University of Alberta
Department of Civil Engineering

Structural Engineering Report No. 164

Nonlinear Dynamic Analysis of Caisson-Type Offshore Structures

by

Ibrahim R. Soudy

and

Terry M. Hrudey

March, 1989

THE UNIVERSITY OF ALBERTA

NONLINEAR DYNAMIC ANALYSIS OF CAISSON-TYPE OFFSHORE STRUCTURES

BY

IBRAHIM R. SOUDY

TERRY M. HRUDEY

STRUCTURAL ENGINEERING REPORT NO. 164

DEPARTMENT OF CIVIL ENGINEERING

UNIVERSITY OF ALBERTA

EDMONTON, ALBERTA, CANADA, T6G 2G7

MARCH 1989

ABSTRACT

During the last two decades oil companies have adopted special types of structures to be used in the arctic. In such environments the existence of ice causes two main problems. First, it permits a very limited open-water season for construction and drilling. Second, the structures must be able to withstand high horizontal forces due to the interaction with the ice.

Many publications, since the late sixties, have dealt with the interaction between ice and narrow structures such as piles, bridge piers, and lighthouses. On the other hand, the interaction between ice and wide structures has not received a comparable amount of attention.

This study is intended to carry out a dynamic analysis on a special type of structure that has been adopted for use in a water depth of 25-50 m. It is a hybrid sand-steel structure consisting of a steel caisson that supports a steel deck which carries accommodation, a drill rig, and personnel facilities. The caisson rests on a sand berm and the core is filled with sand.

The analysis follows two directions. The first one studies the structure response under the effect of a forcing function imposed by the ice. Here, an actual forcing function that has been recorded in the field during an ice event is used. The second direction is to study the problem from an interaction point of view. In that sense, the ice has been included as an element in the overall analysis of the problem considering the related material properties of the ice and assuming known boundary conditions. A comparison between the two approaches will be made and conclusions shall be drawn.

Table of Contents

Chapter Page

Chapter Page

List of Tables

List of Figures

Figure Page

List of Symbols

A	area of contact
a_1 to a_9	constants in yield criterion
a_b	proportionality coefficients
a_T	constant of Sinha's model
b	constant of Sinha's model
[B]	matrix of the spatial derivatives of the interpolation functions
c	empirical coefficient
[C]	damping matrix
c_1	constant of Sinha's model
C_n	contribution of the n^{th} eigenvector in the generalized damping matrix
C_v	radiation damping coefficient
D	indentor width or diameter
d	grain diameter
E	Young's Modulus
[E]	elasticity matrix
F	empirical coefficient
f	natural frequency (Hz)
{F}	vector of body forces
{F(t)}	vector of forcing function

F_{max}	maximum ice force
F_{res}	residual ice force (force after crushing)
g	gravitational acceleration
H	thickness of the ice sheet
K	empirical coefficient
[K]	stiffness matrix
K_n	contribution of the n^{th} eigenvector in the generalized stiffness matrix
L	length of the crushed zone in the ice sheet ahead of the structure
m	lumped mass
[M]	total mass matrix
$[M_a]$	added mass matrix
$[M_s]$	structure mass matrix
M_n	contribution of the n^{th} eigenvector in the generalized mass matrix
n	constant of Sinha's model
[N]	matrix of interpolation functions
P	porosity of ice
$\{q_n\}$	n^{th} eigenvector
{R}	vector of nodal forces
{r}	vector of nodal displacements
s	constant of Sinha's model

S^+	loading slope of the interaction model
S^-	unloading slope of the interaction model
$\{T\}$	vector of surface traction forces
u	displacement in the x direction
V	ice velocity or wave velocity
v	displacement in the y direction
w	displacement in the z direction
$\{x\}, \{\dot{x}\}, \{\ddot{x}\}$	vectors of nodal displacements, velocities, and accelerations, respectively
Θ_1	rotation around the x axis
Θ_2	rotation around the y axis
ε	strain (change in length/original length)
$\{\varepsilon\}$	vector of strain field within a body
$\{\varepsilon_o\}$	vector of initial strain field
ε_d	delayed elastic strain
ε_e	instantaneous elastic strain
ε_v	viscous strain
ε_t	total strain
$\dot{\varepsilon}_{v1}$	viscous strain rate for unit stress
ρ	density of soil or ice
τ_y	yield stress in shear

σ_y	yield stress in tension
ξ_n	damping ratio of the n^{th} eigenvector
ϖ_n	circular frequency of the n^{th} eigenvector (rad/sec)
μ	viscosity of crushed ice
μ_o	initial viscosity of crushed ice

1. INTRODUCTION

1.1 General remarks

Substantial hydrocarbon reserves have been discovered in the Canadian Arctic since the early seventies. Exploration of these reserves in the Canadian Beaufort Sea has been undertaken during that time. In such an area, the offshore exploration activities are faced with severe environmental conditions, in particular ice. The presence of ice causes two main problems. First is the very limited open-water season for construction and drilling. Secondly, structures must be able to withstand large horizontal forces due to impinging ice.

The area of the oil exploration activities in the southern part of the Canadian Beaufort Sea is usually ice-covered for nine months of the year. Freeze up usually starts about early October with new ice formation beginning near shore and slowly advancing offshore. As the ice cover continues to grow, pressure ridges of broken ice become common. The growth of the landfast ice progresses seaward to about 20 m water depth or approximately 48 Kms from shore where the ice cover stabilizes at about January. Beyond the landfast ice exists a transition zone composed of broken moving first-year ice which extends out to the polar or multi-year pack ice.

The extent of the transition zone varies from a few kilometers to hundreds of kilometers depending on the position of the polar pack ice at freeze up. Multi-year ice features might exist within the transition zone and may even be frozen into the landfast ice in some winters. The polar pack ice generally rotates

in a clockwise direction with its movement ranging from 3 to 32 Kms per day in the Beaufort Sea. Break up occurs about late June or early July with the ice in the landfast and transition zones being fragmented into large floes. When these ice floes start moving under the effect of the wind or currents, they exert large horizontal forces on offshore drilling platforms.

In order to conduct oil exploration activities in the arctic areas, artificial gravel islands have been used as drilling platforms. Initially, the islands were constructed in shallow water near shore. The first island was constructed over a two-year period in 3 m of water in 1973. To date, over 22 gravel and sand islands have been constructed in water depths up to 20 m. However, the island costs increase substantially in deeper water because of greatly increased fill volumes required. Therefore in order to extend the exploration activity to deeper waters and at the same time to reduce the increasing costs, another type of structure has been used.

Caisson retained islands have been developed in order to replace the traditional gravel and sand islands in deep water. The volume of fill required in this case is reduced from that used in gravel and sand islands through the use of caissons. The caisson technology developed over the last few years is as follows.

Caisson islands

In 1981 the first caisson-retained island, Tarsiut, was constructed in 22 m of water. The island consisted of four concrete caissons 11 m high, 80 m long, and 14 m wide. The caissons were barged in and placed on a subsea berm. They were separately ballasted into place with water and the core filled with sand.

Single Steel Drilling Caisson

The Canmar SSDC was a segment of an oil tanker that was equipped with a double hull with concrete between the shells. The resulting caisson was 160 m long, 45 m wide, and 23 m high ballasted on a subsea berm. The caisson performed successfully during the winters of 1983, 1984, and also several subsequent winters in the Alaskan Beaufort Sea.

Steel Caisson-retained island

During the winters of 1983 and 1984 an eight-segment steel caisson was used by Esso in the Beaufort Sea. The floating segments were pinned and held together by 16 steel cables to form a large ring shaped structure 90 m in diameter and 17 m high. After ballasting on a subsea berm, the interior core was filled with sand to provide resistance against ice forces.

Conical drilling unit-KULLUK

In 1983 a floating drilling vessel named KULLUK was brought to the Beaufort Sea by Gulf and BeauDrill Limited. It was designed to drill in water depths of 24 to 55 m. It was a conically-shaped floating structure anchored with twelve lines each of 90 mm wire. The diameter of the main deck was about 81 m.

Mobile Arctic Caisson - MAC

The MAC is a mobile arctic caisson (gravity supported) designed to remain on location all winter and withstand ice forces any time of year. It is an octagonal steel annulus that supports a deck which carries the topside modules. After ballasting on a subsea berm the core is filled with sand. The caisson,

approximately 111 by 111 m and 29 m high, is designed to operate in 20 to 50 m of water. A general view of the structure is shown in Fig. 1.1.

In the design of arctic offshore structures one of the most difficult tasks is the determination of the design loads due to ice. From a structural point of view, the designer of such structures is interested in knowing two aspects of the ice load. The first is the global load which controls the overall stability of the structure and the design of the foundations. On the other hand, the local distribution of the ice pressure is more important in the design of the individual structural elements. The time variation of the loads is also an important aspect.

A number of approaches have been proposed in order to determine the design ice loads. However, most of these methods deal with the global ice loads and not the local pressures. Moreover, the problem has been treated from a static point of view while field experience shows that the dynamic effects arising from the interaction between moving ice and the structure can be significant. Jefferies and Wright (1988) reported that dynamic effects were pronounced during the interaction between multi-year ice floes and Gulf Canada's Mobile Arctic Caisson, MAC, in some events. Jefferies and Wright reported that during the most severe ice event (April 12, 1986), the ice loads were very close to the design loads of the structure and measured accelerations were as high as 11% of the gravitational acceleration. There was significant potential for failure during that event due to the possibility of liquefaction of the sand core as a result of the vibrations. This supports the contention that the ice-structure interaction problem should, under some circumstances, be considered as a dynamic problem.

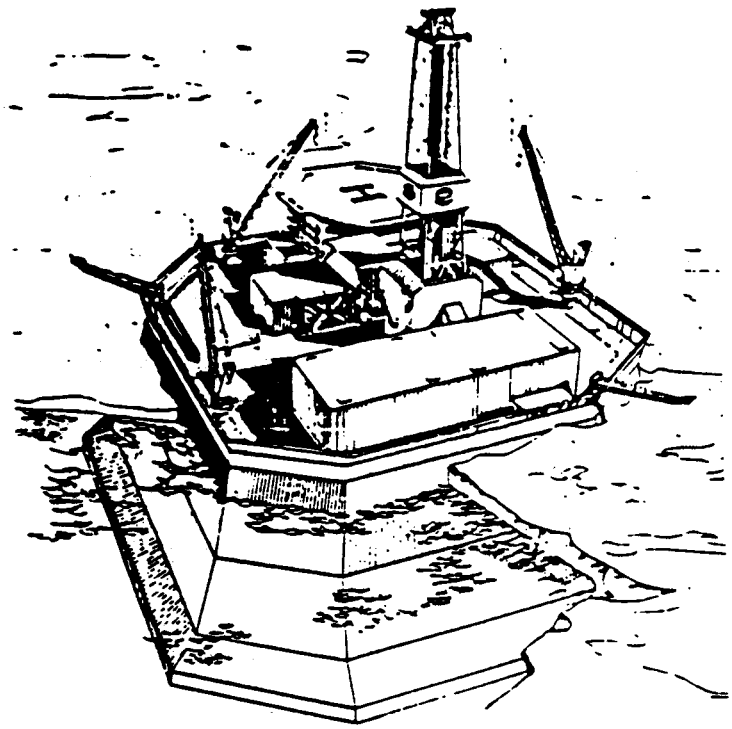

Figure 1.1 General View of MAC

1.2 Object and scope

The study of dynamic ice-structure interaction problems can be carried out following two different approaches. In the first, the ice effect is represented in the analysis as an explicit forcing function that is based on field measurements. Although this is a very useful way of studying the structure response to the moving ice, recording ice forces in the field is very expensive and the results are often kept confidential. On the other hand, there is no guarantee that the same forces will be obtained on a different structure. Another approach in studying the interaction problem is to simulate the moving ice as a structural element in the overall analysis of the problem. The constitutive behavior of such an element is to be developed based on known mechanical properties of ice as well as the general observations of others regarding the interaction between ice and existing structures. The objectives of the present study are as follows.

1- To formulate a fairly detailed finite element model for a representative segment of a typical steel caisson structure.

2- To study the behavior of the finite element model under a specified load time history that has been developed from field measurements.

3- To verify the results of the finite element model against field measurements.

4- To develop an interaction model for the ice based on the mechanical properties of ice and results from indentation tests.

5- To use the interaction model to investigate the effect of certain parameters such as ice velocity and thickness on the dynamic response of the structure as well as the interaction force.

The main purpose of this work is not to conduct a comprehensive parameter study. Rather, it is to establish a methodology for dealing with the analysis of the dynamic interaction problem. A limited parameter study is conducted, however, in order to show that the proposed interaction models are able to capture the effect of parameters such as the ice velocity and thickness on the interaction process.

1.3 Layout of thesis

A review of previous work on ice mechanics and ice forces is mentioned in Chapter 2. Effect of parameters such as temperature , strain rate, confinement, etc. on the mechanical properties of ice is introduced. Current procedures for evaluating ice forces on offshore structures are also discussed. Results of experimental tests of many investigators, both in the field and in labs, are summarized along with analytical models that have been proposed.

A typical caisson-type offshore structure that has been modeled in this study is introduced in Chapter 3. A general description of the different components of the model structure and materials used is presented. Two finite element models have been developed to simulate the structure. A detailed two dimensional (2D) model and a less refined three dimensional (3D) one are introduced. The 3D model is used to refine the 2D model so that the natural frequencies and mode shapes match.

The dynamic analysis of the finite element model under the effect of a recorded ice forcing function is introduced in Chapter 4. The analysis has been conducted using the finite element program ABAQUS mounted on a Cyber 205 supercomputer at the University of Calgary. In this analysis, the added mass

concept is used to simulate the effect of the surrounding water on the structure. The radiation damping technique, used in soil-structure dynamic interaction, has been adopted in this study to represent damping due to ice. The predicted response of the structure is presented in terms of the accelerations, velocities, and displacements as well as stresses in the different structural elements.

The interaction model that is proposed in this study is introduced in Chapter 5. The four parameters required to construct the model are discussed in detail. The implementation of the model in the overall analysis of the ice-structure interaction problem is shown. Also presented is a parametric study to investigate the effect of ice velocity and thickness on the structure response and the resulting interaction force. Results of six cases studied using the interaction model are given and discussed in detail.

Another interaction model is developed and introduced in Chapter 6. In this model the ice is simulated as a viscoelastic material. The viscoelastic model that describes the behavior of ice before crushing is discussed along with the representation of the ice after crushing. The finite element formulation of the viscoelastic dynamic analysis is presented and its implementation in a time stepping solution algorithm is discussed in detail. Results of four cases studied using the viscoelastic model are shown.

Finally, results of this study have been summarized in Chapter 7 along with general conclusions and recommendations for future research work that would be of interest in the area of ice-structure interaction.

2. ICE MECHANICS AND ICE FORCES

2.1 Scope

The successful operation of arctic drilling structures requires their being able to withstand environmental loads, the most severe of which are the horizontal forces due to interaction with multi-year ice. During the last two decades, considerable work has been done in order to obtain an adequate evaluation of the ice loads that can be expected on such structures. This chapter is a review of the mechanical properties of ice and also of previous work done both experimentally and analytically to evaluate the ice loads.

2.2 Mechanical properties of ice

A considerable amount of work has been done during the last two to three decades in order to gain a better understanding of the mechanical behavior of ice. The constitutive behavior of ice is quite complex and many uncertainties are associated with it. The reason is that in nature, ice exists at high homologous temperatures, that is it is very close to its melting point. The mechanical properties of ice depend on many parameters. The internal structure of ice, loading rate, temperature, and degree of confinement are among these. Depending on the surrounding conditions, ice might behave in an elastic, plastic, viscous, or brittle manner. A brief discussion of the effect these parameters have on ice properties follows.

2.2.1 Internal structure

The elementary molecular configuration of ice has a tetrahedral pattern. Each oxygen atom is surrounded by four oxygen atoms at the vertices of a uniform tetrahedron. The continuous arrangement of the oxygen atoms in ice is shown in Fig. 2.1. From this one can see that the crystal structure of ice exhibits hexagonal symmetry and the molecules are arranged in a series of parallel planes. These planes are termed the basal planes and the normal direction to them is referred to as the c-axis or optical axis of the crystal (Michel, 1978).

Freshwater ice

The formation of freshwater ice starts with or without initiation by a snowfall. First, a primary layer (P ice) that has granular crystals is formed. In this layer the c-axes have random orientation. Following that, a secondary layer (S ice) grows in the vertical direction. This layer has columnar grain structure and is usually termed columnar ice. The c-axis in this layer might be vertical (S1 ice) or horizontal (S2 and S3 ice) (Michel and Remseier, 1971).

Sea ice

Peyton (1968) examined the internal structure of sea ice and found that distinct layers exist as follows,

- A snow cover might exist on the top.

- Under the snow cover there is a thin layer of granular ice with fine crystals of about 1 mm size. The thickness of this layer might vary from few millimeters to

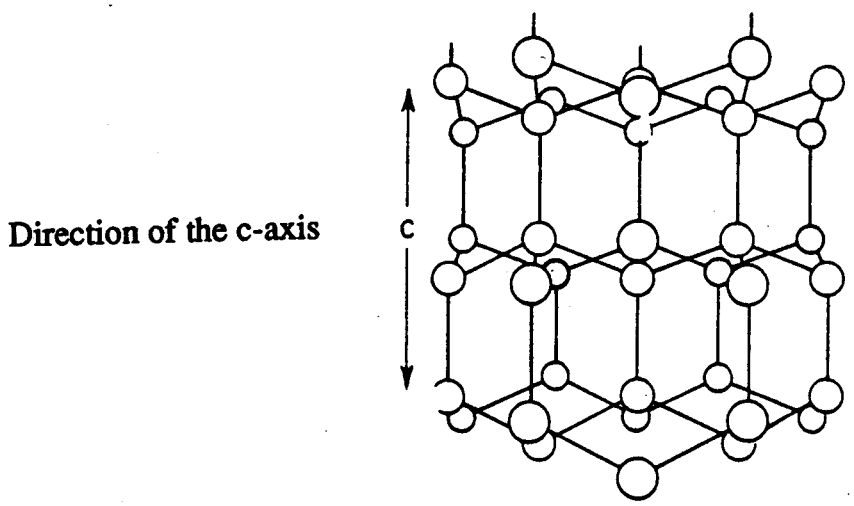

Figure 2.1 Typical Arrangement of Oxygen Atoms in Ice

few centimeters depending on the temperature at formation. The salinity in this layer is from 7 to 14 parts per thousand (0/00).

- Below the granular layer lies a transition zone where the crystals become more elongated. Crystal sizes in this layer are in the order of 4 mm and the salinity is about 9 0/00.

- The main layer of the ice sheet lies under the transition zone. The texture of this layer is columnar and the crystals are elongated vertically with randomly-oriented c-axes in the plane of the ice sheet (the horizontal plane). Crystal sizes up to 24 mm exist with salinity in the order of 5 0/00. A specific feature of this layer is that vertical brine pockets are present between the crystals. The ice is considered as a transversely isotropic material in this layer due to its internal structure.

2.2.2 Parameters affecting the mechanical properties of ice

The effect of some parameters such as the grain size, crystal orientation, loading rate, and temperature are summarized in the following subsections.

2.2.2.1 Grain size

The effect of the grain size on the strength of freshwater ice was studied by Michel (1978). Compressive strength results for both granular and columnar sea ice were reported by Wang (1979). In general, the finer the ice the higher the strength. It might be expected that the different grain sizes that exist in the various layers of a sea ice sheet, will play an important role in determining its overall strength, especially in bending.

2.2.2.2 Crystal orientation

The crystal orientation in the ice determines its isotropy or anisotropy. Granular ice has random crystal orientation and is usually considered to be isotropic. On the other hand, columnar ice is usually oriented and so should be considered as an anisotropic material. Strength values for columnar ice vary significantly depending on the loading direction with respect to the plane of the ice sheet. Tests have shown that the strength in the vertical direction is about three times that in the plane of the ice sheet (Wang, 1979).

2.2.2.3 Porosity

Porosity is the ratio between the volume of voids in a specific sample of material and the total volume. In ice mechanics more than one definition is used for porosity. For freshwater ice the traditional definition is used while air porosity, brine porosity, and total porosity are used for sea ice. The air porosity is the ratio between the volume of voids filled with air and the total volume. Brine porosity is the volume of voids filled with brine over the total volume. The total porosity is the summation of the air and brine porosities. The brine pockets in sea ice reduce the contact area between the crystals and hence reduce the strength. Assur (1958) proposed a simple model to correlate ice strength and brine volume. He assumed that the brine pockets have the shape of vertical cylindrical channels. The strength in a direction perpendicular to the columns can be written as

$$\sigma = \sigma_0 (1 - P) \tag{2.1}$$

where, σ_0 is the strength corresponding to zero porosity and P is the porosity. This model was shown to be in a good agreement with test results.

2.2.2.4 Strain rate

The behavior of ice varies widely depending on the strain rate. In uniaxial constant strain rate compression tests, ice behaves as a ductile material at very low strain rates. The maximum stress reached under such conditions is usually termed the yield stress. The term 'yield stress' used here does not imply that the ice behaves elastically up to that level of stress. Rather, the maximum stress has been called the yield stress in this case because the ice undergoes large strains under almost constant stress once it reaches that level. Thus it is not the same as the yield stress defined in classical plasticity theory. In this range of strain rates, the compressive strength of the ice depends significantly on the strain rate (Wang, 1982).

At high strain rates, on the other hand, ice behaves as a brittle material. Before failure the behavior is essentially elastic until the specimen fractures suddenly. In this range of strain rates, the compressive strength is independent of the strain rate. Figure 2.2 shows typical stress versus strain curves for ice under uniaxial compression at low and high constant strain rates.

A transition range lies between the ductile and brittle ranges of strain rate. The range of strain rates in the transition zone is temperature dependent (Wu et al., 1976). The failure mode in this range can be either ductile or brittle. Michel and Toussaint (1977) plotted ice compressive strength versus strain rate using data from different investigators for S2 freshwater ice at -10^{o}C. Figure 2.3

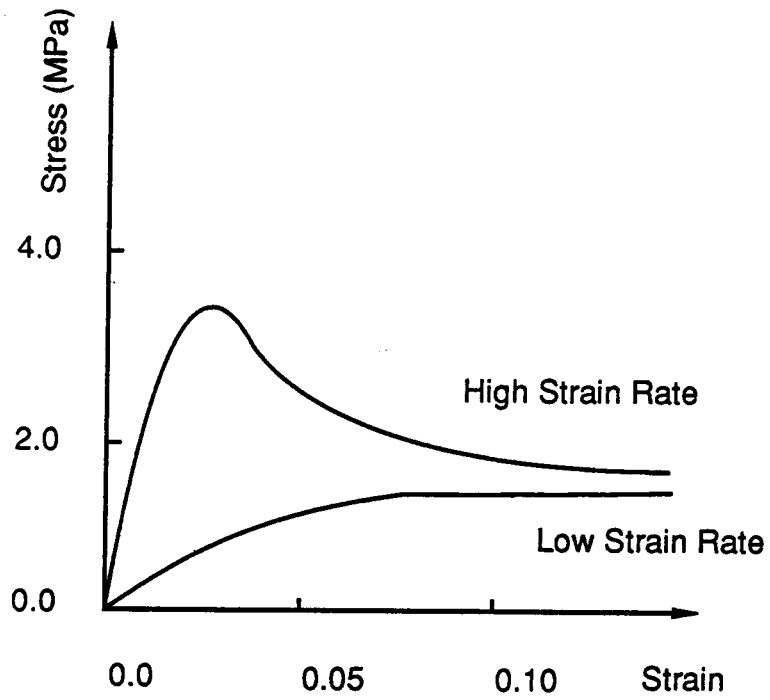

Figure 2.2 Typical Stress-Strain Curves of Ice at Different Strain Rates

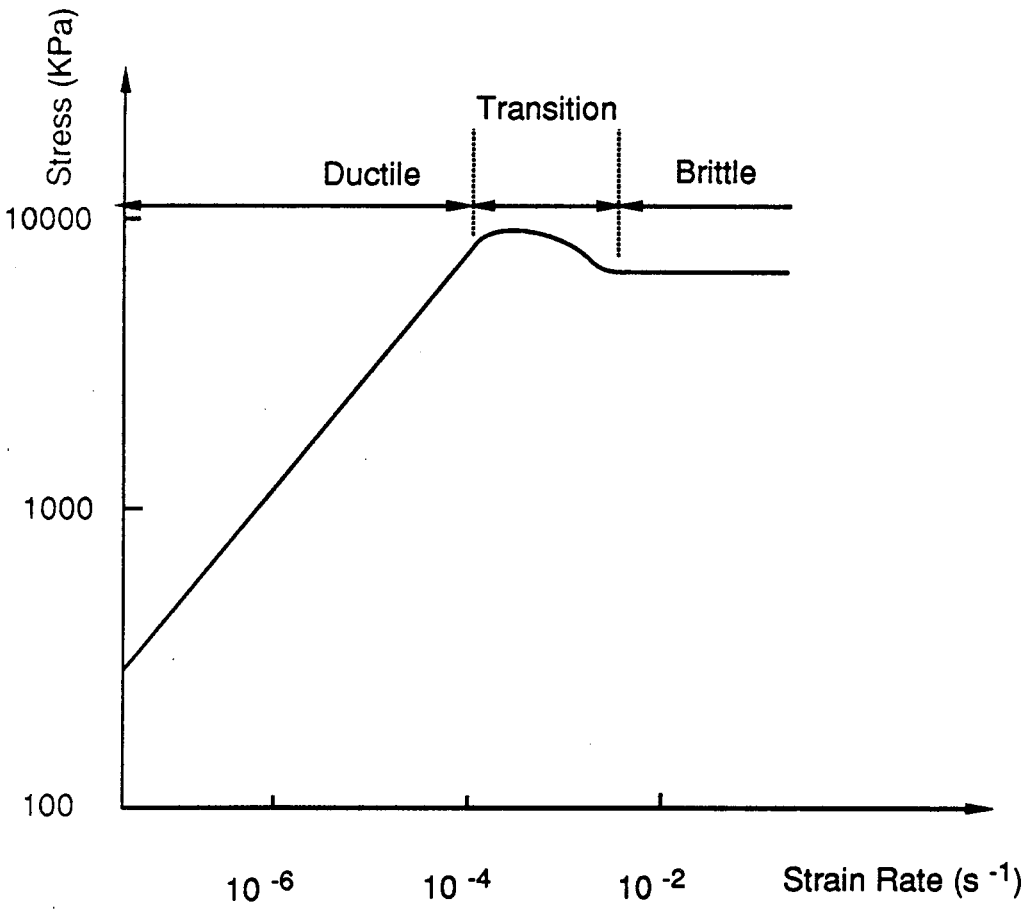

Figure 2.3 Typical Strength- Strain Rate Curve of Ice

shows the variation of the strength with the strain rate and the three ranges are represented.

2.2.2.5 Temperature

Temperature has a significant effect on the compressive strength of both freshwater and sea ice. The problem is further complicated in the case of sea ice because the brine volume, which influences strength, is also temperature-dependent (Frankenstein and Gardner, 1967). In general, the compressive strength of ice increases as the temperature decreases, eventually approaching an asymptotic value.

2.2.2.6 Confinement

Generally, the constitutive behavior of materials under multiaxial states of stress is more complicated than their behavior under uniaxial loading conditions. The material behavior under multiaxial states of stress is of importance in establishing failure criteria under general loading conditions. Biaxial compression tests on freshwater columnar S2 ice at different strain rates and constant temperature of -10^{o}C have been conducted by Frederking (1977). Two types of test, denoted as A and B, were performed on ice under plane strain conditions. The difference between the two types of test was the orientation of the confining plates with respect to the direction of the columns. In type A tests, the confining plates were perpendicular to the columns, while in type B tests, they were parallel to that direction. For type A tests, the confined strength of columnar ice might reach as much as two to three times the uniaxial strength, whereas for granular ice, the increase is only 25% when tested under plane strain conditions. The reason for the significant strength increase in type A tests on

columnar ice, is that plastic flow along the grain boundaries is restricted by that arrangement. For type B specimens the compressive strength is almost the same as the uniaxial strength.

Hausler (1981) conducted triaxial compressive tests on saline ice using brush-type platens in order to minimize the friction between the platens and the specimen. In his experiments, loading of a cubic specimen in three orthogonal directions is possible. According to Hausler, the failure surface for columnar ice in the compression-compression-compression zone is like an ellipsoid whose longitudinal axis is the hydrostatic axis $\sigma_1=\sigma_2=\sigma_3$.

Triaxial tests on laboratory-grown saline ice were also conducted by Nawwar et al. (1983). Five parameters were investigated: salinity, temperature, confining pressure, strain rate, and sample orientation. It was concluded that the strength increases with confining pressure and it might reach two to three times the uniaxial strength. It was also noted that the increase in confining pressure shifts the ductile/brittle transition zone towards higher strain rates.

2.3 Ice forces on arctic offshore structures

The loads exerted on a drilling platform by a moving ice sheet are a function of many parameters such as,

1- Type of ice and its mechanical properties which in turn depend on other factors like temperature, salinity, etc.

2- The overall configuration of the structure; pile-supported or caisson-type, vertical sided or conical form.

3- Rate of loading; impact or long term type of loading.

The problem in such cases is not just the large number of parameters involved in the analysis, rather that there is an interaction between the structure on one side and the moving ice on the other. That is, what happens in the ice affects the structure and in turn the response of the structure influences the behavior of the ice . In addition, the problem is controlled to a great extent by the environmental conditions which determine the available driving forces.

2.3.1 Maximum ice force prediction

When an ice sheet moves against a structure, it exerts a force on the structure. The maximum value of this force is limited by the force required to fail the ice locally in the front of the structure and the maximum environmental driving force. Croasdale (1985) categorized the maximum ice forces in terms of three 'limit states'.

The first limit state is called 'limit stress' in which case it is assumed that the ice is moving under the effect of an infinite driving force and that it fails against the structure. The total ice force is therefore governed by the local failure of the ice ahead of the structure and depends significantly on the failure mode of the ice. The mode in which the ice fails depends mainly on the geometry of the structure. For slender structures such as piles, the problem of the ice-structure interaction can be treated as an indentation one. Korzhavin (1962) proposed a formula to calculate the maximum force exerted on a slender indentor by a moving ice sheet as

$$F = K D H \sigma \qquad (2.2)$$

where σ is the crushing strength of ice and K is an empirical factor that takes account of biaxial indentation stress, indentor shape, imperfect contact between the ice and the structure, non-simultaneous failure, and the aspect ratio D/H(indentor width/ice thickness).

Kry (1980) defined four modes of failure for an ice sheet against a structure, these are: flexure, rubble formation, buckling, and crushing. It is expected that ice fails in crushing against a vertically sided structure and in bending against a sloping one. Buckling occurs usually with very thin ice sheets, of the order of several centimeters thick, and rubble formation appears if the broken ice cannot clear around the structure and instead starts to accumulate ahead of it. Among the four modes of failure, the crushing mode produces the maximum forces.

If the ice floe has insufficient kinetic energy to envelope the structure completely, then the ice force will be less than that estimated using the limit stress approach. In this case, a second limit state can be used in evaluating the ice force that is the "limit kinetic energy". In this limit state the force is estimated from an energy balance that equates the initial kinetic energy of the ice to the work done by force on the ice sheet.

The third limit state is based on the assumption that the available driving forces are limited. These are due to wind and current drag, and pack ice acting against the ice floe. In this case the maximum ice force is limited by the available driving forces. Generally, the ice force associated with this limit state is the least of the three limit states. Many difficulties are encountered in this limit state especially in estimating the environmental driving forces.

Comparing the three limit states, it is apparent that the ice load cannot exceed the force calculated from the limit stress state and it may be less. Hence, the limit stress state, using an appropriate failure mode, is frequently used to estimate the maximum global ice forces.

The methods discussed so far are concerned only with estimating the maximum global ice forces. Also, they neglect two important aspects of the ice-structure interaction problem. The first is that the problem has been dealt with from a static point of view. The static approach is a reasonable starting point but field experience indicates that dynamic effects may be significant. Consequently there is a need to know the time history of the ice force not just the maximum value. The second point is that the global forces estimated by any of the three limit states do not take into account the interaction between the structure and the moving ice which governs the local distribution of the ice pressure.

2.3.2 Measurements of ice forces

In order to get actual time histories for the forces exerted by moving ice on offshore structures, measurements have been conducted on both drilling platforms operating in the field and small models in labs. Also, since ice forces are a major design factor for bridge piers in many places, field measurements have been conducted to estimate the forces exerted by river ice on bridge piers.

Since the discovery of offshore oil in Alaska in the summer of 1962, the upper part of Cook Inlet has been the site of intensive offshore oil development activity. Peyton (1966, 1968(a), and 1968(b)) measured the forcing functions resulting from continuous indentation of ice by circular indentors. Because of the complexity of the problem and the large economic risk, it was decided to

determine the design loads from measurements on a field test structure. The test structure was a simply supported beam attached to one of one leg of a temporary drilling platform. The beam, 0.91 m in diameter and 6.1 m long, was hinged at both ends with a load cell to measure the reaction. At the same time Peyton carried out experimental work on a laboratory test pile. The measured forcing functions were found to be very much dependent on the velocity of the ice. At low velocities the load histories showed a large amplitude saw-tooth pattern with a frequency of 1 Hz. Although the natural frequency of the supporting platform was also approximately 1 Hz, Peyton concluded, based on the experimental work, that the forcing frequency is related to the material properties of the ice and has little to do with the natural frequency of the structure. In general, the largest ice forces occurred when the ice velocity was very low. This was attributed to the fact that as the loading rate decreases, the ice strength increases. The conclusion of Peyton that the force frequency is affected by the material properties of the ice but not by the structure does not seem to be very realistic since the problem is an interaction one between the ice on one side and the structure on the other. It should be expected, however, that the effect of the structure on the force frequency decreases as the stiffness of the structure increases since the displacement of the structure will be very small.

Blenkarn (1970) presented results of ice force measurements made in Cook Inlet between 1963 to 1969. Measurements were made on a specially instrumented test pile and records were taken on a number of different platforms. Blenkarn observed that ice loading of a structure is generally accompanied with dynamic or vibratory phenomena. He divided the ice loads into two components, an effective or steady component and a vibratory component. While the transient

or vibratory component can be a function of the ice properties as well as the structure itself, the steady component is related more to the material characteristics of the ice. The explanation of Blenkarn emphasizes the importance of the effect of the structure on the crushing frequency of the ice.

Measurements of ice forces on several bridge piers have been conducted in Alberta, Canada. Neill (1972, 1976) proposed that the frequency of the ice force is a function of the velocity of the ice as well as the size of the crushed zone ahead of the structure. Based on experimental observations, Michel (1978) gave a similar explanation that the speed of the ice and the size of the damaged zone in front of the indentor determine the frequency of the ice force.

Lipsett and Gerard (1980) and Montgomery et al. (1980) presented results of forcing functions recorded at Hondo bridge site where a massive pier has been instrumented to measure ice forces. Because the pier has a sloping face, the mode of ice failure was a combination of bending and crushing. Montgomery and Lipsett (1981) used an indirect method to deduce the ice forcing functions from the acceleration response of the pier recorded in the field. The structural characteristics of the pier have been determined by performing the suitable tests in the field both statically and dynamically. The ice forces calculated by them were in good agreement with the measured ones.

Schwarz (1970) presented measurements on an instrumented pile fixed on a bridge pier in the Eider River in Germany. A total of 50 separate pressure-measuring plates were used to measure the total force and its distribution along the pile. In general, the maximum local pressures were found to be greater than

the average pressure across the pile. That confirms the importance of the local distribution of the ice pressures.

Maattanen (1979, 1981) conducted some tests at CRREL (Cold Regions Research and Engineering Laboratory) to investigate the dynamic interaction between moving ice and piles. The results were in agreement with the conclusion of Peyton that the frequency of the forcing function is dependent on the velocity of the ice sheet.

In addition to the measurements of the ice forces on full scale structures, experimental work has been conducted on reduced scale models. Frederking and Gold (1975) carried out a series of laboratory indentation tests on columnar S2 freshwater ice plates. The tests were limited to low aspect ratios (maximum of 3) and very low indentation rates so that the behavior was ductile without significant cracking. It was found that the yield stress depends on the width of the indentor but not on the ice thickness. In fact, this is expected because for the range of aspect ratio used in the experiments there was a plane strain state in the ice sheet ahead of the indentor. This is in general agreement with the results of Schwarz et al. (1974) who found that for small values of aspect ratio, the ice thickness has no significant effect on the ice pressure.

Michel and Toussaint (1977) carried out indentation tests on freshwater columnar S2 ice plates. They studied the effect of the strain rate, scale, and the aspect ratio on the effective indentation pressure and mode of failure. For very low strain rates, the failure was purely ductile. A plastification zone with high intensity of microcracks was formed and extended a distance about 1.6 times the indentor width ahead of it. Very little cracking was observed beyond a distance

2.5 times the indentor width. The force reduced to almost 60% of the peak after yielding and then remained constant. This failure process appeared to be valid up to an effective strain rate of about $2.5x10^{-5}$ s^{-1}. At higher strain rates, the stress concentrations at the corners of the indentor caused major cracks in the ice plate before yielding. These macrocracks were not sufficient to fail the plate and the microcracking mechanism continued as for pure ductile behavior. This mechanism was called transition failure and occurred up to a strain rate of about $5x10^{-4}s^{-1}$.

For strain rates higher than $2.5x10^{-2}$ s^{-1}, the failure was brittle and no plastification zone was formed. Major cracks like those in the transition range formed first and complete failure occurred with flaking of the ice on both sides of the plate. The flaking took place over a very short distance ahead of the indentor.

In their study, Michel and Toussaint found that the ice thickness does not influence the failure modes significantly. This is in agreement with the conclusions of both Frederking and Gold (1975) and Schwarz et al. (1974). The major factor that affected the failure process is the strain rate which governed the mode of failure. It was also concluded that the aspect ratio does not have significant effect on the indentation strength for constant strain rate conditions. To interpret the experimental data, they used the plane strain solution for the flat punch indentation of a half space, with a von Mises failure criterion. It was concluded that the indentation strength of laboratory grown S2 ice is approximately three times the uniaxial compressive strength.

Croasdale et al. (1977) conducted both laboratory and field tests in order to investigate the relationship between small scale ice strength and maximum ice forces on vertical piers. Results from the field tests showed that the pressure increased to a peak value at which the ice failed. After the initial failure, the ice pressure usually dropped to about half the peak value before rising again. This is consistent with the observations of Michel and Toussaint (1977). The failure mode during the tests was the flaking type.

Croasdale et al. conducted a theoretical analysis in order to evaluate the indentation coefficient of Korzhavin's indentation equation, Eq. 2.2. The analysis was done using the lower-bound and upper-bound limit theorems of plasticity (Prager and Hodge, 1951). The ice was assumed to be as isotropic, homogeneous, and ideal elastic-plastic material obeying the Tresca yield criterion. Because columnar ice is anisotropic, nonhomogeneous, and not an ideal elastic-plastic material, good correlation between the analytical results and the test observations was not achieved.

Michel and Blanchet (1983) conducted indentation tests in the brittle range on S2 freshwater ice plates. The range of aspect ratio in these experiments varied between 0.5 and 83. Modes of failure similar to those found by Michel and Toussaint were observed (ductile, transition, and brittle). In the brittle range of failure, four modes were observed, depending on the aspect ratio. For aspect ratios less than 1, a cleavage mode of failure occurred. For aspect ratios in the range of 1 to 5, the failure mode changed to one in which a plastified triangle formed ahead of the indentor followed by extrusion. For aspect ratios between 5 and 20, the failure mode was mainly a shear mode. Radial cracks originated initially from the edges of the indentor. These cracks propagated either outside to

form wedges in the ice sheet or inside to form large broken triangles in front of the indentor. When the aspect ratio was more than 20, the predominant failure mode was buckling.

Maattanen (1983) carried out an experimental program at CRREL to study the dependence of ice forces and crushing frequency on the properties of the ice and the structure, in this case, a pile. The study was limited to the continuous crushing mode of failure at low values of ice velocity. Maattanen found that the variation of both ice force and pile displacement with time exhibited a sawtooth pattern. He observed that the maximum ice forces occurred when the strain rate was at the transition zone from ductile to brittle. The frequency of the recorded ice forces was directly proportional to the ice velocity and inversely proportional to the difference between the maximum and minimum ice force. These results raised doubts about Peyton's suggestion that the ice has a characteristic failure frequency of 1 Hz.

Sodhi and Morris (1986) conducted small scale indentation tests to investigate the effect of pile diameter and ice velocity on the ice forces during interaction between ice and rigid, vertical, cylindrical structures. The characteristic frequency of crushing was found to depend on the ice velocity but not on the pile diameter. It was concluded that the average length of the damage zone during a crushing cycle varies between 0.1 and 0.5 of the ice thickness. This is in agreement with the results of both Neill (1976) and Michel (1978).

Timco (1986) published the results of small scale indentation tests on S2 freshwater ice in the brittle range. The range of strain rates used varied between 10^{-2} and 10 s^{-1}, and the aspect ratio ranged between 0.5 and 22. Five failure

modes were observed: pure crushing with no cracks or very short radial cracks, crushing with spalling, crushing with radial cracks, crushing with circumferential cracking, and radial/circumferential cracking and buckling. The factors that control these modes of failure were the aspect ratio and the ice velocity.

During the interaction process for all the failure modes, there was a region immediately in front of the indentor that contained a very high density of microcracks. The region was as wide as the indentor and extended in front of it to a distance of one to one and a half times the width. From these tests it was concluded that there is a strong correlation between the peak pressure and the aspect ratio. On the other hand, the dependence of the peak pressure on the strain rate is not significant. This is consistent with the conclusion of Michel and Toussaint that the ice strength is independent of the strain rate in the brittle range.

Both Michel and Toussaint and Croasdale et al. used failure criteria that have been developed for applications in metal plasticity. These criteria describe behavior of isotropic materials that have equal tensile and compressive strengths and are not sensitive to hydrostatic pressure. The strength of columnar-grained ice is, however, rate and temperature dependent, anisotropic, sensitive to hydrostatic pressure, and differs in tension and compression. In plastic limit analysis of the indentation problem, an appropriate failure criterion must be employed in order to obtain reasonable results. The failure criterion must take into consideration the anisotropy, sensitivity to hydrostatic pressure, and difference in tensile and compressive strengths of ice.

Reinicke and Ralston (1977) developed an anisotropic yield criterion suitable for columnar ice. The yield function is a generalization of the von Mises yield criterion and is defined by 9 parameters as follows:

$$F = a_1 (\sigma_y-\sigma_z)^2 + a_2 (\sigma_z-\sigma_x)^2 + a_3 (\sigma_x-\sigma_y)^2 + a_4\tau_{yz}^2 + a_5\tau_{zx}^2 + a_6\tau_{xy}^2 + a_7\sigma_x + a_8\sigma_y + a_9\sigma_z - 1 \quad (2.3)$$

This anisotropic yield criterion predicts different tensile and compressive strengths and is a function of the hydrostatic stress.

Imposing isotropy in the x-y plane reduces the number of the parameters to five and the yield criterion can be written as:

$$F=a_1[(\sigma_y-\sigma_z)^2+(\sigma_z-\sigma_x)^2]+a_3(\sigma_x-\sigma_y)^2+a_4(\tau_{yz}+\tau_{zx})^2 + a_6\tau_{xy}^2+a_7(\sigma_x+\sigma_y) + a_9\sigma_z - 1 \quad (2.4)$$

where, $a_6=2(a_1+2a_3)$. The values of these parameters can be determined by performing the appropriate tests on the material, however this is a formidable experimental task. Reinicke and Remer (1978) proposed a three-parameter isotropic yield function that is suitable for modelling the behavior of granular ice. The function is deduced by adding another plane of isotropy in Eq. 2.4 and can be written as :

$$F=a_1[(\sigma_y-\sigma_z)^2+(\sigma_z-\sigma_x)^2+(\sigma_x-\sigma_y)^2]+6a_1(\tau_{yz}^2+\tau_{zx}^2+\tau_{xy}^2) + a_7(\sigma_x+\sigma_y+\sigma_z) -1 \quad (2.5)$$

Using the anisotropic relation given in Eq.2.4, Ralston (1978) obtained upper bound and lower bound solutions for the indentation of a sheet of ice with

uniform temperature through its thickness. In the analysis, a Prandtl type mechanism was assumed to develop ahead of the indentor. The indentation pressures obtained by Ralston were in good agreement with the experimental results of Michel and Toussaint (1977).

Reinicke and Remer (1978) proposed upper and lower bound solutions for the indentation problem assuming a flaking mode of failure. They used the 3-parameter isotropic yield criterion mentioned above. The solution in this case is limited to granular ice and cannot be used with columnar ice.

2.3.3 Hans Island

In all the studies mentioned above, the main consideration has been the interaction of ice with narrow structures such as piles and bridge piers. Caisson-type offshore drilling platforms are wide structures with lateral dimensions of the order of tens of meters. Since it is known that ice forces are very scale-dependent (Bercha and Brown, 1985), results from narrow structures cannot easily be extrapolated for use with wide structures. However, small scale tests can be very useful in helping one understand the interaction between ice and large scale structures. On the other hand, measurements of ice forces exerted on wide structures are of great importance for the design of arctic caissons.

In 1979, Dome Petroleum started a project aimed at measuring full scale ice forces exerted by multi-year ice floes on a stationary object (Metge et al., 1981). They decided to measure large scale ice forces by measuring the deceleration of large ice floes as they contacted a natural obstruction. The site chosen was Hans Island, located in the middle of Kennedy Channel between Greenland and Ellesmere Island.

The methodology used was to estimate the mass of the ice floe and use Newton's second law (force=mass x acceleration) to evaluate the ice force. Only some qualitative observations have been given by Metge et al.. Perhaps the most important, is that the mode of failure of ice during impact is a crushing mode, with very little evidence of flexural failure. Some of the data obtained during the measurements have been released and used in preparing pressure versus aspect ratio/area curves. One of the most important conclusions of their study is that the average ice pressure decreases significantly as the contact area increases.

2.4 Ice-structure interaction models

It has been shown above that many investigators have conducted studies in order to measure ice forces in the field and in laboratories. Field measurements are very important but, in general, some difficulties related to them cannot be avoided. Measuring ice forces is expensive, and time consuming. Moreover, the recorded forces are controlled by the available driving forces during the ice event. Mathematical modelling of the ice-structure interaction problem is an attractive approach which, with a good physical model and reasonable assumptions, allows parametric studies to be undertaken. Such studies can encompass broad ranges of variables and provide reasonable insight into the relative importance of these factors.

Matlock et al. (1969) proposed a simple model for the ice-structure interaction problem. The model considered the structure as a single degree of freedom system and the ice as a train of elastic-brittle cantilevers attached to a rigid base that moves with a constant velocity. The model can be defined by the deformation of the ice tooth at which brittle failure occurs, the pitch between each

two successive teeth, and the maximum force at failure. At the maximum deformation, the ice tooth fractures completely and the interaction force remains at zero until the next tooth comes in contact with the structure. The model is clearly an empirical one and field measurements must be made to provide some of the data required. In addition to that, the ice is assumed to be an elastic-brittle material and the dependence of its mechanical properties on parameters like loading rate, temperature, and time are not considered. On the other hand, the model produced structural responses that are qualitatively similar to those observed in the field. The main conclusion is that the structure response is influenced by the ice velocity. This is in agreement with the conclusion of Peyton (1968).

Reddy et al. (1975a) developed a response spectrum that could be used for normal mode analysis of structures. They also used average power spectral density functions of Blenkarn's ice force records (Blenkarn, 1970) to establish a random vibration analysis of the structure (Reddy et al., 1975b). This technique predicts the response of the structure under artificially generated random ice forces. In order to have confidence in the results obtained using this method, a wide date base for generating random ice forces has to be available. This is not usually easy to obtain. The applications of these techniques in determining ice forces in an interaction analysis is not possible because the mechanical properties of the ice are not simulated.

Maattanen (1978) proposed a physical model that depends mainly on the strong relationship between the ice strength and loading rate as described by Peyton(1966). Assuming that the lighthouses under investigation respond elastically, Maattanen wrote the equations of motion in terms of the normal modes

of vibration of the structure. The ice force was expressed in terms of the relative velocity between the ice and the structure as well as an idealized strength versus stress rate curve for the ice. The forcing function contributed a term in the equations of motion that is proportional to the velocity. This term, under certain conditions, gave rise to what Maattanen called negative damping. This force, in fact, worked as a driving force as explained earlier by Blenkarn(1970).

Maattanen established an approximate criterion to examine the stability of the vibration solution to see if large ice-induced vibrations might occur. Also, using a step-by-step integration technique for the equations of motion, force and displacement time histories could be obtained. The model is limited in its use to slender flexible structures.

Eranti et al. (1981) developed an ice-structure interaction model based on laboratory indentation tests. It was observed during the tests that the interaction process can be divided into two phases. The indentor first penetrated into ice and during this phase the ice force increased until it reached a critical value. Then the ice failed suddenly within a finite zone that depended on the critical force. After that, the structure was almost in a free vibration mode until complete contact with the ice developed. The system of equations of motion was also solved in a step-by-step fashion using a modal analysis. Solving the system of equations, both forces and displacement records could be found. Their approach is similar, to some extent, to that proposed by Matlock et al. (1969) since the stiffness of the ice is added to the stiffness of the structure when the structure is in contact with the intact ice. The model is considered to be a semi-empirical and field measurements must be available in order to provide some parameters.

Eranti et al. obtained qualitatively good agreement between the ice forces derived theoretically using their model and those measured experimentally.

Croteau (1983) developed a nonlinear model for the ice-structure interaction problem. The model is based on Korzhavin's equation to evaluate the ice force before and after failure of the ice. He used the model to study ice floe impact problems with hypothetical rigid platforms using the energy balance approach. He also studied the response of slender structures in the indentation process with ice. A study of a platform subjected to earthquake motion while surrounded by ice was also undertaken. The model failed to reproduce force records measured by Lipsett and Gerard (1980) at Hondo bridge pier, Alberta, Canada. It was explained by Croteau that some aspects related to fracture of ice at very rapid loading are not described by the model. All the other cases studied by him were hypothetical and assessment of the model performance against field data was not made.

2.5 Summary and conclusions

From the literature review, it can be seen that a large number of studies have been conducted on the ice-structure interaction problem. Many investigators carried out indentation tests both in field and labs in order to study the effect of moving ice on structures. It is noted, however, that most of these studies have been conducted using slender indentors. Only one study dealt with a wide structure, that is Hans Island. The main purpose of that project was to evaluate the effective ice pressure when ice fails over a large area. Since Hans Island is effectively a rigid structure, the effect of the stiffness of the structure on the interaction process was not a factor.

A number of analytical models have been developed to study the ice-structure interaction problem. The simulation of the mechanical properties of ice in the analysis is not possible in some of these models. Other models are either limited to a specific type of structure or need field measurements to complete the formulation of the model.

Caisson-type drilling platforms are wide structures in the order of 10's to 100's of meters. These structures are not totally rigid. Analyses of these structures under ice load histories that have been recorded in the field during ice events have not been published yet. To conduct such analyses, several aspects must be dealt with. The representation of the structure in the analysis is an important issue, especially with the large dimensions of the structure and the complicated structural details. Damping due to ice is another problem that has to be solved in the analysis.

Development of analytical interaction models that can predict the forces exerted by moving ice on the structure is of great importance. These models provide a good opportunity to study the effect of parameters like ice velocity and thickness on the response of the structure. Controlling these parameters can not be done easily in the field. In this study, these tasks are pursued.

3. FINITE ELEMENT MODEL

3.1 Introduction

In order to carry out an analysis to study the behavior of caisson-type offshore structures under ice loads, a representative structure has to be modeled. Gulf Canada's Mobile Arctic Caisson, MAC, is a typical of caisson retained island and therefore the structure used in this study is modeled on it. However, the intent is not to produce a model of MAC per se but rather to have a structure that is representative of those that have been used in the Arctic.

In this chapter, a description of the structure is given and details of the different structural elements are shown. Loads on the deck are mentioned and properties of the sand core and berm are given. In order to conduct a dynamic analysis on the structure, two finite element models have been developed: a detailed two dimensional model and a less detailed three dimensional one. The two models are described and a comparison is made of the vibration mode shapes predicted by each.

3.2 Basic design requirements of the structure

A bottom founded structure called the MAC, was built by Gulf Canada Resources for use in the Canadian Beaufort Sea at water depths in the range of 20 to 50 m. Bruce and Harrington (1982) have summarized the basic design requirements of the structure. These are that the structure must have the ability to operate all year round and be relocated without great difficulty. Another, and

perhaps the most important design requirement, is that the fill volume be significantly less than the volume required for constructing traditional gravel and sand islands in deep waters. The structure has been designed to meet these requirements and has been used successfully in more than one location. In the following section a general overview of the structure is given.

3.3 General layout of MAC

The structure consists of an annular steel caisson, approximately 111 by 111 m in plan, and about 29 m high. The topside modules are erected on a box girder deck that is simply supported on rubber bushings. The core of the annular caisson, 72 by 72 m, is filled with hydraulically placed sand, and provides most of the resistance to the horizontal ice forces. A sand berm is required so that the caisson is supported uniformly and to provide a setdown depth of about 20 m.

The construction sequence of such a structure is that after preparation of the foundation and berm, the structure is ballasted by pumping water into tanks inside the caisson and then the core is filled with sand. Figure 3.1 shows a typical cross section of the structure.

3.4 Structural details

In the following subsections, details of the different structural elements are presented. The structural arrangement of the steel caisson is given first followed by the steels used. Also shown are details of the box girder deck, core, and the berm.

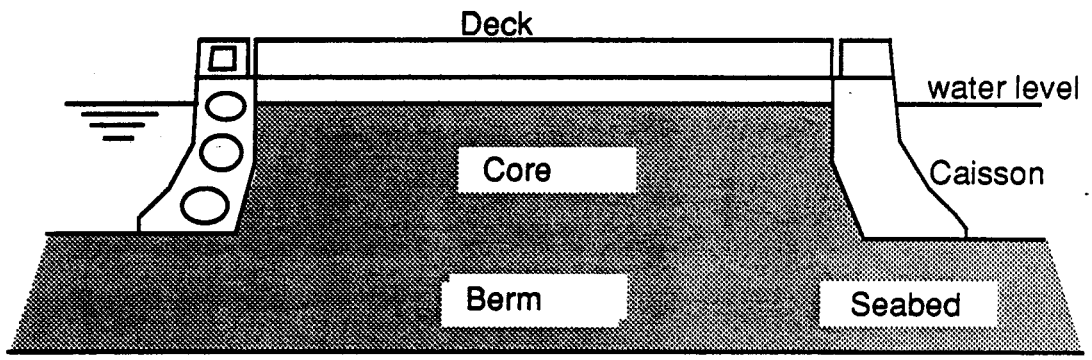

Figure 3.1 Cross Section of MAC

3.4.1 Steel caisson

The structural system of the caisson is similar to that used in naval architecture. The steel structure of the caisson consists of a group of main bulkheads spaced every 2.44 m. An intermediate bulkhead exists between each two successive main bulkheads. The intermediate ones are supported on horizontal girders which in turn are supported by the main bulkheads. The bulkheads support the skin shell of the caisson which consists of a system of closely spaced ribs (or stiffners) to withstand intense local ice pressures. The general arrangement of the different structural elements in the caisson is shown in Fig. 3.2.

3.4.2 Materials

Since the structure operates in temperatures as low as -20^{o}C, special consideration is given to brittle fracture problems in selecting steels. The steels used in the caisson are as follows. Referring to the base of the caisson as elevation 0.0 m, skin plate steel above elevation 19.8 m is type EH36-060. The exterior face shell is type EH36 below elevation 19.8 m. The interior face below elevation 19.8 m and the caisson base consist of type DH36 and CLASS70 steel. All the steels used satisfy the requirements of the American Bureau of Shipping (A.B.S.)

3.4.3 Steel deck

The box girder steel deck carries the topside modules and is simply supported by the caisson in order to avoid buckling problems in the deck under horizontal ice loads. The deck is provided with two north and south drilling

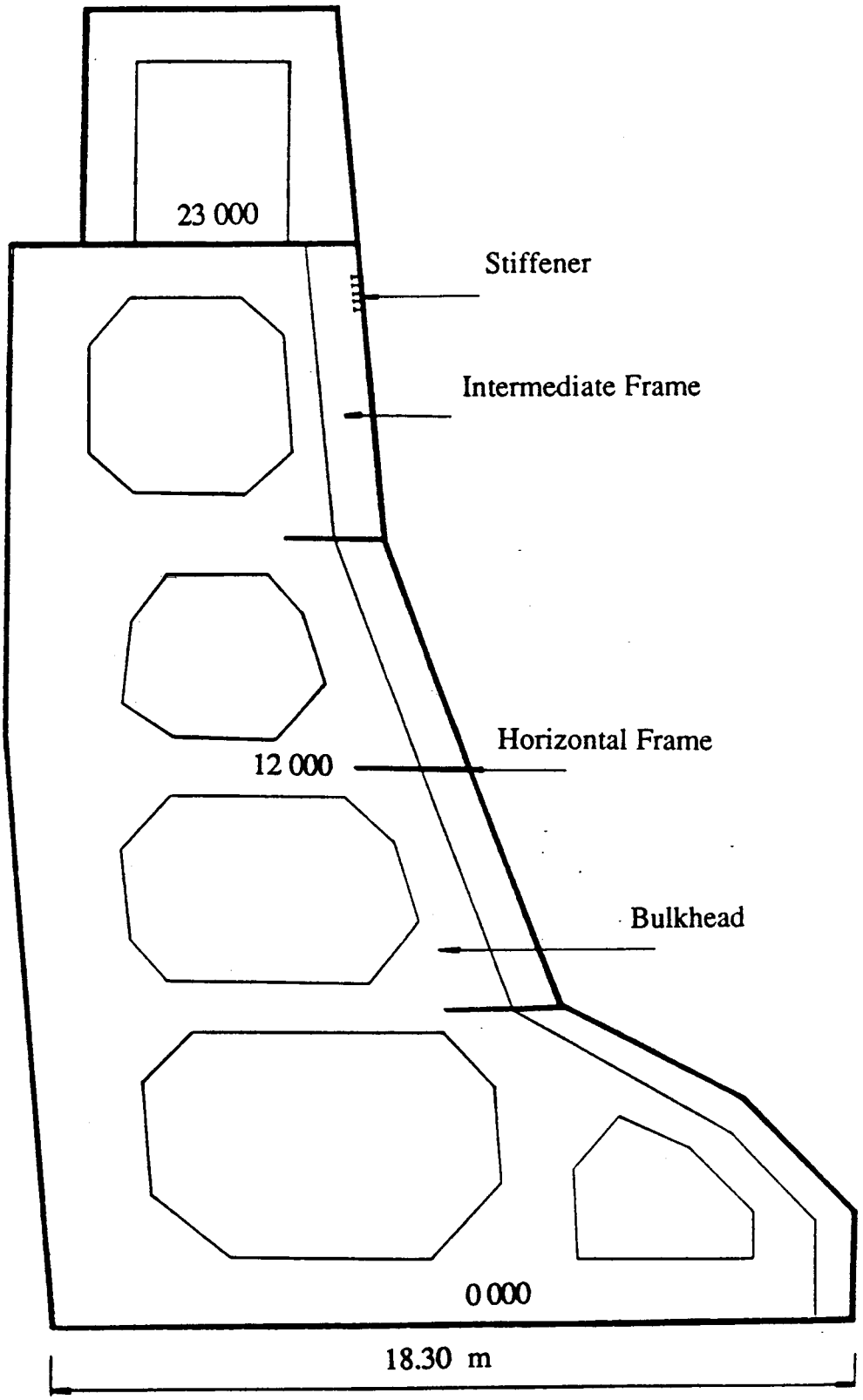

Figure 3.2 Structural Arrangement of The Caisson

openings so that drilling through either of them can be done without moving the caisson. In addition, there are five dredging hatches in the deck for discharging sand in the core area. The total vertical load on the deck including its selfweight is 13,406 metric tonnes.

3.4.4 Sand core and berm

The sand core is the main element by which the structure resists the horizontal loads due to ice. The fill material consists of hydraulically placed uniform fine to medium grained sand. The properties of the sand vary from one site to another. In this study, the MAC site Amauligak I-65 is chosen since the structure encountered its most severe ice loads at that location (Jefferies et al., 1986).

3.5 Finite element representation

In the following sections a detailed description of the finite element model which has been used in this study is given. Two models have been developed, a detailed two dimensional model and a less refined three dimensional one. The three dimensional model is used as a check on the two dimensional model to assure that it adequately represents the global behavior of the structure. In the following, the assumptions on which the two dimensional model is based are discussed.

3.5.1 Quasi plane strain assumption

Since the structure is of significant dimensions (111 by 111m), under a uniform symmetric case of loading like that shown in Fig. 3.3, the behavior of the adjacent panels near the center line will not be considerably different from one

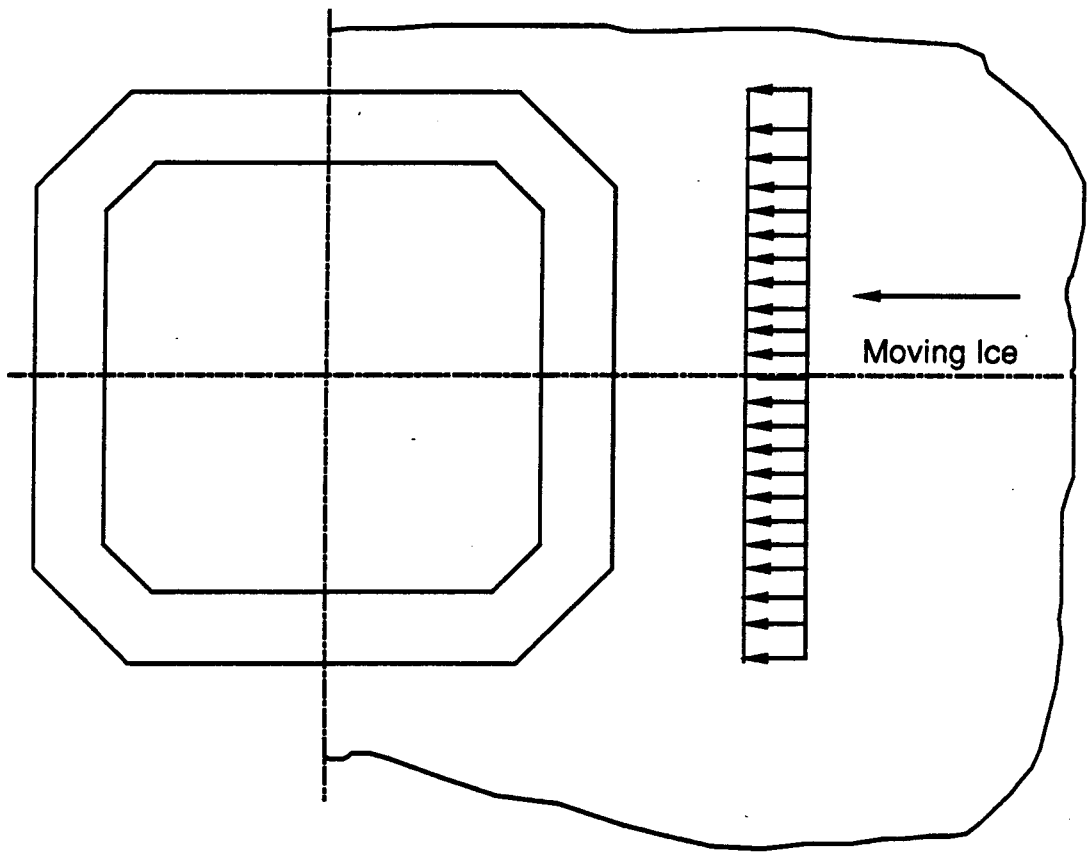

Figure 3.3 A Uniform Case of Loading on MAC

another. The term panel here refers to a segment of the structure that is bounded by two successive bulkheads. In such case, a representative strip of the structure can be modelled using the proper boundary conditions as shown in Fig. 3.4. In this strip, the sand core and berm are under boundary conditions very close to the usual plane strain situations where motion is completely restricted in one direction. The situation is different for the portion of the steel caisson. Because of the large number of adjacent panels, each behaving the same, there can be no lateral displacement at their boundaries. On the other hand, the skin plate spanning the bulkheads can move in the lateral direction. To differentiate this situation from the classical plane strain problem the term quasi-plane strain is used.

Studying a single strip of the structure is quite advantageous since it reduces the problem size significantly and allows the different components to be represented in a reasonable level of detail. However, since the overall configuration of the MAC gives rise to a ring action in the global behavior of the structure, the representative strip must be modified to reflect the actual characteristics of the full caisson. This can be achieved by adding extra springs to connect the front and back sides of the caisson. The method followed in evaluating the stiffnesses of the extra springs is discussed in detail in a subsequent section.

3.5.2 Two dimensional finite element model

The finite element gridwork of the representative strip is called the two dimensional finite element model. The strip is represented in a 3D space and all the nodes on the boundaries are allowed to undergo displacements in two

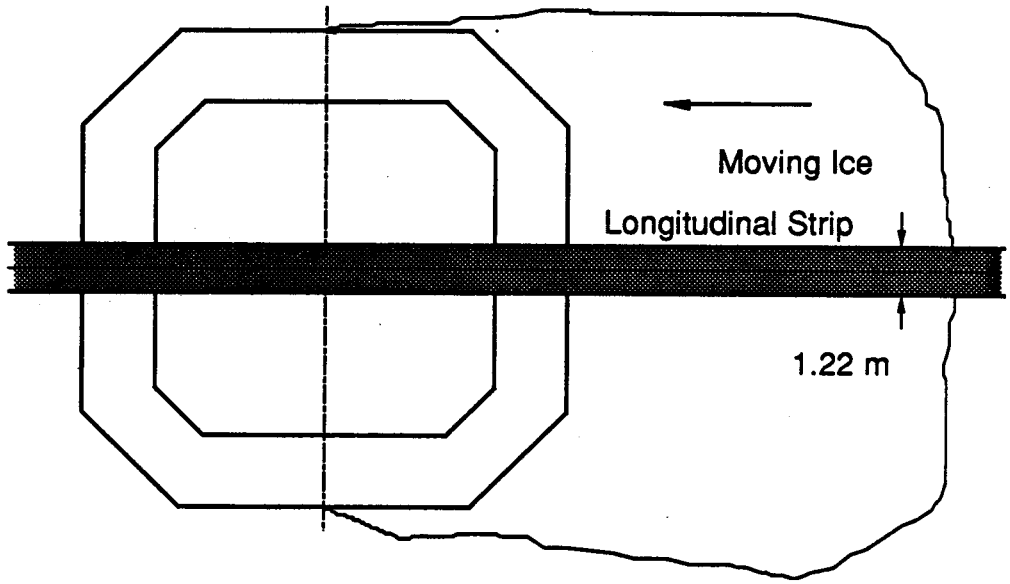

Figure 3.4 Longitudinal Strip of MAC

directions only according to the imposed "quasi-plane strain" condition. Because of that, the gridwork of the strip is named the two dimensional finite element model. Details of the finite element representation of the different components are now given.

Core and berm

In representing the sand core and berm, brick elements with 8 nodes at the corners are used. These elements are bi-linear displacement elements. In total there are 84 elements representing the core and 52 elements for the berm. In order to keep the problem size as small as possible, the berm slopes have been eliminated and the nodes at the edges of the berm have been constrained to move only in the vertical direction. To account for any stress concentrations in the sand, the gridwork has been designed to be relatively finer around the caisson. An elevation view of the finite element representation of the sand core and berm is shown in Fig. 3.5.

Steel caisson

Since a system of closely spaced ribs is used in the skin shell throughout the entire perimeter of the caisson, representing each and every stiffener in the finite element model would result in an extremely large number of degrees of freedom. In order to avoid that, the stiffened plate has been represented in detail only at the areas subjected directly to the ice pressure. Elsewhere, a uniform thickness plate is used in the model instead of the actual one. The thickness of the equivalent uniform plate has to be calculated in such a way that its behavior adequately approximates the actual plate. With the structural arrangement of the caisson, where the stiffened plate is supported on the bulkheads, it is expected that

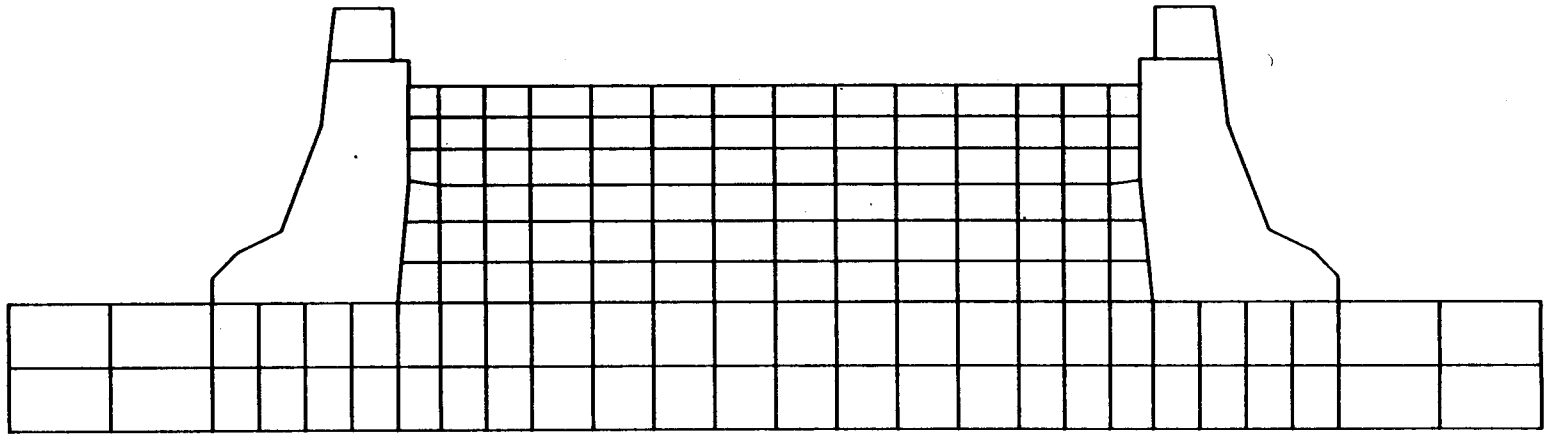

Figure 3.5 An Elevation View of the Finite Element Mesh of the Soil Elements

the plate will carry the load mainly by bending in its shorter span (between the bulkheads). In other words the stiffened plate carries the load in a one-way plate action where most of the load is transmitted to the supports by bending in one direction(the shorter span). On this basis, the thickness of the equivalent uniform plate is calculated so that the two plates have identical bending stiffnesses in the shorter direction.

The effect of this approximation on the behavior of the bulkheads must be considered, since the skin plate works as a flange for them. In order to test the validity of this approximation, and to determine its effects on the behavior of the bulkheads, a special case of loading has been studied. In this loading case, the two dimensional model is loaded as shown in Fig. 3.6 where symmetric loads are applied both horizontally and vertically on the two sides of the structure. In the finite element model, the exterior face shell is represented in an exact manner from elevation 17.4 m to the top of the caisson on the ice side. The uniform thickness approximation is used to represent the corresponding portion of the skin plate on the opposite side. In the test case, comparison is made between the behavior of those two corresponding portions of the skin plate. Table 3.1 shows the results on both sides in terms of displacements at different points. It can be seen from the table that the agreement between the two representations is quite satisfactory.

Shell elements are used to represent the various components of the steel caisson. The bulkheads are represented using bi-linear elements and bi-quadratic elements are used for the horizontal girders and the stiffened plate. Both these elements have five degrees of freedom at each node; three displacements and two out-of-plane rotations as shown in Fig. 3.7 (Ashwell and Gallagher, 1976).

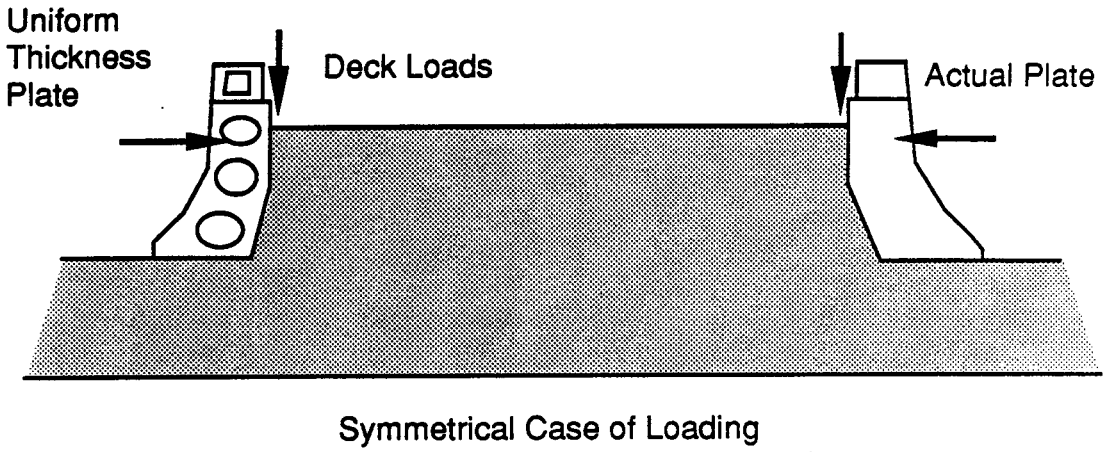

Figure 3.6 Test Case for The Uniform Thickness Plate Assumption

Table 3.1 Comparison Between Actual Stiffened Plate And Uniform Plate

	Actual Plate	Uniform Plate
Displacement at caisson top (mm)	7.05 (vertical) 63.50 (horizontal)	6.96 63.30
Displacement at deck level (mm)	6.62 (vertical) 59.90 (horizontal)	6.50 59.86
Displacement at horizontal load level (mm)	6.10 (vertical) 55.70 (horizontal)	6.02 55.67

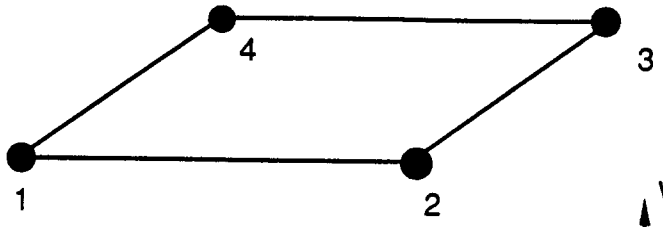

4-Node Element

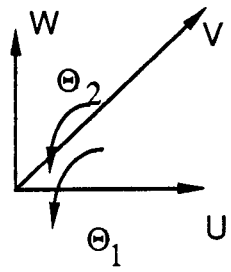

Nodal Degrees of Freedom

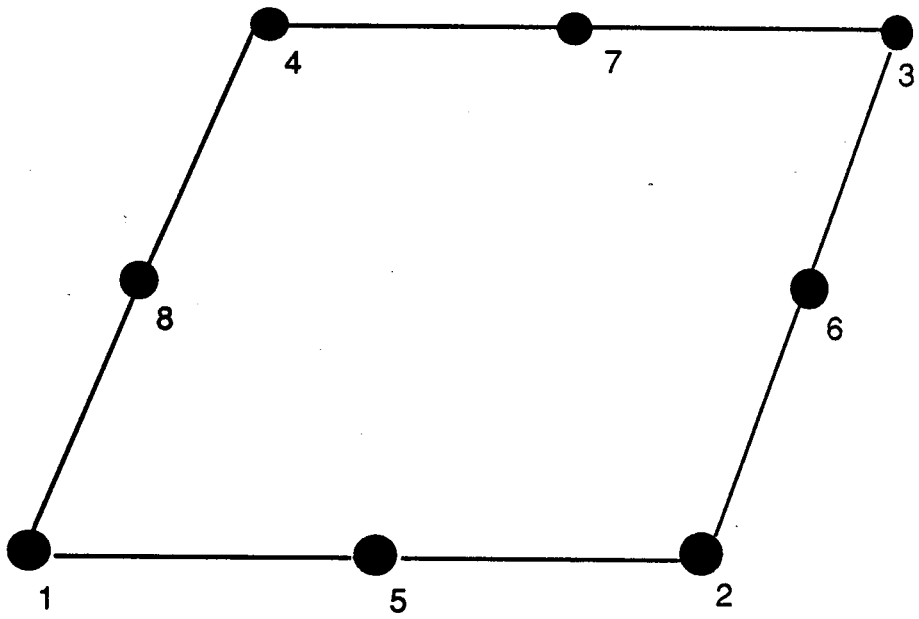

8-Node Element

Figure 3.7 Shell Elements

Details of the finite element gridwork for the caisson are shown in Figs. 3.8 through 3.10.

After validating the use of the equivalent uniform thickness plate as an approximation to the actual stiffened one, the effect of that approximation on the mass matrix must be considered. Since a dynamic analysis is conducted using this finite element model, the actual mass of the strip should be represented in the overall formulation. To achieve that, the steel density for the equivalent uniform plate has been adjusted in order to give the same mass as that of the actual plate.

Steel deck

The deck is not considered an integrated part of the structural system since it is simply supported on the caisson. For this reason, the deck has not been represented as a structural element in the finite element model. However, the loads from the deck on the caisson should be considered and its mass has to be represented in the total formulation. Figure 3.11 shows the vertical loads and lumped masses that represent the effect of the deck. It should be pointed out that these loads and masses correspond to the strip studied and have been calculated assuming uniform distribution of the loads along the inner perimeter of the complete steel caisson.

Soil-Structure interface

Since the structure consists of different structural components (caisson, core, and berm) and since there is no physical bond between these elements, relative motion between them can occur. In fact horizontal sliding of the entire caisson along the berm, is considered a limiting case of failure (Jefferies et al.,

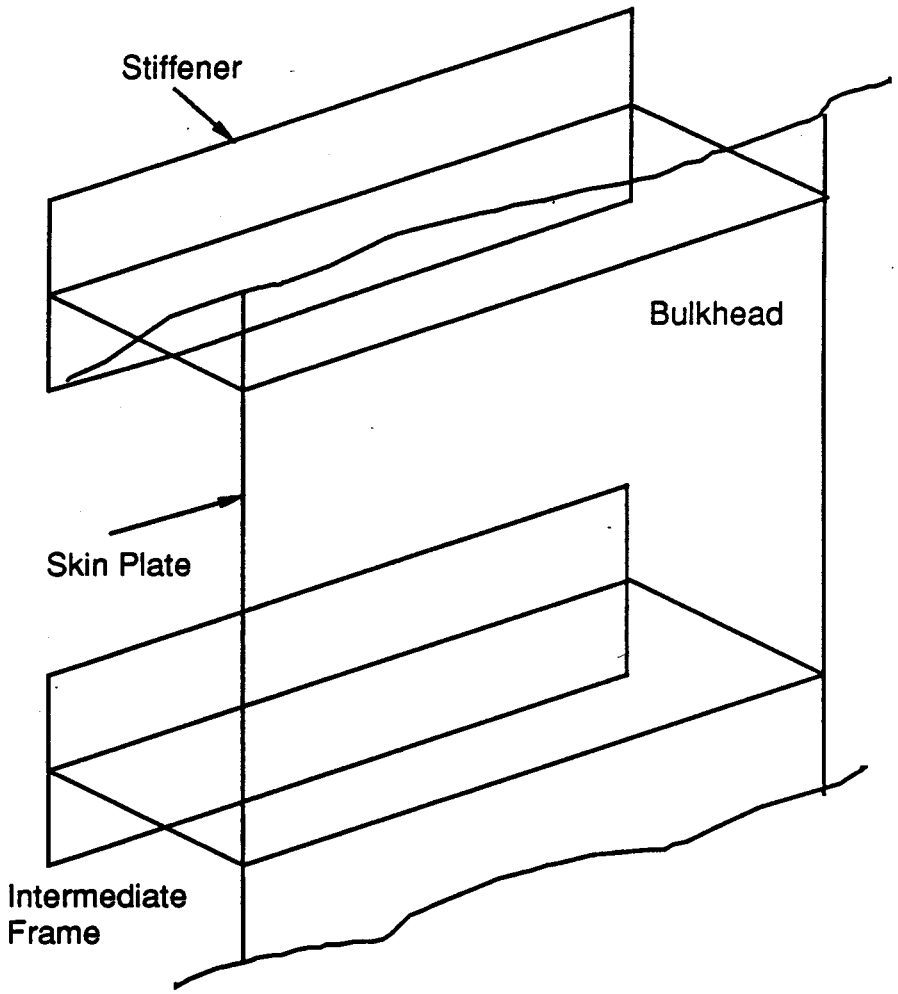

Figure 3.8 Caisson Gridwork - Stiffened Plate

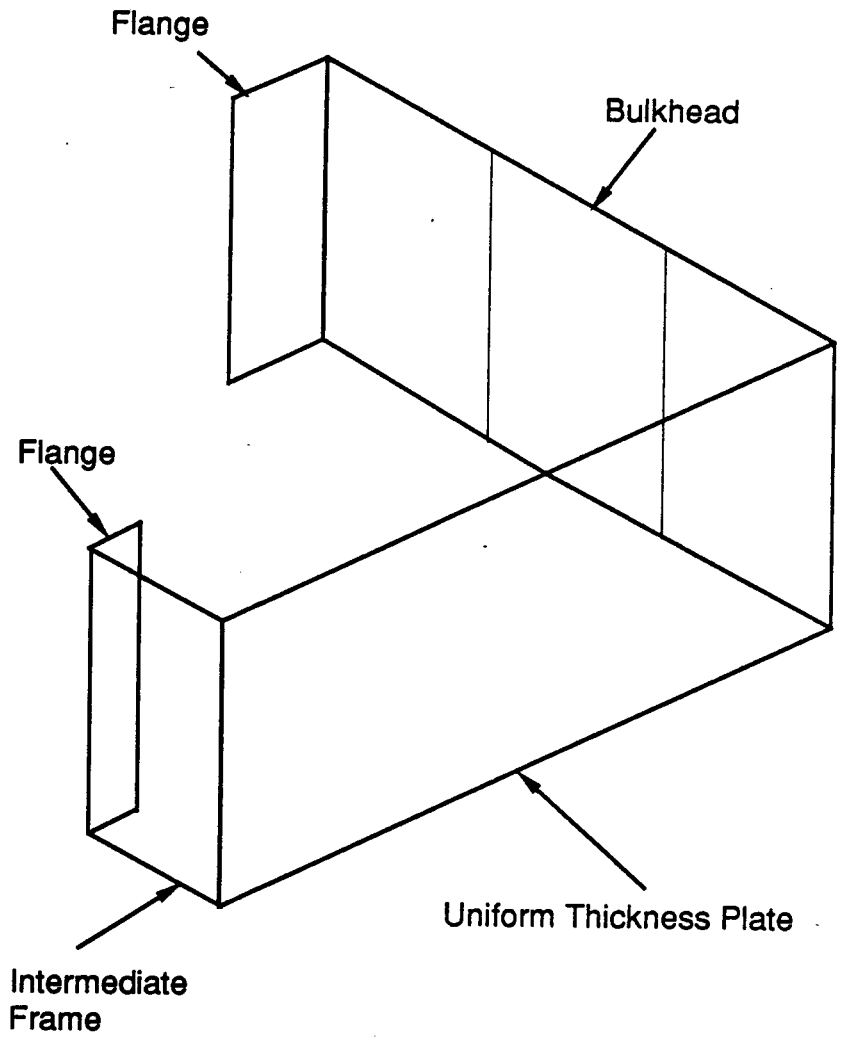

Figure 3.9 Caisson Gridwork - Uniform Thickness Plate

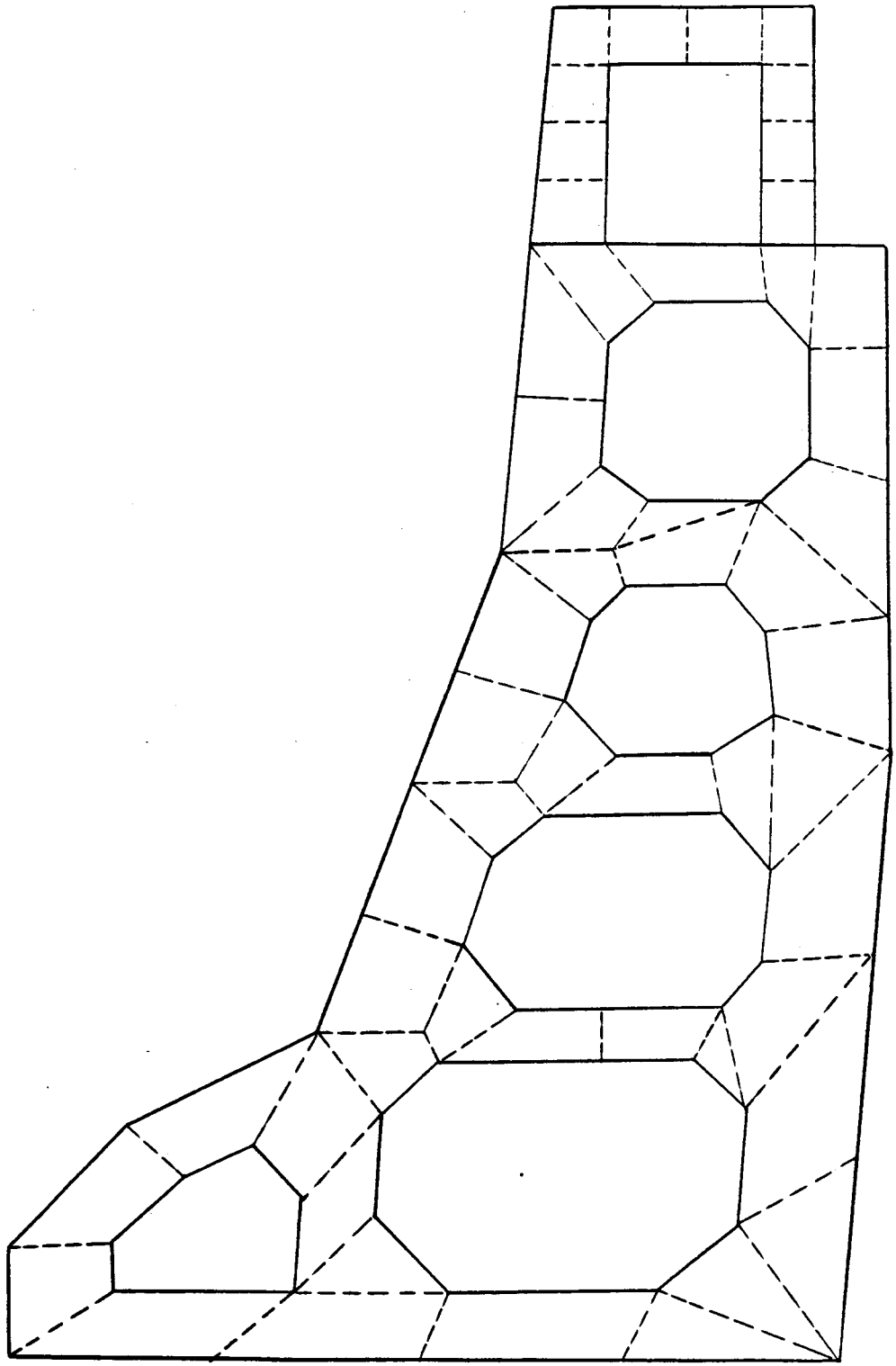

Figure 3.10 Caisson Gridwork - Bulkhead Unloaded Side

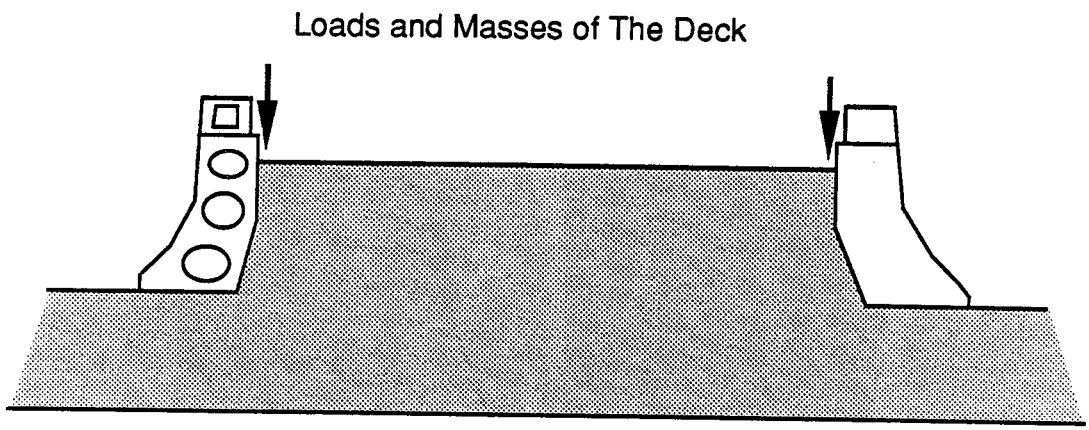

Figure 3.11 Deck Loads and Masses

1985). If this slip was considered in this study, interface elements should be used in order to account for any relative motion between the caisson and the berm. The limiting cases of failure of the structure are not within the scope of this study. Also, the effect of any relative motion between the caisson and the berm is expected to be negligible. This is because of the large difference in the stiffnesses of the steel and the sand elements. In this case, it is expected that the sand will deform according to the deformation of the steel caisson and a complete contact between them will be maintained. Hence, no interface elements are used along the horizontal interfaces (caisson-berm and core-berm). On the other hand, as the main load on the structure is in the horizontal direction, relative motions along the vertical interfaces, if any, are not expected to have significant effect hence, no interface elements are used vertically.

3.5.3 Three dimensional effect in two dimensional model

The actual structure is three dimensional and its overall shape gives rise to a ring action in the global behavior of the structure. The two dimensional finite element model must be able to simulate the overall characteristics of the three dimensional structure. Since a dynamic analysis is carried out in this study, the finite element model has to reflect the global behavior of the actual structure in both a static and dynamic sense. An appropriate test for the two dimensional model is to compare its mode shapes of vibration and the corresponding natural frequencies with those of a three dimensional model of the structure.

Figure 3.12 shows a three dimensional model for the MAC where the following approximations have been used in developing the model:

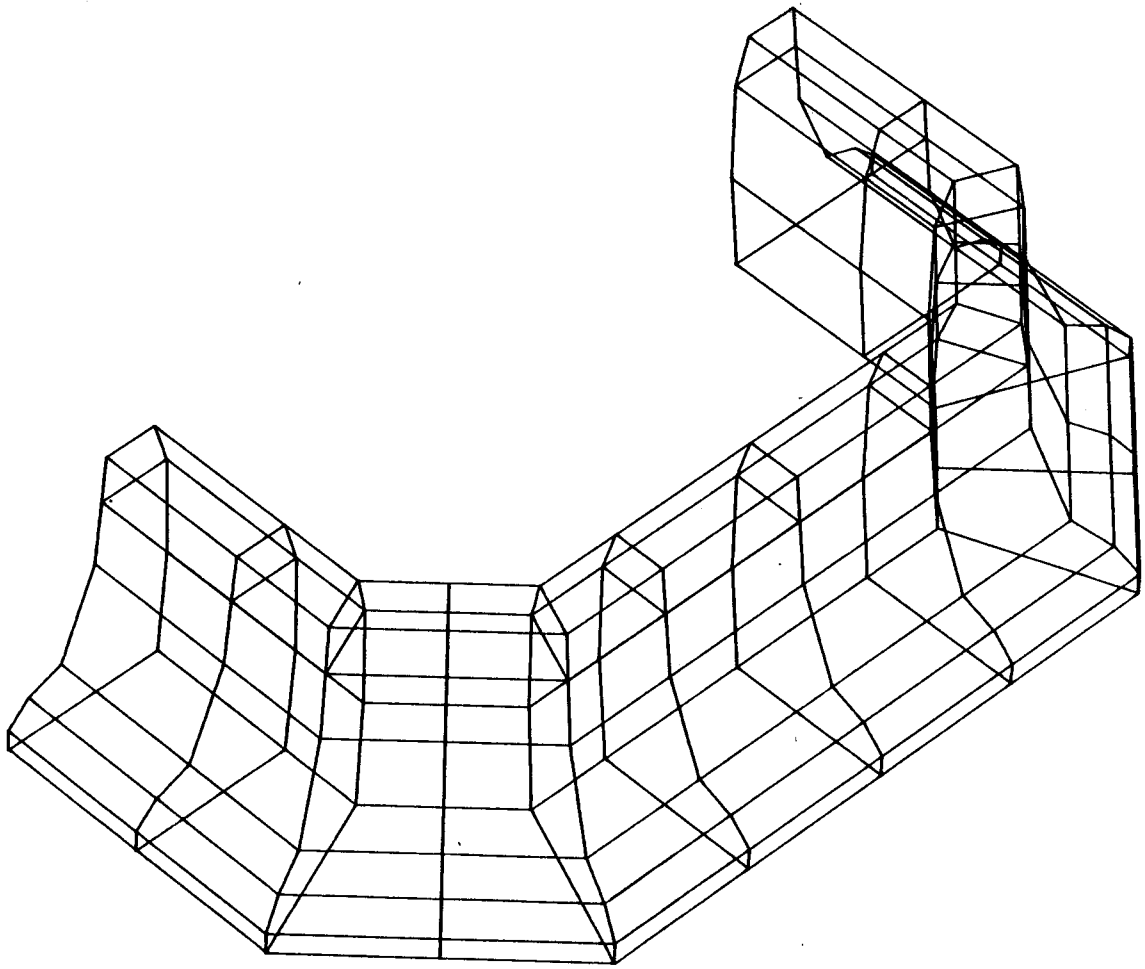

Figure 3.12 Three Dimensional Finite Element Model for MAC

1- Groups of bulkheads have been lumped together to form fewer, more massive bulkheads. In this regard, every five bulkheads in the actual structure are replaced in the 3D model by a single one that has the same mass as the original five bulkheads.

2- The caisson cross section has been modified slightly in order to reduce the number of elements required.

3- The stiffened skin plate has been replaced by a uniform thickness plate that has the same cross sectional area as the stiffened plate.

The first five symmetric natural modes of vibration and the corresponding frequencies are shown in Figs. 3.13 through 3.17. For the sake of clarity, the soil elements are not shown in these figures but they were present in the analysis. In general, the soil motion in the modes of vibration of the 3D model is similar to the corresponding motion in the 2D modes. It is noted that the first two modes involve motions that are mainly in the horizontal direction while the last three modes are mainly vertical.

In order to reflect the ring action of the actual structure in the two dimensional finite element model, some extra springs have been added to the strip as shown in Fig. 3.18. In this figure, the heavy lines that connect the two portions of the caisson represent the extra springs.

Some trials have been made on the 2D model with the extra springs in order to get mode shapes and natural frequencies as close as possible to those of the 3D model. Figs. 3.19 through 3.23 show the first five mode shapes of the 2D model with the extra springs. It is noted that there is a one to one correspondence

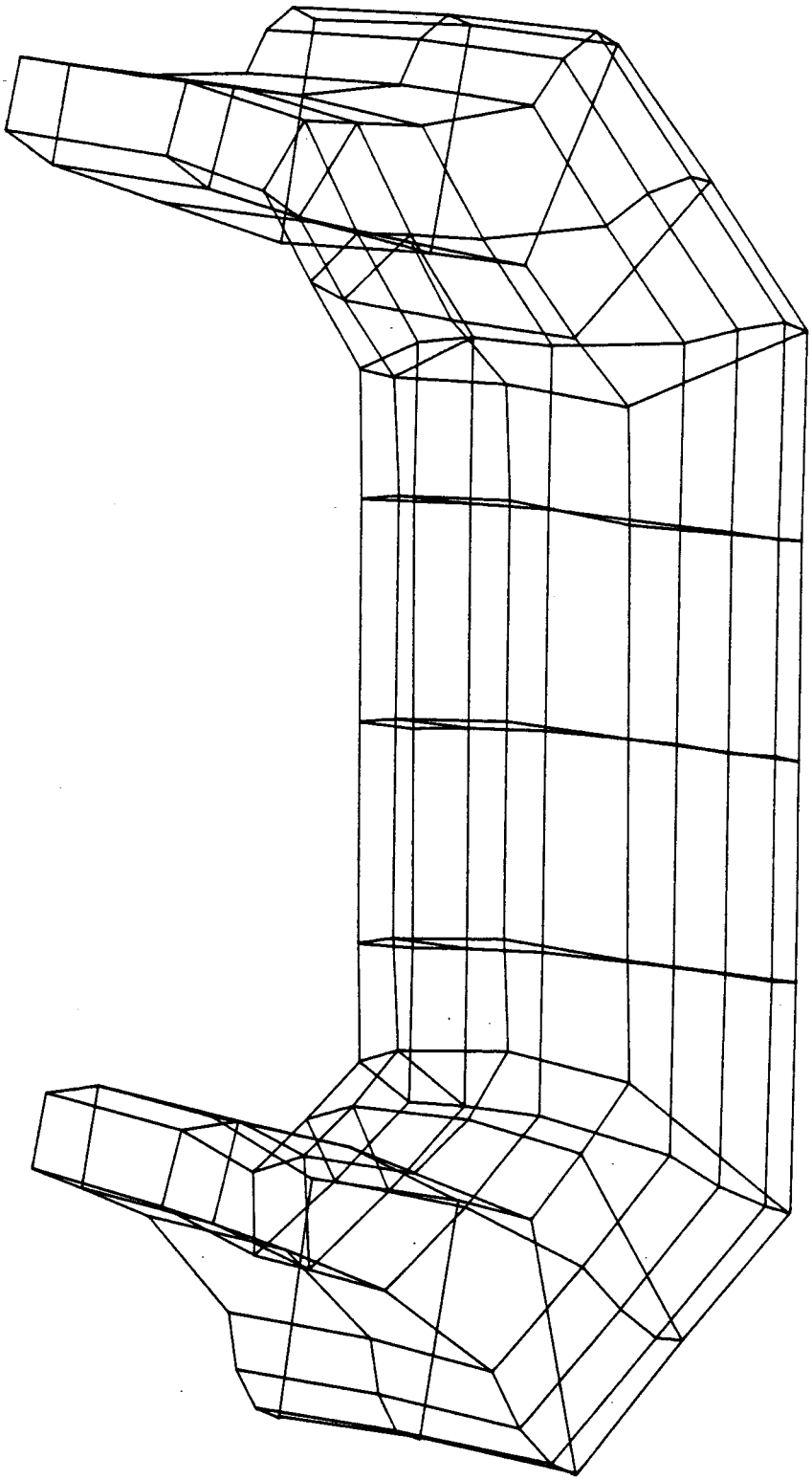

Figure 3.13 First Mode of Vibration - f = 1.60 Hz

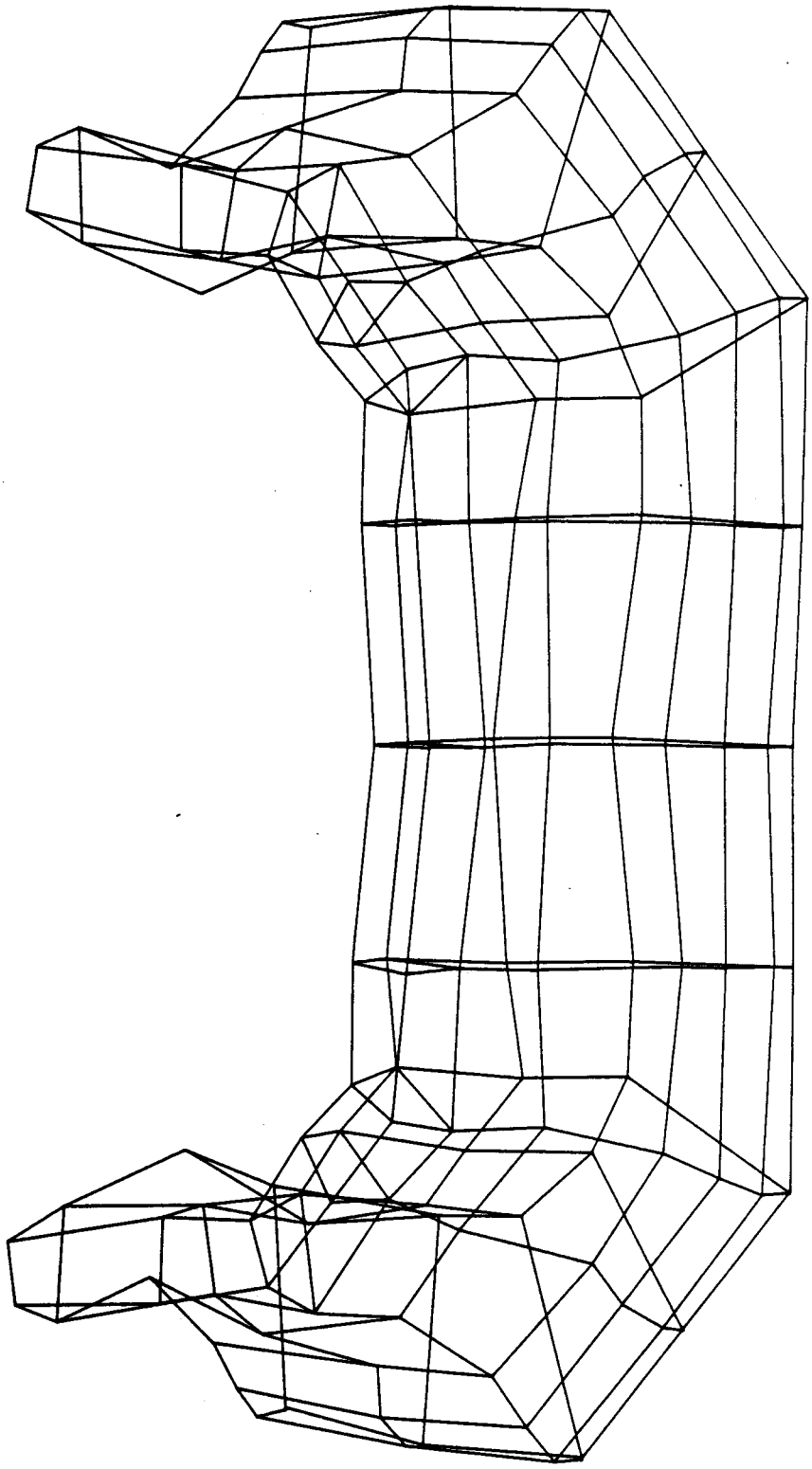

Figure 3.14 Second Mode of Vibration - f = 2.0 Hz

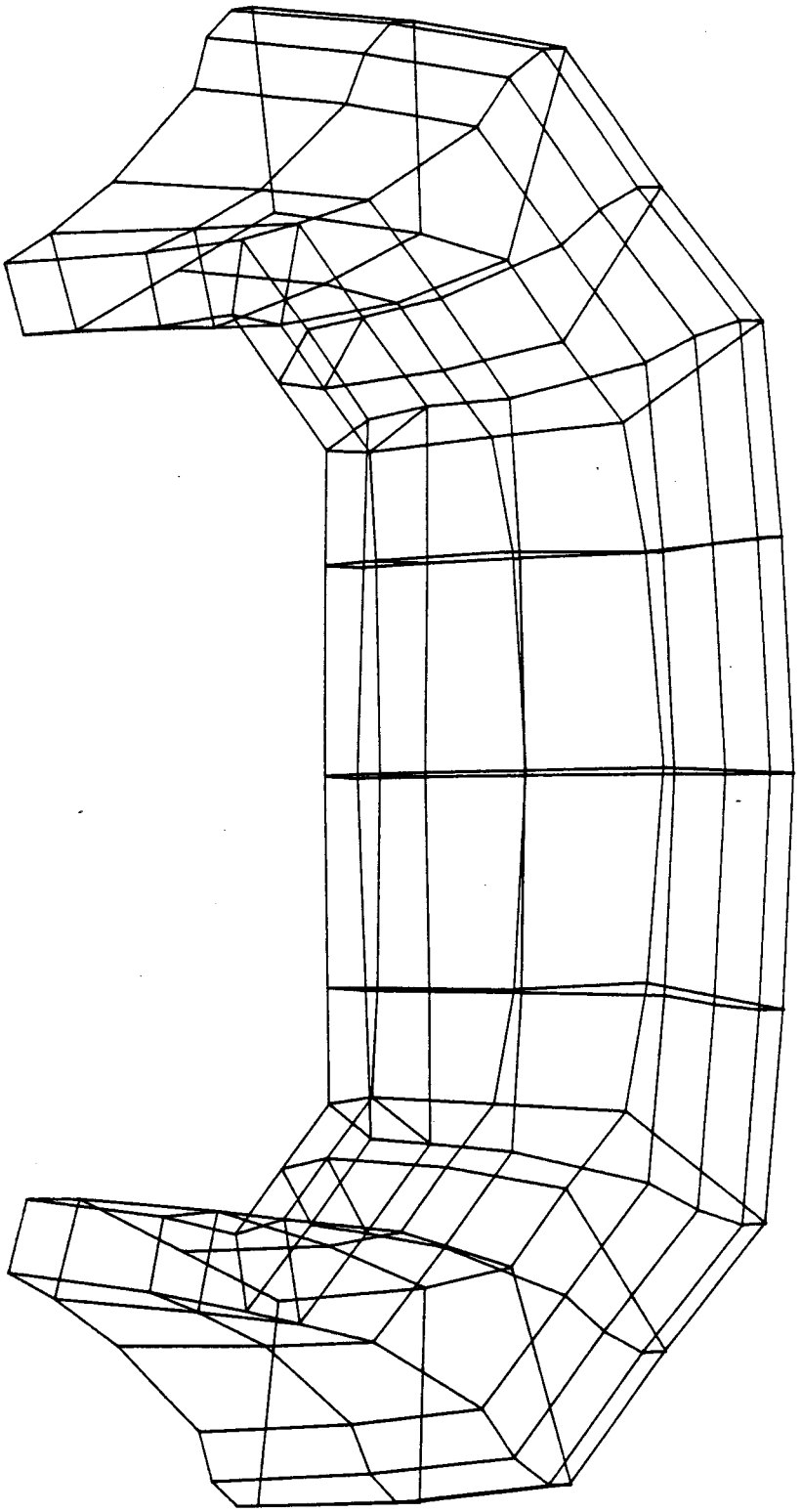

Figure 3.15 Third Mode of Vibration - f = 2.15 Hz

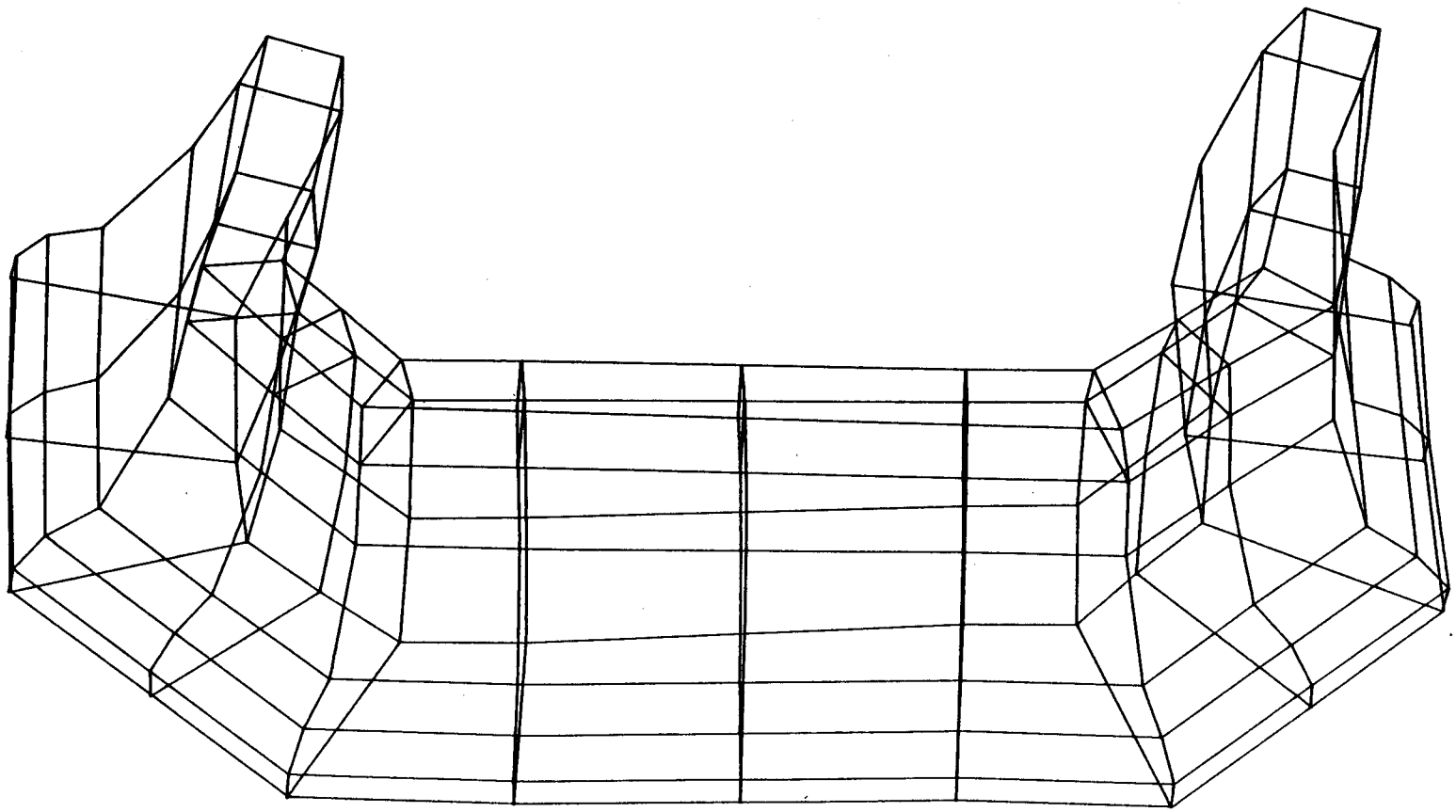

Figure 3.16 Fourth Mode of Vibration - f = 2.20 Hz

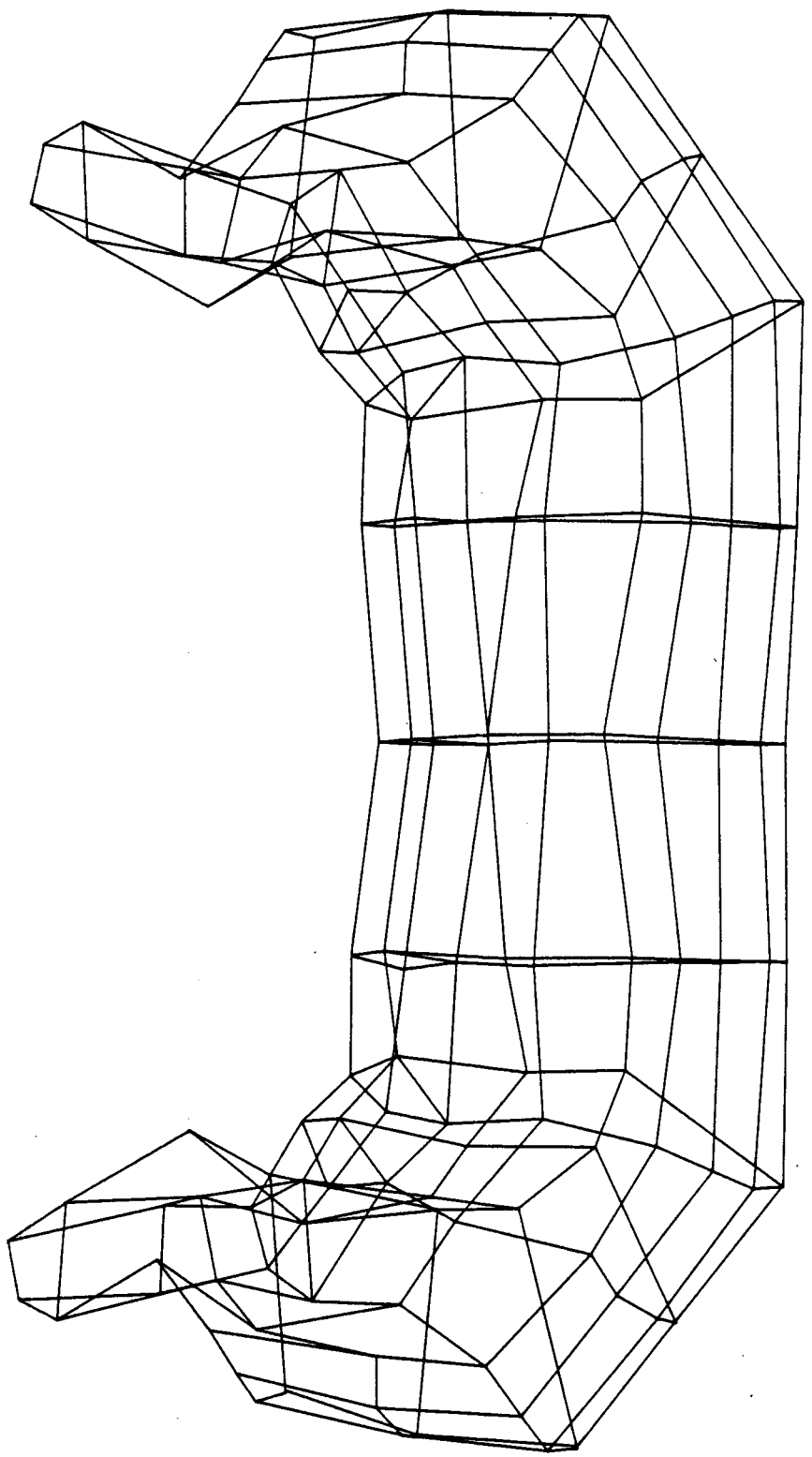

Figure 3.17 Fifth Mode of Vibration - f = 2.30 Hz

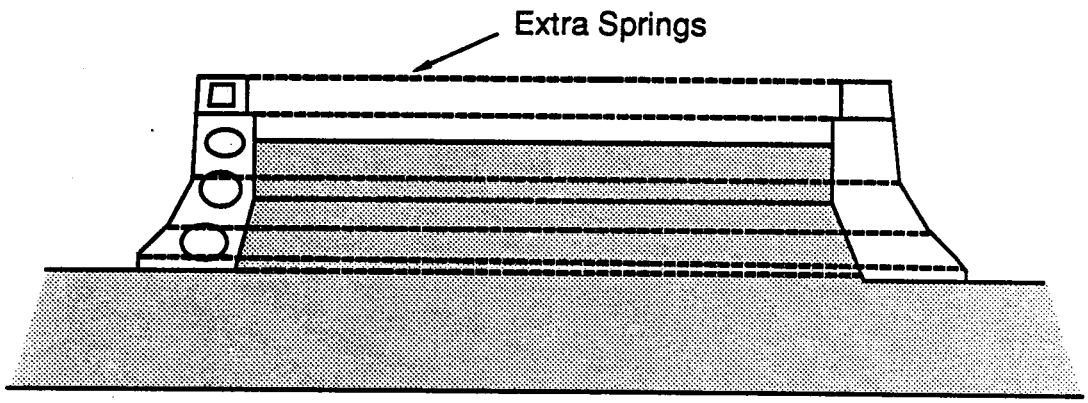

Figure 3.18 Two Dimensional Model with Extra Springs

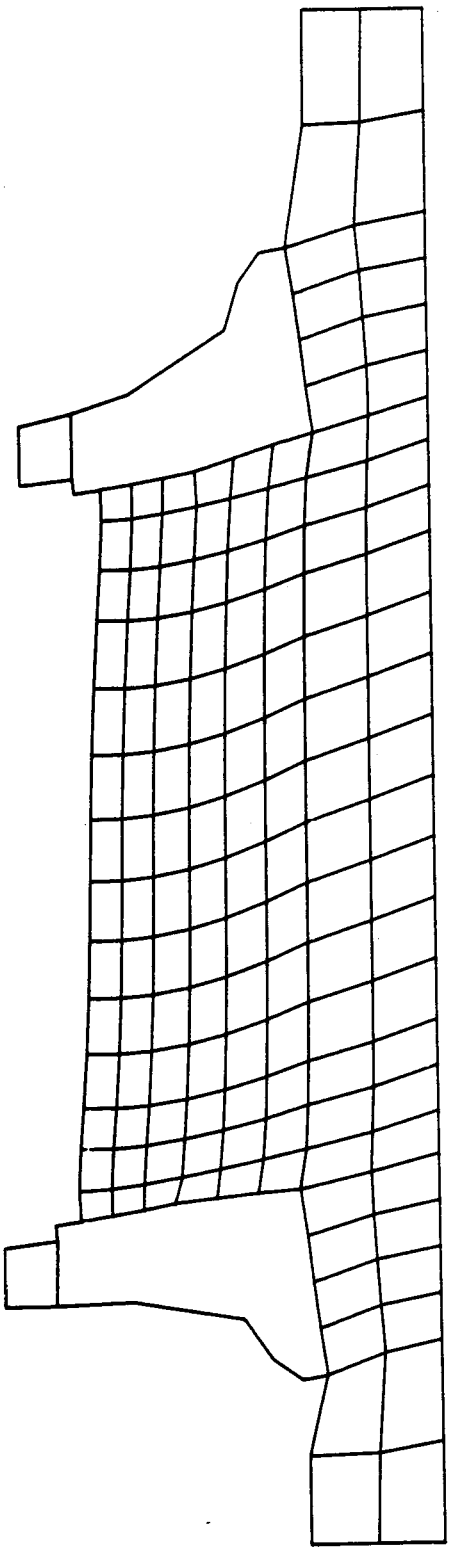

Figure 3.19 First Mode of Vibration - f = 1.40 Hz

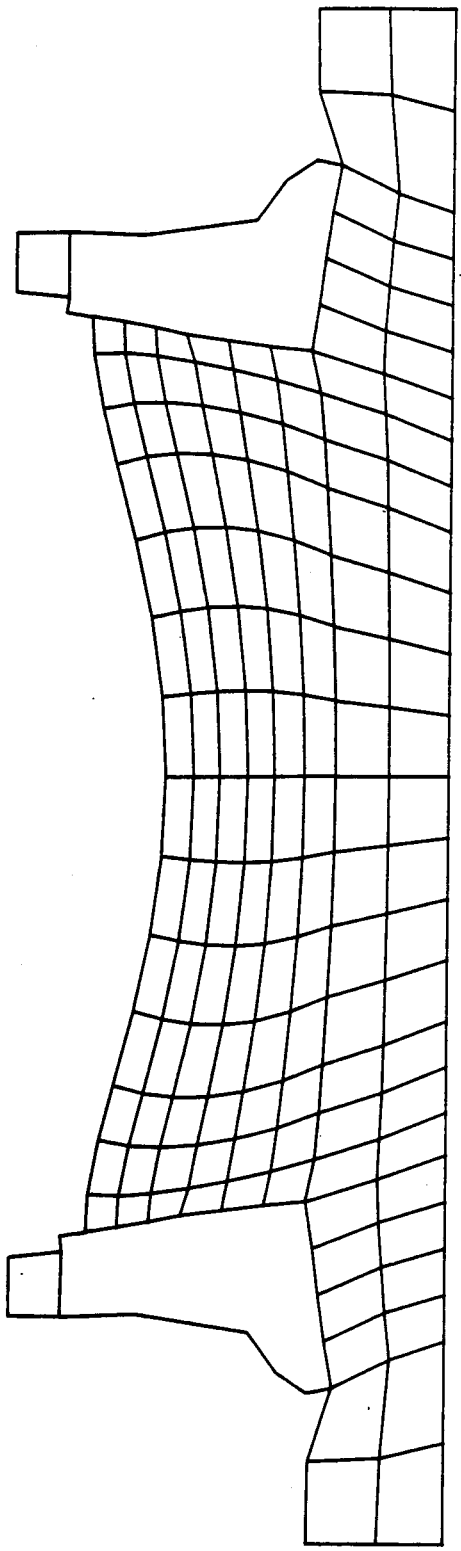

Figure 3.20 Second Mode of Vibration - f = 1.95 Hz

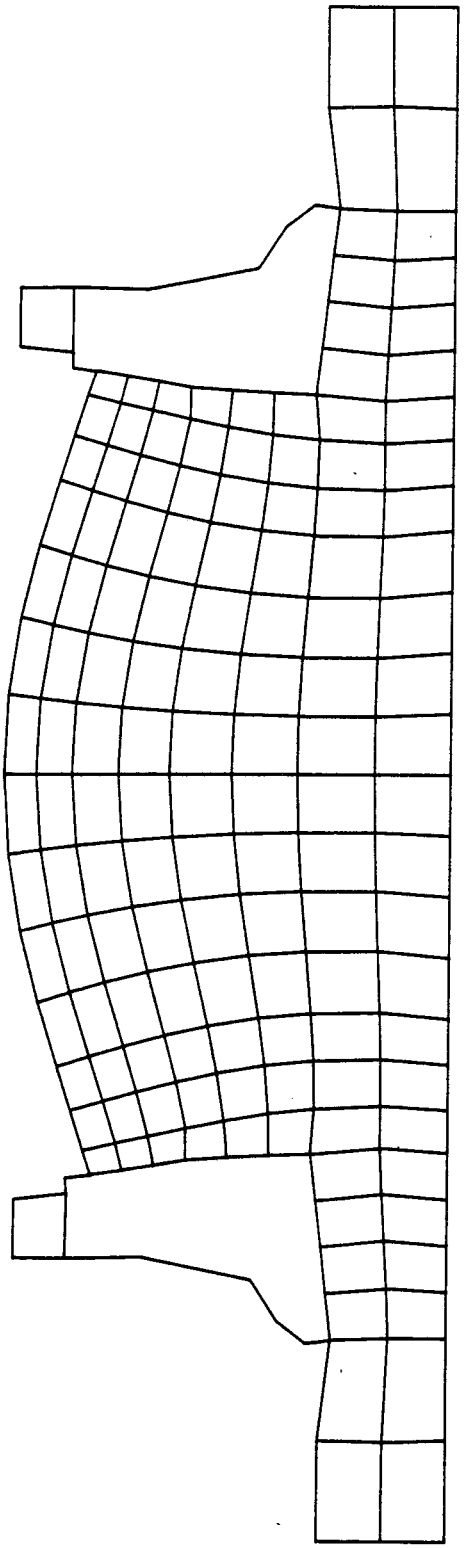

Figure 3.21 Third Mode of Vibration - f = 2.24 Hz

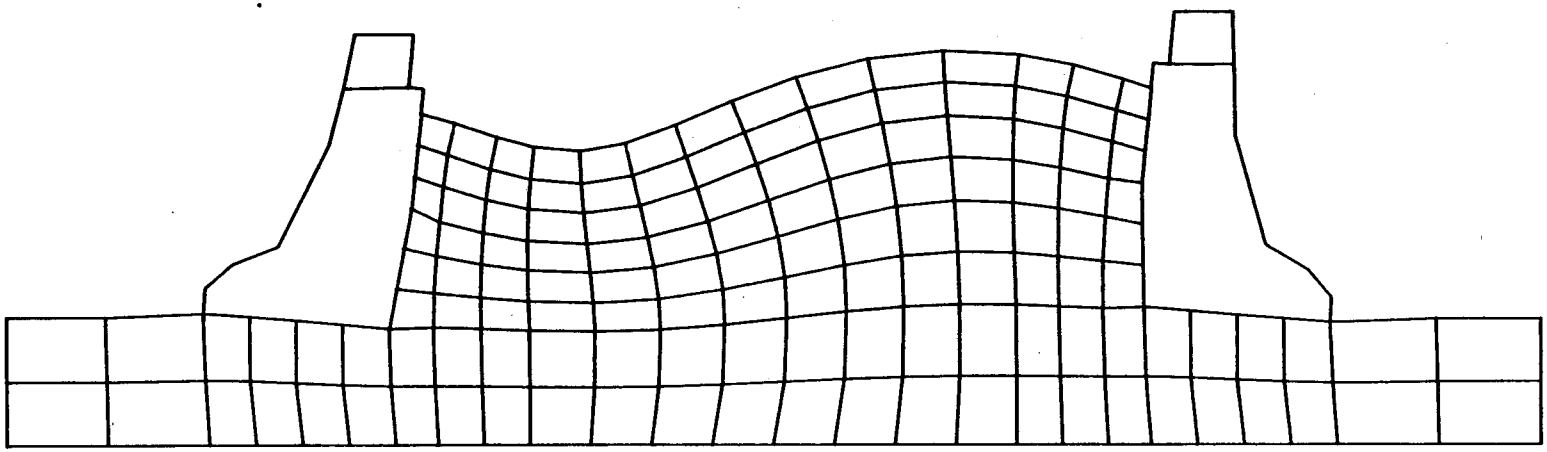

Figure 3.22 Fourth Mode of Vibration - f = 2.34 Hz

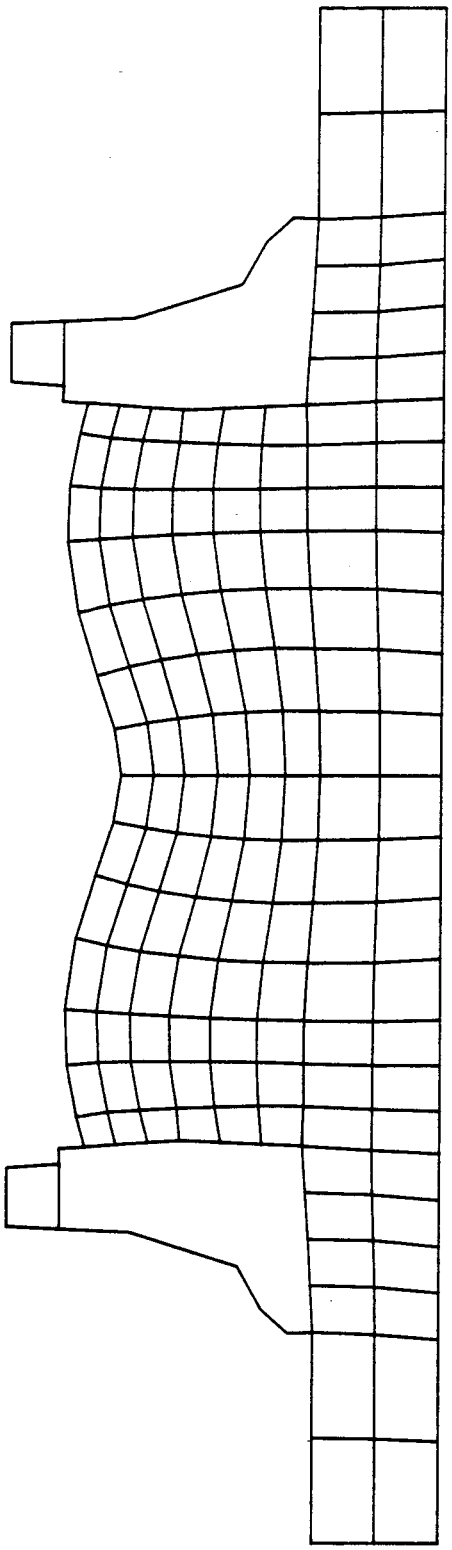

Figure 3.23 Fifth Mode of Vibration - f = 2.76 Hz

between the two sets of modes of vibration of the two finite element models. A comparison between the dynamic characteristics of the two models shows that they are in a good agreement. The stiffnesses of the extra springs used in this model are found to be in agreement with the stiffness of a connecting rod required to simulate the ring action of the caisson in a 2D static analysis (M. Jefferies, personal communications).

4. DIRECT DYNAMIC ANALYSIS

4.1 Introduction

In this chapter dynamic analysis of the model structure is introduced. In this analysis, the finite element model has been studied under the action of a forcing function that was recorded in the field during an ice event. The overall system of the equations of motion is presented first, followed by detailed explanations of the different terms in these equations. The added mass concept is used to take into consideration the effect of the surrounding water, on the response of the structure. To represent the damping effect due to ice, the radiation damping technique, which is used in soil-structure interaction problems, has been adopted. Brief discussions of both the added mass and the radiation damping concepts are given. A complete section is devoted to the forcing function used in the analysis. Finally the predicted response of the structure is presented in terms of accelerations, velocities, and displacements. Normal and shear stresses in different structural elements are also presented.

4.2 Equations of motion

Structural analyses can be divided into two main categories, static and dynamic. The main difference between the two is whether the inertia forces are significant or not. If the inertia forces are significant, a dynamic analysis has to be carried out.

In performing such an analysis, if one represents the structure under consideration as a linear elastic system with viscous damping and discretizes it using say, the finite element technique, then the equations of motion can be written as :

$$[M]\{\ddot{x}\} + [C]\{\dot{x}\} + [K]\{x\} = \{F(t)\} \tag{4.1}$$

where [M], [C], and [K] are the mass, damping and stiffness matrices respectively. The vector {x} contains the nodal degrees of freedom, usually displacements, and a superposed dot indicates time differentiation. The forcing function applied to the structure is represented by the vector {F(t)}. A detailed explanation of the mass, damping, and stiffness matrices used in the present study is given in the following subsections.

4.2.1 Mass matrix

For a massive structure like the MAC, the inertia of all the different components is important and therefore should be considered. That includes the inertia of the caisson, deck, and berm. The inertia of the ballasting water inside the caisson as well as the hydrodynamic effect of the surrounding water should also be included in the analysis.

The mass matrix of a structure like the MAC can be written as:

$$[M] = [M_S] + [M_a] \tag{4.2}$$

where [M] is the total mass matrix of the system, $[M_S]$ is the mass matrix of the structure that includes masses of the different components (caisson with ballasting water, deck, core, and berm) , and $[M_a]$ is the added mass matrix which takes into

consideration the effect of the surrounding water. A brief explanation of the added mass concept is now given.

Added mass

When a partially or fully submerged structure vibrates, its motion is influenced by the surrounding fluid. The inertia forces of the fluid exert hydrodynamic pressures on the structure. Due to this coupling, the dynamic properties of the vibrating structure, for example its natural frequencies, are affected.

To take the effect of the hydrodynamic pressures into consideration, when carrying a dynamic analysis of a submerged structure, two approaches can be followed. The first is to perform a coupled fluid-structure analysis by representing the fluid itself in the gridwork. In such an approach the size of the problem gets bigger due to the additional degrees of freedom that represent the fluid. For a structure like the MAC, the number of degrees of freedom required to represent the structure itself is already very large. Adding fluid degrees of freedom will make the problem worse and therefore using such a technique in this case is impractical.

Another way of taking the hydrodynamic pressures into consideration is to use the added mass concept. In this approach, analysis of the structure can be undertaken by adding the mass of a certain volume of the fluid, to the mass of the structure (Newmark and Rosenblueth, 1971). The determination of the added mass comes from a fluid-structure interaction analysis.

Nilrat (1980) carried out a fluid-structure interaction study both experimentally and analytically in order to determine the hydrodynamic pressures exerted on large volume structures. Large storage tanks used in the offshore oil industry are a typical example of this problem when being used in earthquake areas. The finite element formulation of the problem was made first and after verifying its results experimentally the formulation was used to estimate the suitable coefficients of added mass for different cases. Partially and fully submerged structures with different frequencies vibrating both horizontally and vertically were studied, and the corresponding added mass coefficients were given. One of the conclusions of Nilrat, is that if the water is treated as an incompressible fluid, and the effect of the surface waves is neglected, the added mass coefficient is frequency independent. These two conditions are assumed in the present study.

The total added mass is the product of the added mass coefficient, times the volume of the fluid displaced by the structure, times the density of the fluid. In the present study a coefficient of horizontal added mass of 0.35 is used for the MAC. This is based on the results given by Nilrat. No vertical added mass is considered since the motion of the structure under the ice forces is mainly horizontal.

4.2.2 Damping matrix

Damping characteristics of vibrating systems are function of many parameters such as the damping properties of the materials used, and the existence of physical dampers in the system. Although it is possible to quantify the damping behavior of different materials and structural elements on an individual basis, it

remains a difficult, if not impossible task, to predict the damping characteristics of the assembled structure (Clough and Penzien, 1975).

For steel structures, the damping coefficient is found experimentally to vary between 2 and 10 to 15 percent of the critical damping coefficient, depending on the level of stress in the steel, and the type of connections used (riveted or welded) (Newmark and Hall, 1973). For a structure like the MAC, there is no practical way to determine the damping coefficients experimentally. On the other hand, damping in such a structure is expected to play an important role in determining its response. Damping is also present in the MAC due to sand inside the core and the friction between the different structural components (caisson, core, and berm).

It has been reported (Jefferies and Wright, 1988), on the basis of an analysis of the structural response of the MAC during an ice event, that the damping coefficient of the structure is between 15 and 30 percent of its critical damping. This seems reasonable since sand forms a significant volume of the structure, and damping ratios for sand have been reported by investigators to be as high as 15 percent of the critical damping (Prakash, 1981).

The terms "damping ratio" and "coefficient of critical damping" are based on individual modes of vibration. For multi-degree of freedom structures, there is a coefficient of critical damping and a corresponding damping ratio associated with each vibration mode. In the present study, uncoupling the equations of motion of the structure, through modal analysis, is not possible because of the nonlinearities included as discussed later in the interaction analysis. Therefore, dynamic analysis of the problem must be performed on the coupled

system of equations of motion. Hence, a full damping matrix has to be used in the overall system of equations of motion.

One way of evaluating a full damping matrix is that suggested by Rayleigh, in which the damping matrix is taken as a linear combination of the mass and the stiffness matrices. In equation form, this can be written as

$$[C] = a_0 [M] + a_1 [K]. \tag{4.3}$$

The values of the coefficients a_0 and a_1 can be determined by specifying damping ratios for any two modes of vibration of the structure. In fact, it is possible to construct a full damping matrix that satisfies desired modal damping ratios for any number of free vibration modes of the structure (Clough and Penzien, 1975). The procedure is as follows.

Writing [C] in a more general form as

$$[C] = [M] \Sigma a_b \{ [M]^{-1} [K] \}^b \tag{4.4}$$

where a_b are proportionality coefficients and as many terms as desired, can be included in this equation. The contributions of the n^{th} eigenvector, $\{q_n\}$, in the generalized mass, damping, and stiffness matrices, of any vibrating system can be written as

$$M_n = \{q_n\}^T [M] \{q_n\} \tag{4.5a}$$

$$C_n = \{q_n\}^T [C] \{q_n\} = 2\xi_n \varpi_n M_n \tag{4.5b}$$

$$K_n = \{q_n\}^T [K] \{q_n\} = \varpi_n^2 M_n \tag{4.5c}$$

where ϖ_n is the circular frequency of mode n and ξ_n is the damping ratio of the same mode. If [C] is given by Eq. (4.4), the contributions of any term b to the generalized damping matrix is

$$C_{nb} = \{q_n\}^T \{a_b [M] [[M]^{-1}[K]]^b\} \{q_n\} \tag{4.6}$$

and it can be shown that this expression is equivalent to

$$C_{nb} = a_b \varpi_n^{2b} M_n \tag{4.7}$$

The term C_n can now be written in a general form as

$$C_n = 2\xi_n \varpi_n M_n = \Sigma C_{nb} = \Sigma a_b \varpi_n^{2b} M_n \tag{4.8}$$

from which the damping ratio of the n^{th} mode of free vibration can be written as

$$\xi_n = 1/(2\varpi_n) \; \Sigma a_b \varpi_n^{2b} \tag{4.9}$$

Using Eq. (4.9) for any number of mode shapes results in a system of simultaneous equations in the coefficients a_b. Substituting the values of a_b into Eq. (4.4), the full damping matrix is obtained.

To demonstrate the effect of the mass and stiffness matrices on the damping matrix, when this method is adopted, it is useful to study two limiting cases. When the damping matrix is proportional to the mass matrix only ([C] $=a_0$[M], b=0), the damping ratio is inversely proportional to the frequency of vibration, as seen from Eq. (4.9). This means that the higher modes of vibration are lightly damped and hence, their contribution to the damping matrix is insignificant. On the other hand, if the damping matrix is proportional to the stiffness matrix only ([C]=a_1[K], b=1), the damping ratio is in direct proportion

with the frequency of vibration. In this case the higher modes of vibration have high damping ratios and therefore contribute heavily to the damping matrix.

From the first few modes of vibration of the MAC, as shown in the previous chapter, it is expected that under a horizontal forcing function the response of the structure will depend mainly on the lower vibration modes. The modes of vibration starting from the third, have predominantly vertical motion and therefore they are not expected to play a significant role in the response to ice loads. Although there can be higher modes of vibration that have mainly horizontal motion, there contribution to the response of the structure is negligible. This is due to the big difference between the frequency of these modes and the frequency of the ice loads. Hence, the contribution of the higher modes of vibration in the equations of motion should be minimal since it is expected that they do not participate significantly in the response of the structure. For this reason, the damping matrix is taken to be proportional to the mass matrix only ($[C]=a_0[M]$). The value of the proportionality coefficient a_0 can be determined using Eq. (4.9), taking only one term from the series. Thus Eq. (4.9) degenerates to

$$\xi_n = a_0 \omega_n / 2. \qquad (4.10)$$

Substituting in this equation the values of the circular frequency for any mode of vibration, and the corresponding damping ratio, one obtains a_0. In this analysis, the natural frequency of the first vibration mode of the MAC is used with a damping ratio of 20 percent. This value is chosen as a reasonable one that lies in the range of 15 to 30 percent reported by Jefferies and Wright (1988).

Damping due to ice

In the discussion to this point, no contribution from the ice has been considered in the damping matrix. To the writer's knowledge, no study has been done in order to determine the damping effect due to the presence of ice in ice-structure interaction problems. This section describes how this effect might be considered in a dynamic analysis.

Ice is a highly rate dependent material since it creeps significantly in a short period of time when being subjected to permanent stress (Sinha, 1978). This means that ice is a dissipative material and has its own damping characteristics. This kind of damping is called material damping. To date, there is no widely accepted values for the material damping properties of ice. More experimental work is required in order to provide sufficient data on the damping characteristics of ice.

In dynamic soil-structure interactions, when a structure moves against the adjacent soil, stress waves originate at the contact surface and spread outwards. These waves carry away some of the energy transmitted into the soil by the structure. This loss of energy from the soil-structure system constitutes damping. This kind of damping is called radiation or geomertic damping (Richart et al., 1970).

For the type of ice events considered in this study, the ice floes moving against the structure are of significant dimensions in the order of 10's to 100's of kilometers. Due in part to the large size of the ice floes and the dissipative nature of ice, the net effect is the same as it would be for an infinite floe. In this case,

some of the stress waves which originate at the ice-structure interface are not returned.

By analogy with the soil-structure interaction problem, the radiation damping concept can be used in the dynamic analysis of ice-structure interactions. The ice sheet extends fairly long distances ahead of the structure and all of the energy carried by the stress waves will be dissipated before it is reflected back.

In the present study, the radiation damping concept can also be used at the interface between the berm and the foundation to take into consideration the effect of the infinite extent of the soil underneath the structure. However, this has not been considered, since it is assumed that the foundation is totally rigid and all the nodes at the foundation level are fixed. This implies that all the stress waves will be reflected back at the foundation level.

Gazetas and Dobry (1984) proposed a simple radiation damping model for soil-foundation systems. In this model the radiation damping is represented by a frequency-dependent viscous dashpot whose damping coefficient is given as

$$C_V = \rho V A F, \tag{4.11}$$

where ρ is the soil density, V is the wave velocity, A is the contact area between the soil and the structure, and F is a frequency-dependent factor. Gazetas and Dobry introduced solutions for both axisymmetric and plane strain loading conditions using their model. In the present study, since the structure is very wide so that a representative strip has been considered in the analysis, the wave propagation is one-dimensional. In this case C_V is frequency independent and F is equal to unity.

This completes the formulation of the full damping matrix required in the system of equations of motion. It is noted that the hydrodynamic damping due to the surrounding water has been neglected. This is in accordance with the conclusion of Nilrat (1980) that the hydrodynamic damping is negligible if the water is assumed to be incompressible fluid and no surface wave effect is considered.

4.2.3 Stiffness matrix

The stiffness matrix for the system is formed using standard finite element procedures. It includes contributions from the steel caisson, the sand core, and the berm, in addition to the extra springs required to simulate the ring action of the caisson. The total mesh for the strip contains 2007 structural elements, 136 soil elements, and with over 4000 displacement degrees of freedom.

In the analysis, the steel has been assumed to behave as a linear elastic material. This assumption is made, since no plastification has occurred in the caisson during ice events (M. Jefferies, personal communications). The results of the analysis confirm this.

The sand core and berm form a significant volume of the structure. The sand core is considered the main resisting element to ice loads. Under dynamic loading, there is significant potential for liquefaction of the sand core as a result of vibrations. Liquefaction of the sand depends on several parameters. Material properties of the sand, characteristics of the dynamic loads, and duration of the vibrations are among these. In the analysis of dynamic soil-structure interactions,

constitutive models that represent the mechanical behavior of soils under dynamic loads must be used in order to obtain reasonable results.

Erbatur and Maddock (1985) conducted a comprehensive study on the response of the sand core and berm of the MAC due to horizontal ice loads. In their analysis, they used the modified Cam-clay constitutive model to simulate the sand. The model, developed by Roscoe (1970), is based on work hardening/softening behavior of normally consolidated materials. According to the analysis of Erbature and Maddock, stress concentrations occurred in the sand at the lower inside corner of the steel caisson, as shown schematically in Fig. 4.1. In fact, because of the large dimensions of the sand core (72 by 72 m), it is expected that under a horizontal force on one side of the caisson most of the sand will be free from stress concentartions.

Based on the results of Erbatur and Maddock and since most of the sand is free from stress concentrations, a linear elastic constitutive behavior is used for the sand in this study. Representing the sand as an elastic media in the analysis might not be the best way to reflect the actual behavior of the material. Behavior of soils, in general, under dynamic loads is quite complex. The occurrence of plastic deformation in the sand under dynamic loads is probable. To take that into consideration one has to solve a system of coupled diffusion/deformation equations. Looking at the recorded forcing function, shown in Fig. 4.2, one can see that the ice event continued over 22 minutes. The ice force reached its maximum value after almost 20 minutes from the begining of the event. Since plastic deformations are history dependent and since the maximum response is expected to take place when the ice force reaches its maximum value, one has to solve a system of coupled diffusion/deformation equations under a load history of

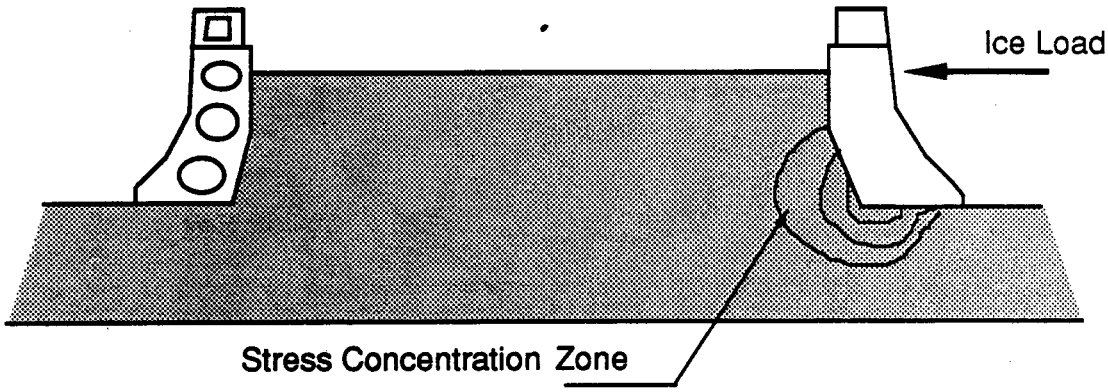

Figure 4.1 Stress Concentrations in The Sand

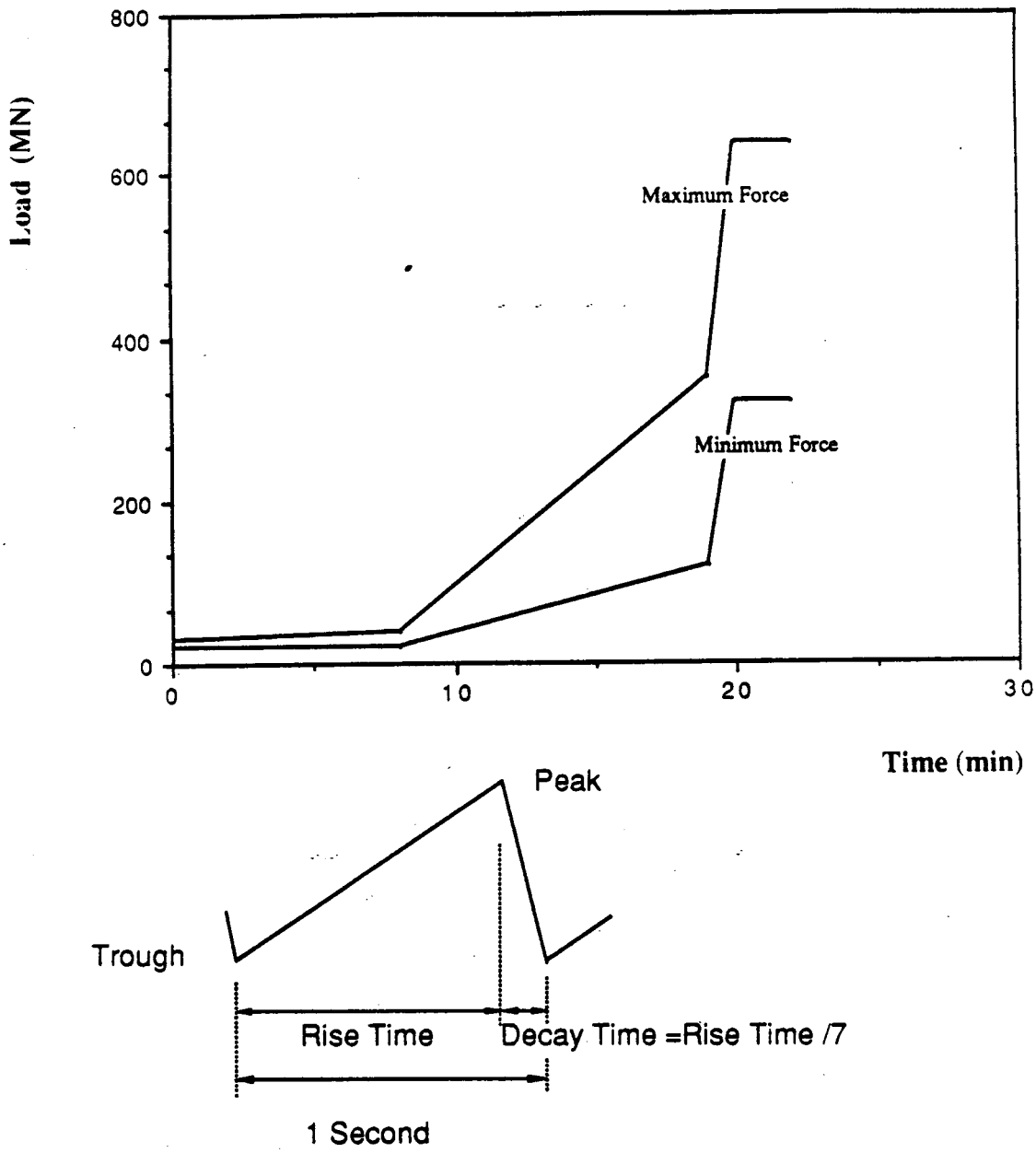

Figure 4.2 Recorded Forcing Function

over 20 minutes. With a problem of large size like the one encountered here, this is a formidable task. In order to avoid that, the sand is assumed to be an elastic media in this study. Although one can vary the elastic properties of the sand as a function of the depth in the core and berm, this is not expected to have a significant effect on the results since the sand contributes in the system mainly by its inertial and damping terms. This assumption is expected to give reasonable results in addition to its attractive feature from a computational point of view. This is an important factor especially with a structure as large as the MAC. The material properties used in this analysis are listed in Table 4.1. The properties of the sand core and berm have been provided by M. Jefferies, personal communications.

4.3 Forcing function

The time history for the ice load used in this analysis is shown in Fig. 4.2. This forcing function is an idealized load history based on the field measurements during an ice event. That event happened on April 12, 1986, when a multi-year ice floe was continuously crushed against the side of the MAC. The ice velocity was about 0.06 m/s and the floe thickness was about 9.0 m. During that event, the maximum recorded ice force was comparable to the design load of the structure and the acceleration response was in excess of 11 percent of the gravitational acceleration (Jefferies and Wright, 1988).

To find out the load that corresponds to the strip analyzed here, the total load is assumed to be distributed across the width of the structure as shown in Fig. 4.3. In this distribution the force intensity is assumed to decrease linearly from its maximum value to zero at both ends in order to take the effect of the sloping

Table 4.1 Material Properties

	Material	Young's Modulus MPa	Poisson's Ratio	Yield Stress MPa
Steel	EH36-060	200×10^3	0.3	353.0
	EH36	200×10^3	0.3	353.0
	DH36	200×10^3	0.3	353.0
	CLASS70	200×10^3	0.3	686.0
Sand	CORE	94.0	0.18	-----
	BERM	171.0	0.40	-----

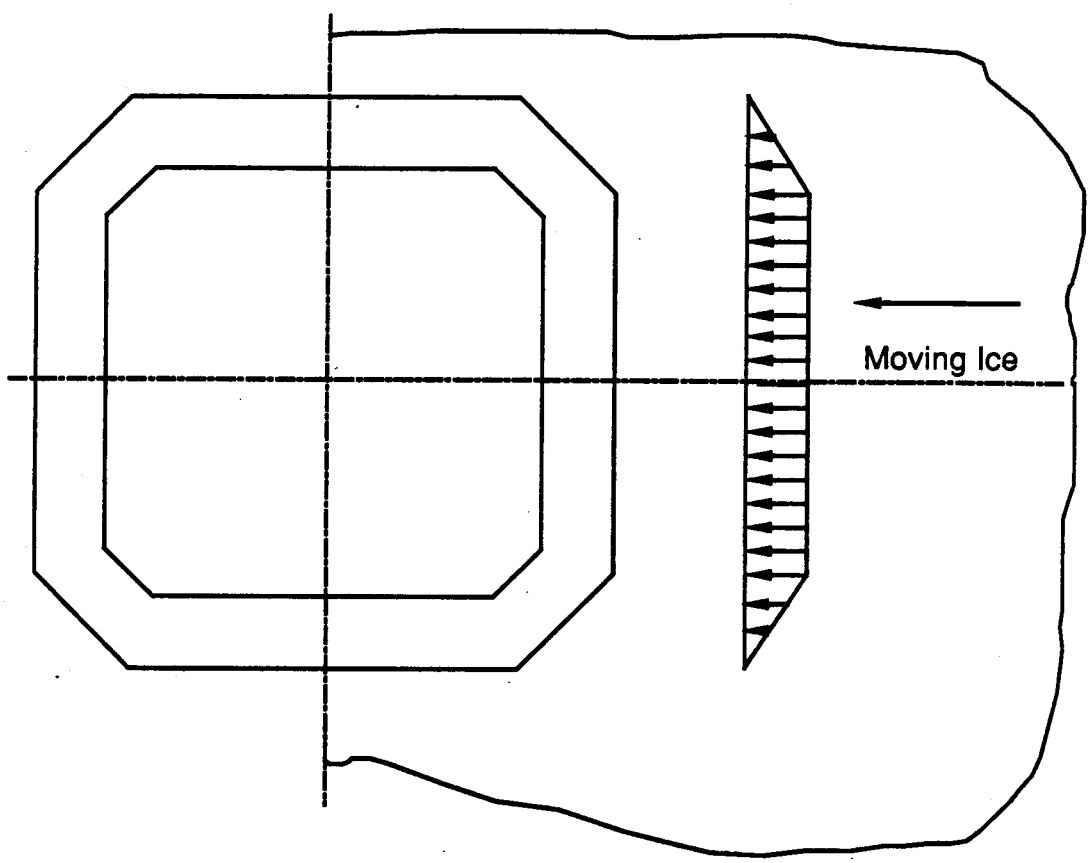

Figure 4.3 Force Distribution Across The Structure

corners of the caisson into consideration. The loading steps followed in the analysis are discussed in the following section.

4.4 Loading sequence

4.4.1 Static loading

A static loading step should be carried out at the beginning in order to provide the initial conditions (displacements) for the dynamic analysis. In this step the model is subjected to static forces that represent the vertical loads from the deck in addition to the body forces.

4.4.2 Transition loading

The ice forcing function varies as shown in Fig. 4.2, where both the peak and trough increase gradually from one load cycle to the next. Finally, when the ice floe completely envelopes the structure, the load cycle becomes steady (periodic with constant amplitude). Under such a forcing function one would expect a steady-state condition to be reached. However, to perform an analysis over the duration of the entire event, more than 20 minutes, would be very expensive computationally. In addition, the peak loads and response are expected to occur in the steady-state range, and so it is that part of the response that is of most interest.

In an attempt to generate a steady-state response of the structure as quickly as possible, a transition load function has been used. This forcing function consists of a static load plus a modified dynamic load history. The static load is a horizontal force that has a value equal to the average of the dynamic load

($F_{max}+F_{min}$ /2). Starting from the results under the horizontal static load, the dynamic analysis is conducted using the transient dynamic load shown in Fig. 4.4.

In developing this transient dynamic load history, the main parameter that has been varied is the unloading time. It is noted that in the recorded load history, the unloading time is much smaller than the loading time. The main reason for this is that the ice fails in a brittle manner. It is expected that due to the very short unloading time, the transient response of the structure can take a long time to reach the steady-state condition. In order to shorten the duration of the transient response, the unloading time is decreased gradually in the transient load history from one load cycle to the next.

4.4.3 Steady-state loading

The last load cycle in the transition load history is the same as the load cycle for the steady-state phase of the ice forcing function. From that point on, the structure is subjected to the same load cycle until the response of the structure repeats itself in consecutive cycles. The loading sequence discussed above is shown in Fig. 4.5.

The solution of the equations of motion is done using the Newmark-β time integration scheme (Newmark, 1959). This is an implicit time integration technique in which it is assumed that,

$$\dot{x}_{t+\Delta t}= \dot{x}_t +[(1-\delta)\, \ddot{x}_t +\delta\, \ddot{x}_{t+\Delta t}\,]\Delta t, \text{ and}$$

$$x_{t+\Delta t}= x_t +\dot{x}_t\Delta t + [(0.5-A)\, \ddot{x}_t +A\ddot{x}_{t+\Delta t}]\Delta t^2$$

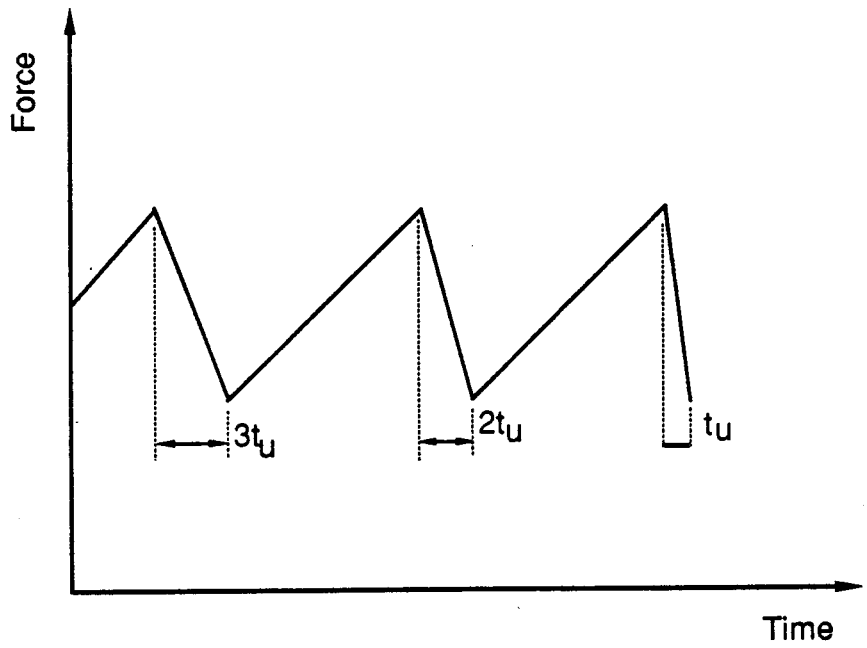

t_u is the unloading time during the steady state condition

Figure 4.4 Transient Load History

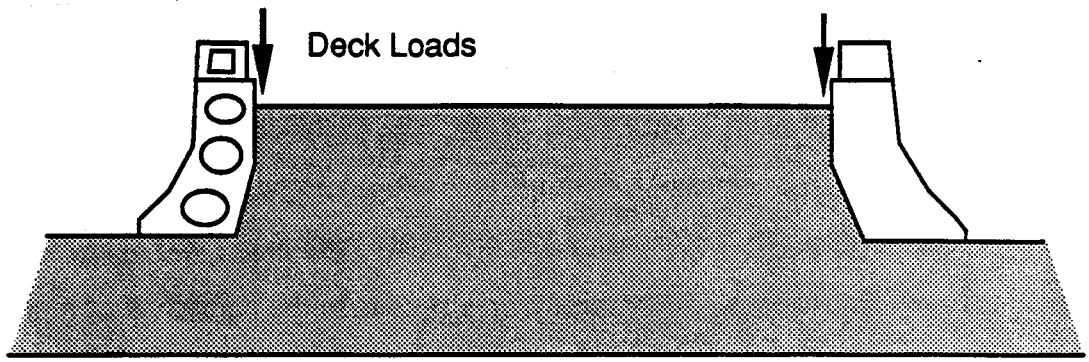

Step 1, Static Vertical Loads

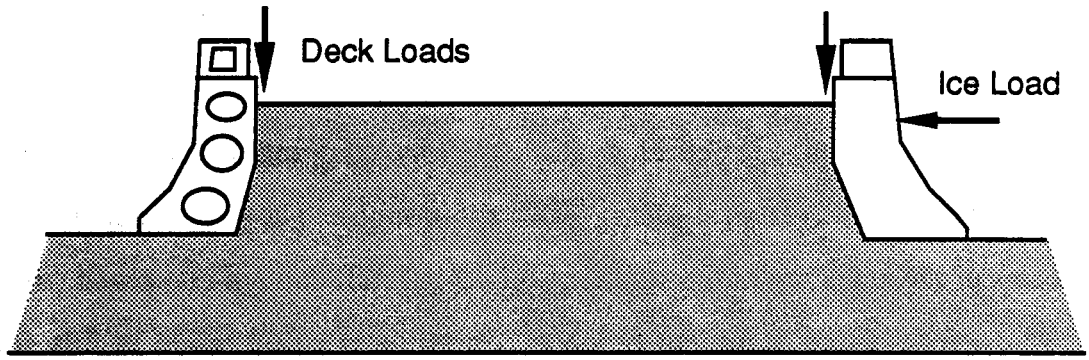

Step 2, Transient Dynamic Load

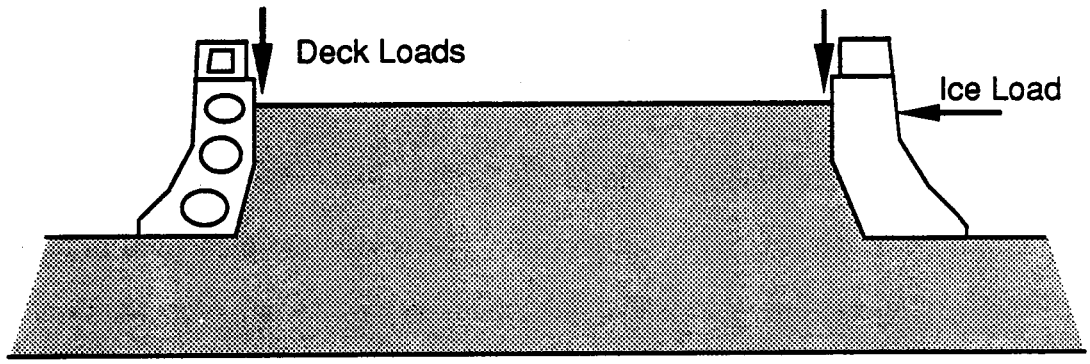

Step 3, Steady-State Dynamic Load

Figure 4.5 Loading Sequence on MAC

where the subscripts t and $t+\Delta t$ refer to the response at time t and $t+\Delta t$ respectively. The parameters δ and A can be chosen to control the stability and accuracy of the solution. Newmark proposed, as an unconditionally stable scheme, the constant average acceleration method in which case $\delta=0.5$ and $A=0.25$. Using these two expressions one can write both $\dot{x}_{t+\Delta t}$ and $\ddot{x}_{t+\Delta t}$ in terms of $x_{t+\Delta t}$ only. Substituting the resulting expressions in the equations of motion at time $t+\Delta t$, the displacement response can be obtained. From the expressions of $\dot{x}_{t+\Delta t}$ and $\ddot{x}_{t+\Delta t}$ in terms of the displacements at time $t+\Delta t$, the velocities and accelerations can be calculated.

The dynamic analysis has been undertaken using a time increment of 1/16 of a second. This value is chosen to allow the time stepping process to match the forcing function at its critical points (peak and trough). The value is also suitable in terms of the accuracy of the solution since it is small enough compared with the natural period of the dominant mode of vibration, the first mode in this study (Clough and Penzien, 1975). Also this value of the time increment is found to be reasonable from computing costs point of view. The response of the structure as predicted by the dynamic analysis is shown in the next section.

4.5 Predicted response of the structure

The dynamic response due to the horizontal ice force during the steady-state condition is discussed in this section. The results are presented in terms of the kinematic quantities, that is displacements, velocities, and accelerations. As well, the normalized normal and shear stresses, (σ/σ_y) and (τ/τ_y), in different structural elements are given during a typical cycle. In the analysis, the steady-state condition occurred after about 6 to 7 seconds from the initial loading. In all

the figures that represent the predicted response of the structure, only the steady-state portion is shown. For the sake of convenience the start of the steady-state response is taken to be t=0.

Displacement response

The displacements at the top of the steel caisson on both the loaded side and the unloaded side are shown in Figs. 4.6 and 4.7 respectively. It is noted that the vertical scales are different in the two figures. Comparing the values of the displacements on the two sides, one can see that the displacements on the unloaded side are much smaller than those on the loaded side. This means that the unloaded side of the structure feels very little effect of the ice loads. Jefferies et al. (1985) indicated that the load paths for the ice load are through the friction between the caisson and the berm (about 10 percent) and the rest (about 90 percent) goes to the foundation by the sand core. In fact, it is expected that most of the 10 percent that takes the friction path, will be transmitted by the caisson on the loaded side. That explains why the response on the unloaded side of the caisson is much smaller than that on the loaded side. An interesting point here is that although the ice force drops to half of its maximum value, the range within which the structure moves is only a few millimeters. Only 20 percent of the maximum displacement is recovered upon unloading. The reason is that the time between the start of unloading and the next loading is very short, hence, there is little chance for the structure to recover much of the displacement from the maximum ice load.

Figure 4.6 shows that the displacement response on the loaded side has the same pattern as the forcing function, however, due to the existence of damping in the system there is a phase shift between the load and the response. This shift is

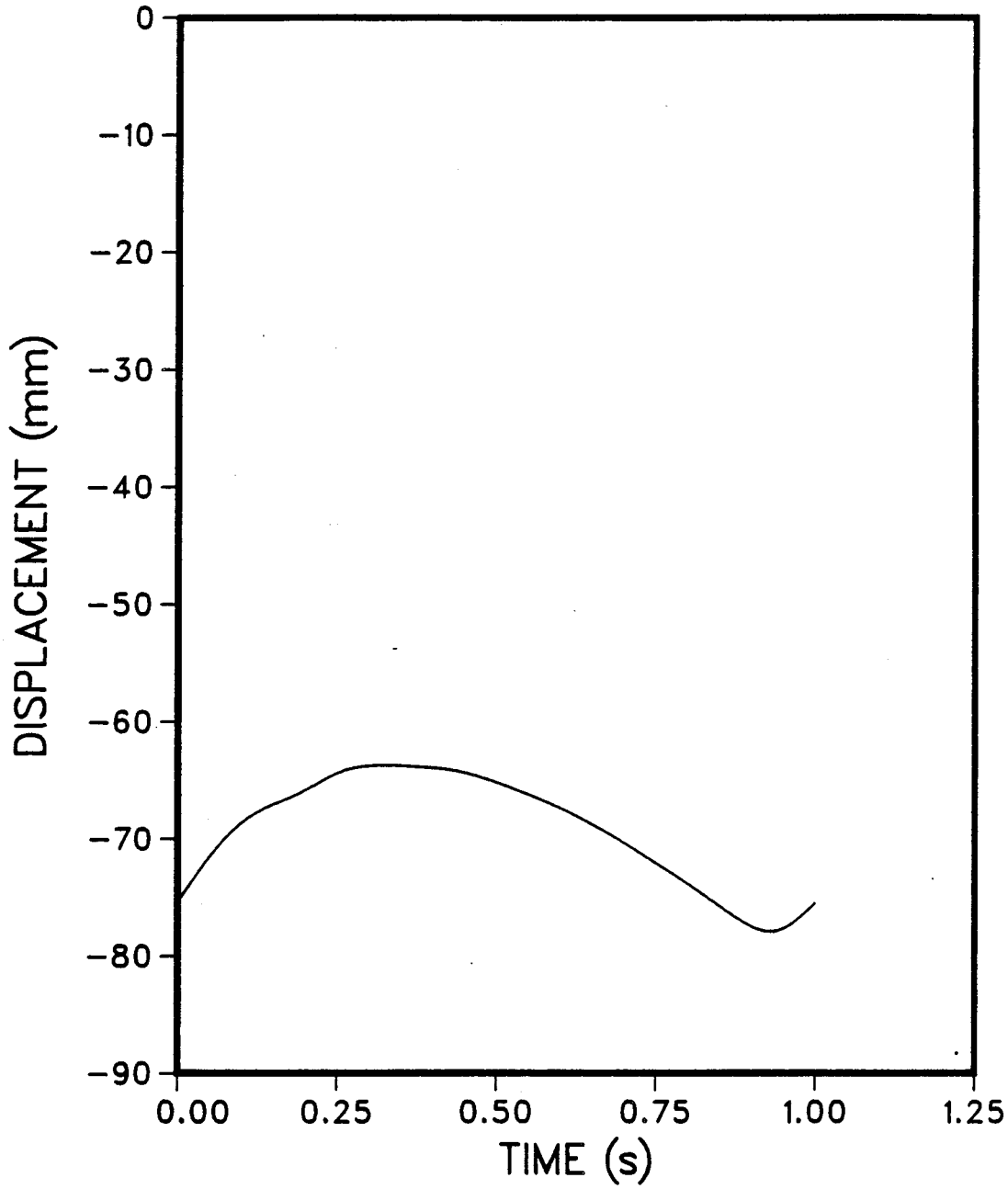

Figure 4.6 Displacement Response - Loaded Side

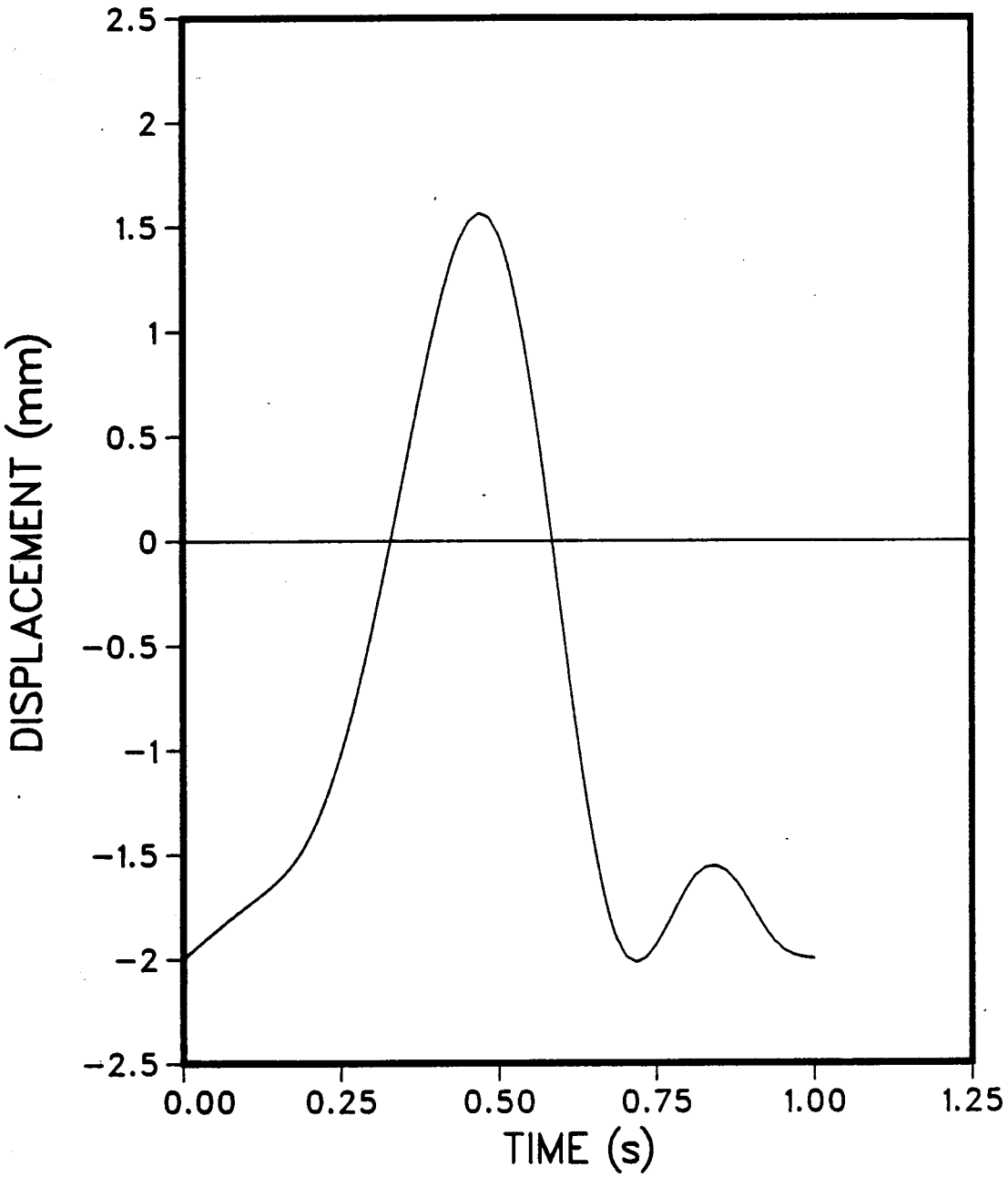

Figure 4.7 Displacement Response - Unloaded Side

not uniform throughout the cycle because the loading and unloading phases are not equal. On the other hand, the displacement response on the unloaded side of the caisson has a different pattern. The maximum displacement on the loaded side is a little less than 80 mm and on the unloaded side about 2 mm which is an indication that the structure does not move significantly (compared with its dimensions) under the ice force.

Velocity response

The velocity response at the top of the caisson on the two sides of the structure is shown in Figs. 4.8 and 4.9. The general shape of the response differs between the two sides in almost the same way the displacement response does. Again the velocity on the unloaded side is much smaller than that on the loaded side. The maximum velocity on the loaded side is about 80 mm/s and on the unloaded side is about 25 mm/s.

Acceleration response

Figs. 4.10 and 4.11 show the acceleration response at the top of the caisson on the loaded side and the unloaded side respectively. The maximum acceleration on the loaded side is about 1.4 m/s^2 which is about 14 percent of the gravitational acceleration (g). On the unloaded side, the maximum acceleration is in the order of 3.6 percent of g. These values are in agreement with the measured response in the field. Jefferies and Wright (1988) mentioned that the maximum recorded acceleration during this ice event was in excess of 11 percent of g on the loaded side and 3.5 percent of g on the unloaded side of the caisson.

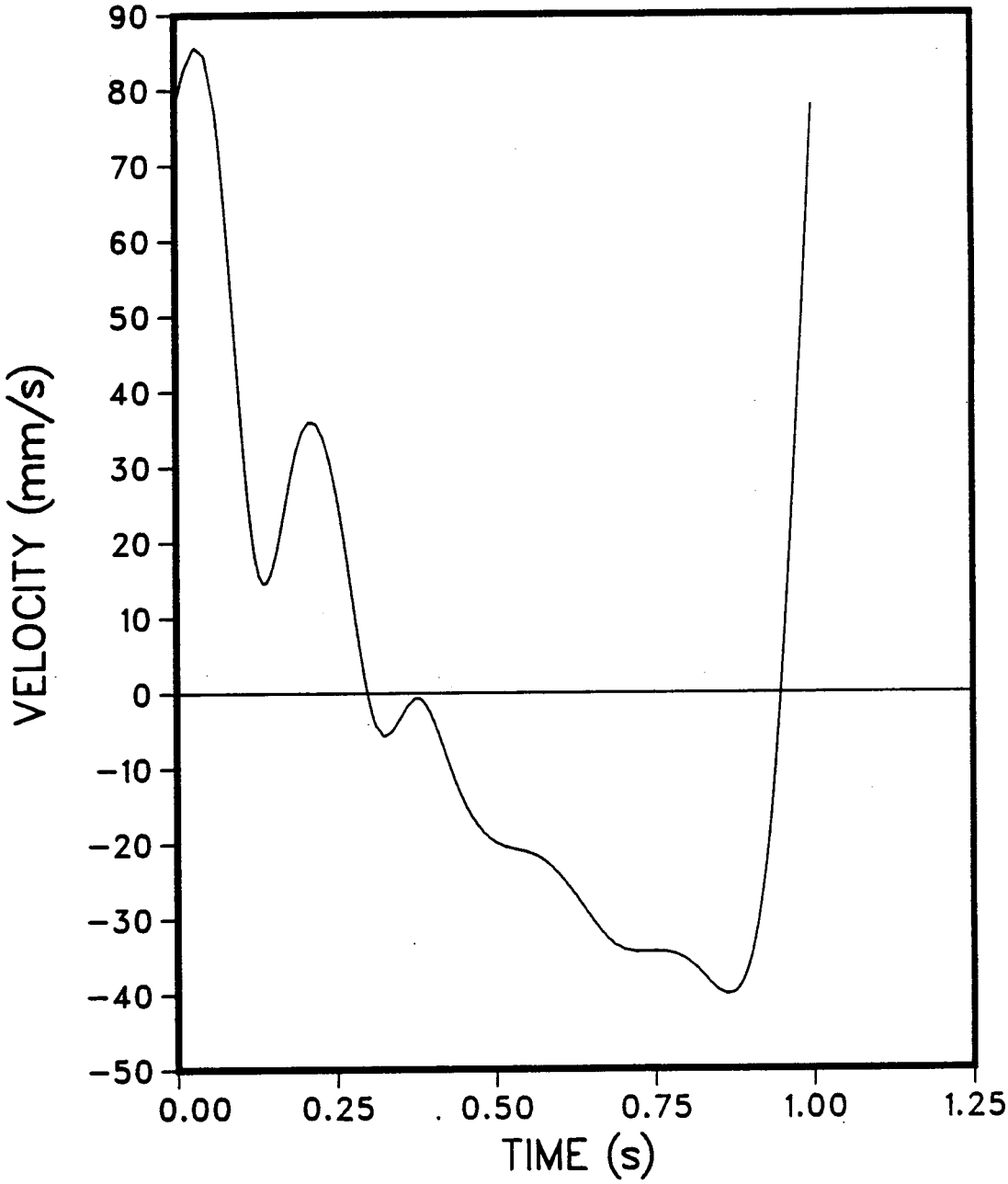

Figure 4.8 Velocity Response - Loaded Side

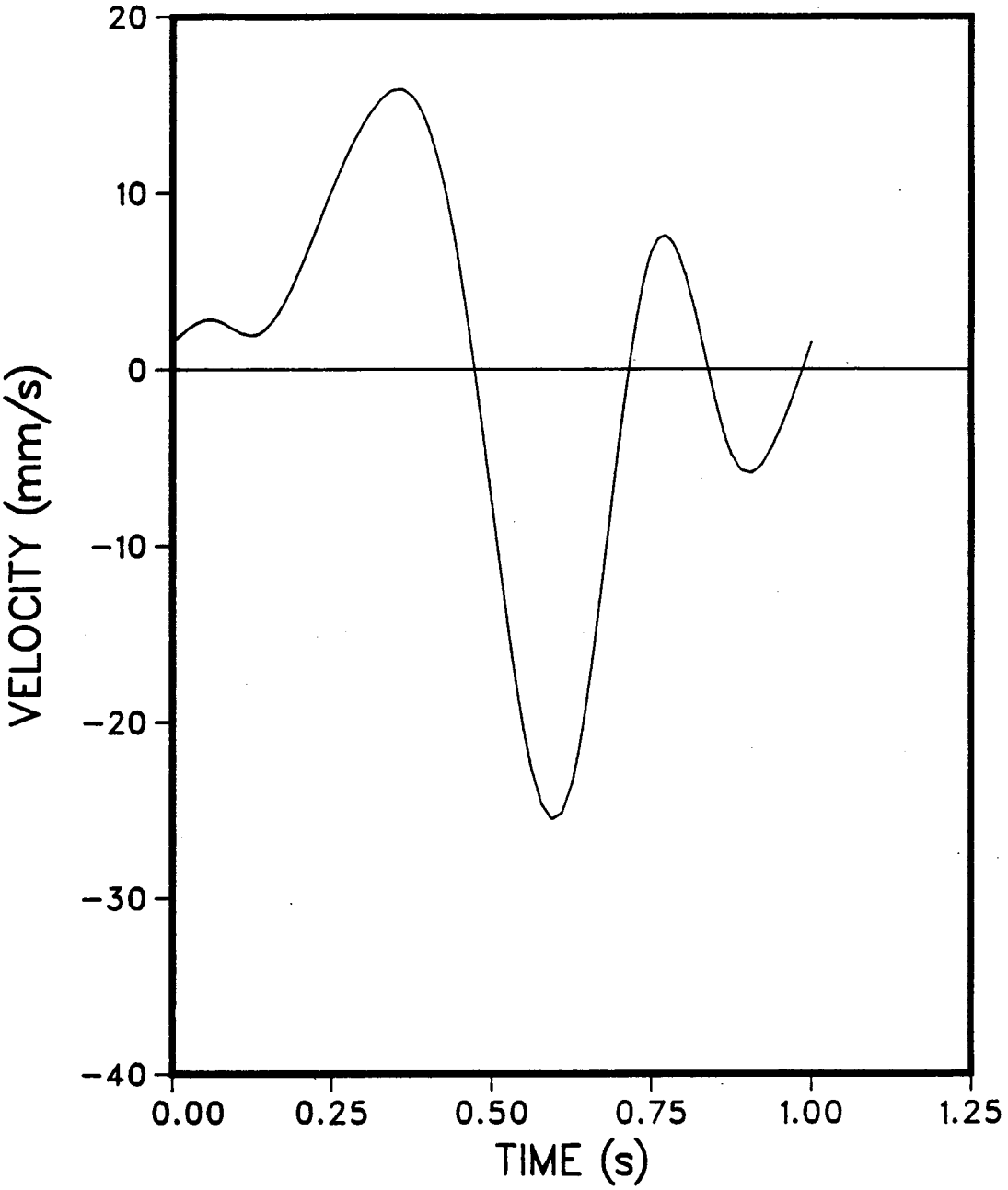

Figure 4.9 Velocity Response - Unloaded Side

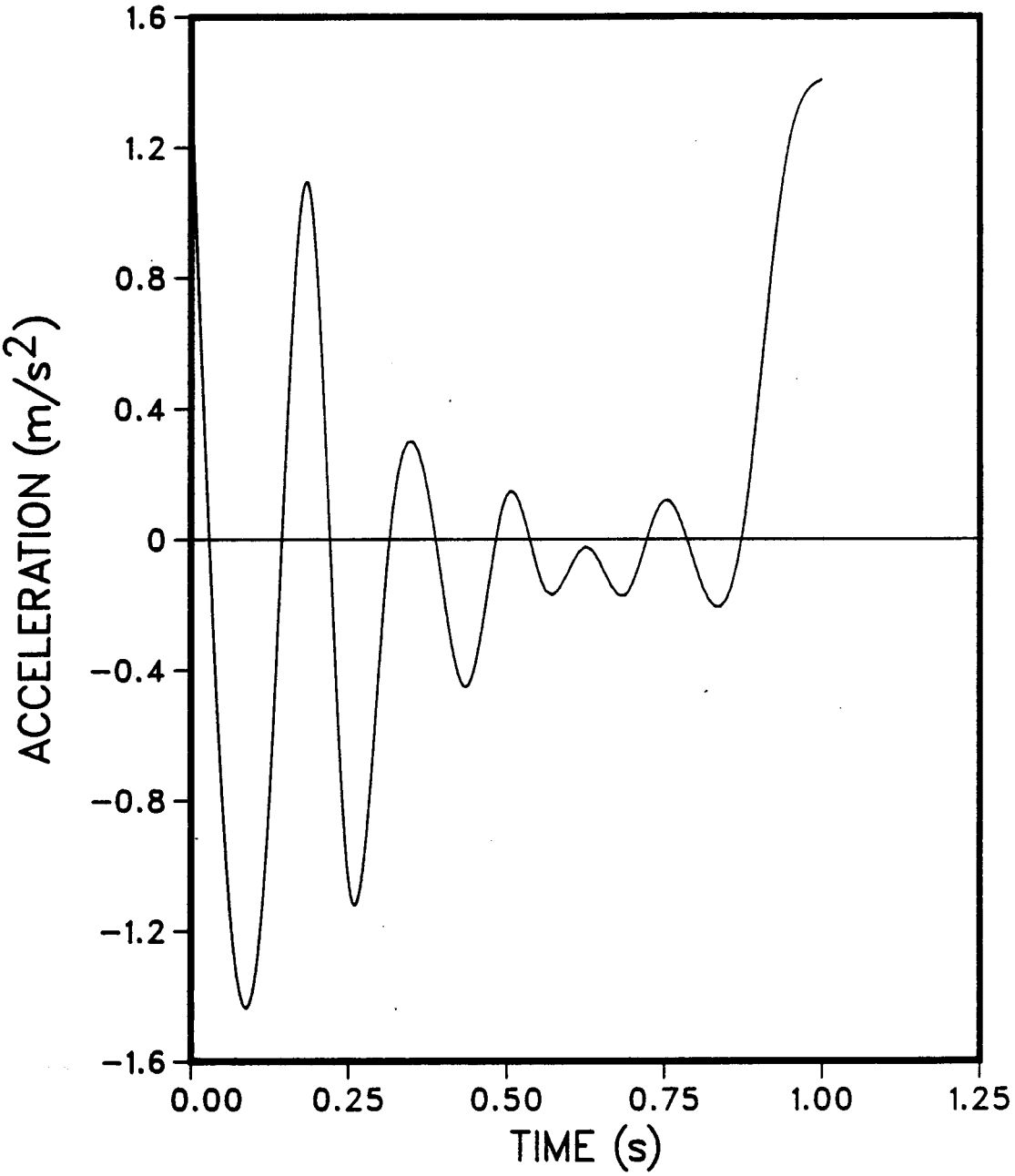

Figure 4.10 Acceleration Response - Loaded Side

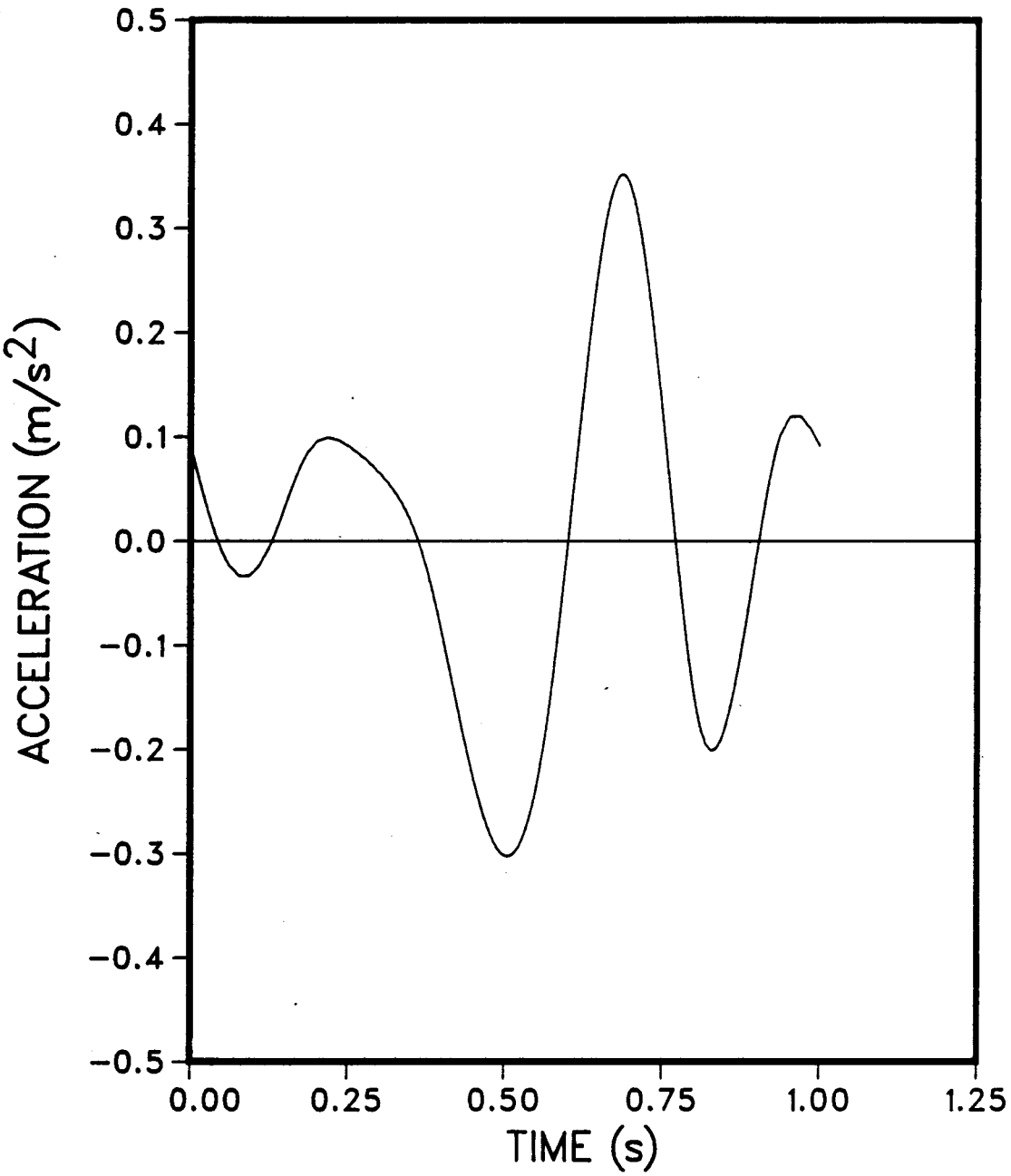

Figure 4.11 Acceleration Response - Unloaded Side

Stresses in structural elements

Nondimensionalized normal and shear stresses in different structural elements are shown in Figs. 4.12 through 4.19. The normalization scheme used in these figures is with respect to the yield stress. The normalized normal stress is the ratio between the normal stress and the uniaxial yield stress (σ_y) and the normalized shear stress is the ratio between the shear stress and the yield stress in shear according to the von Mises yield condition ($\tau_y=0.577\sigma_y$).

A typical stiffener, as well as elements in the intermediate bulkhead, horizontal girder, and main bulkhead are chosen in plotting these figures. It is noted that these values do not represent the maximum values within the entire structural element. Merely, they represent the maximum values within the "finite element" itself. All the representative elements are chosen to be as close as possible to the point of ice load application. Fig. 4.20 shows the locations of the representative elements used in plotting the normalized stresses. General remarks can be drawn from the figures as follows:

1- The stresses in all the representative elements vary with time in the same way as the displacement does. This is expected since the stresses are direct functions of the displacements.

2- The stresses in the different elements are significantly lower than the elastic limit of the steel. However, since a global forcing function has been used in the analysis the resulting stresses are expected to be small. In actual design of the different elements, higher values of local ice pressure should be used.

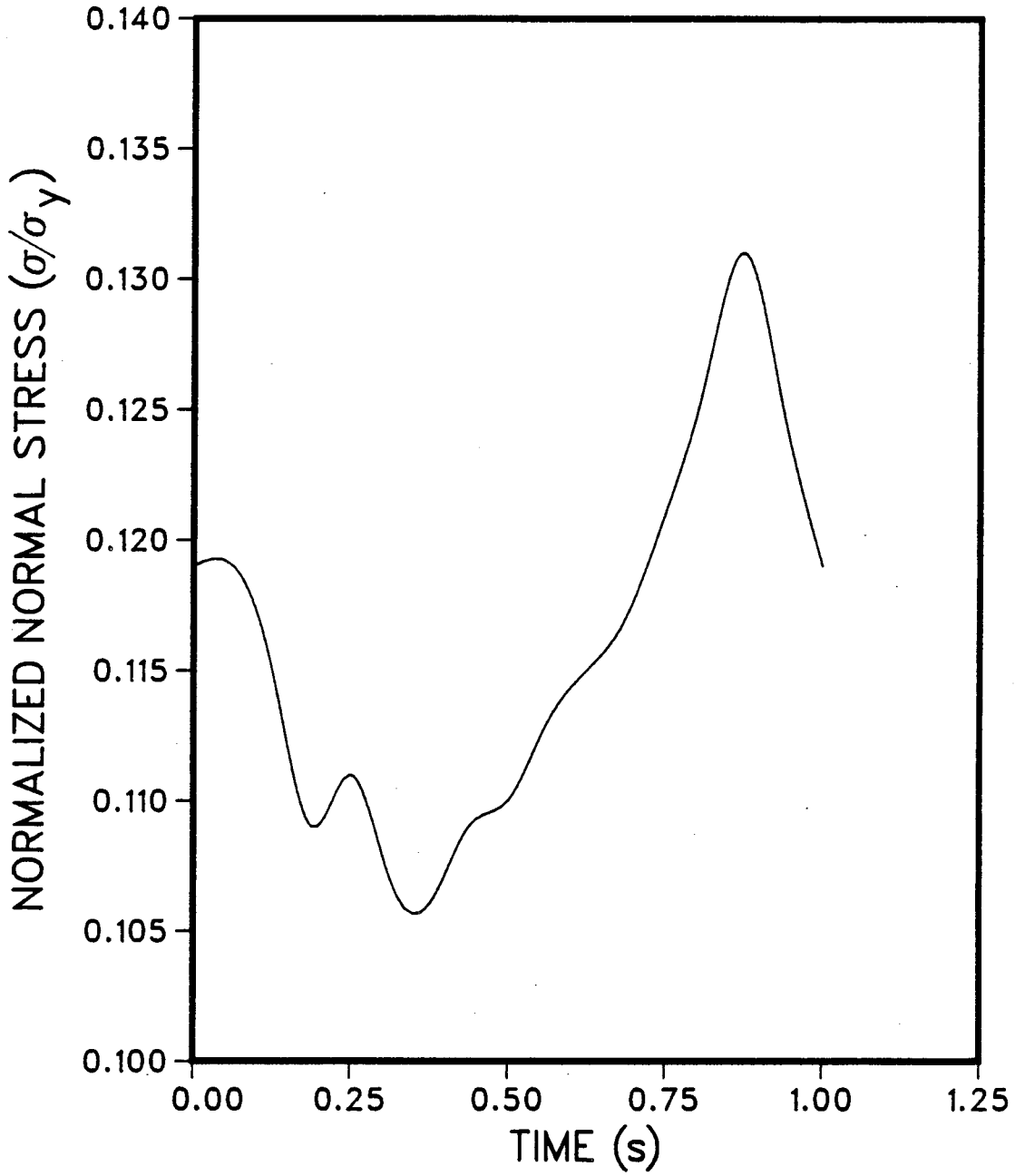

Figure 4.12 Normalized Normal Stress - Stiffener

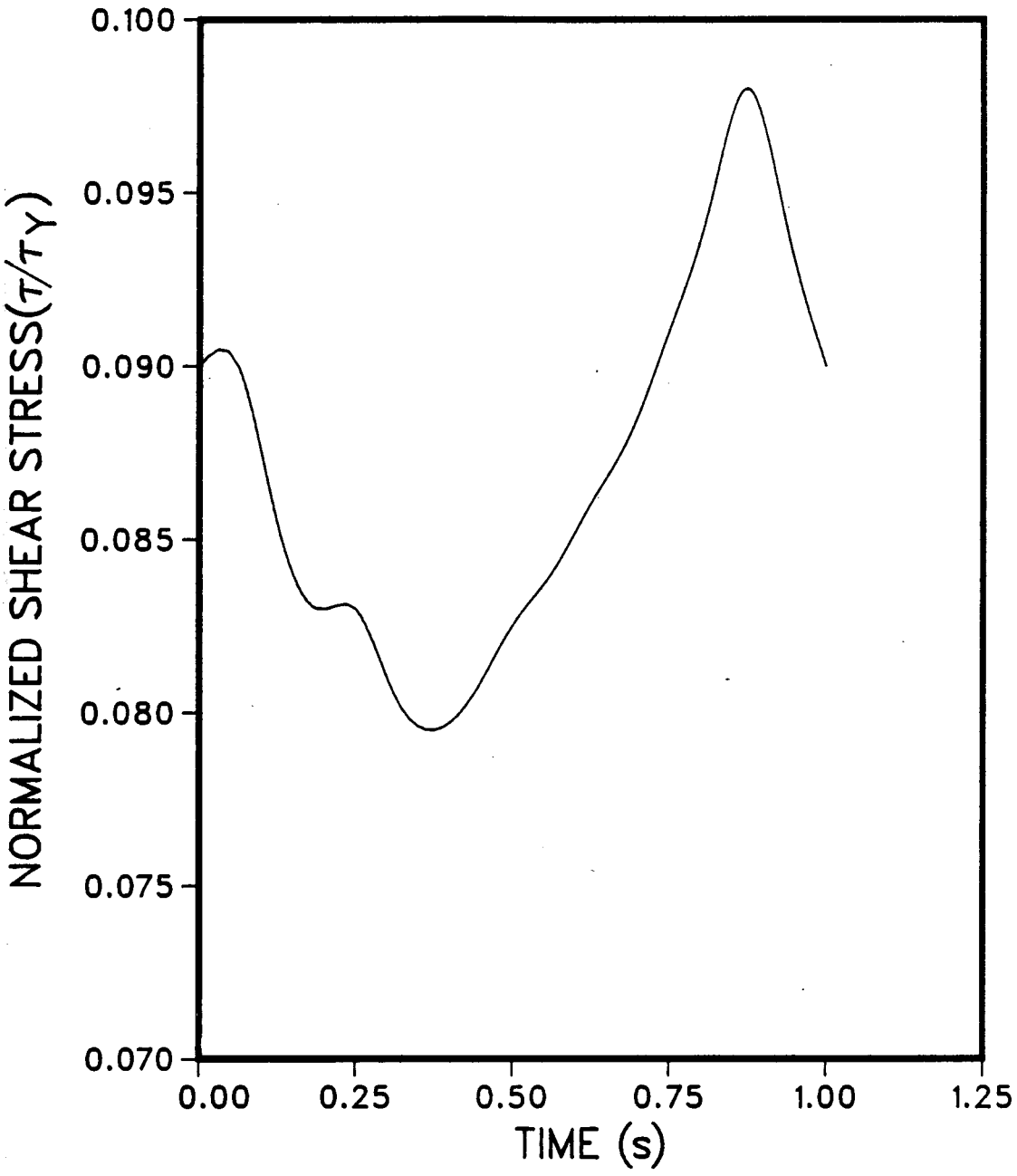

Figure 4.13 Normalized Shear Stress - Stiffener

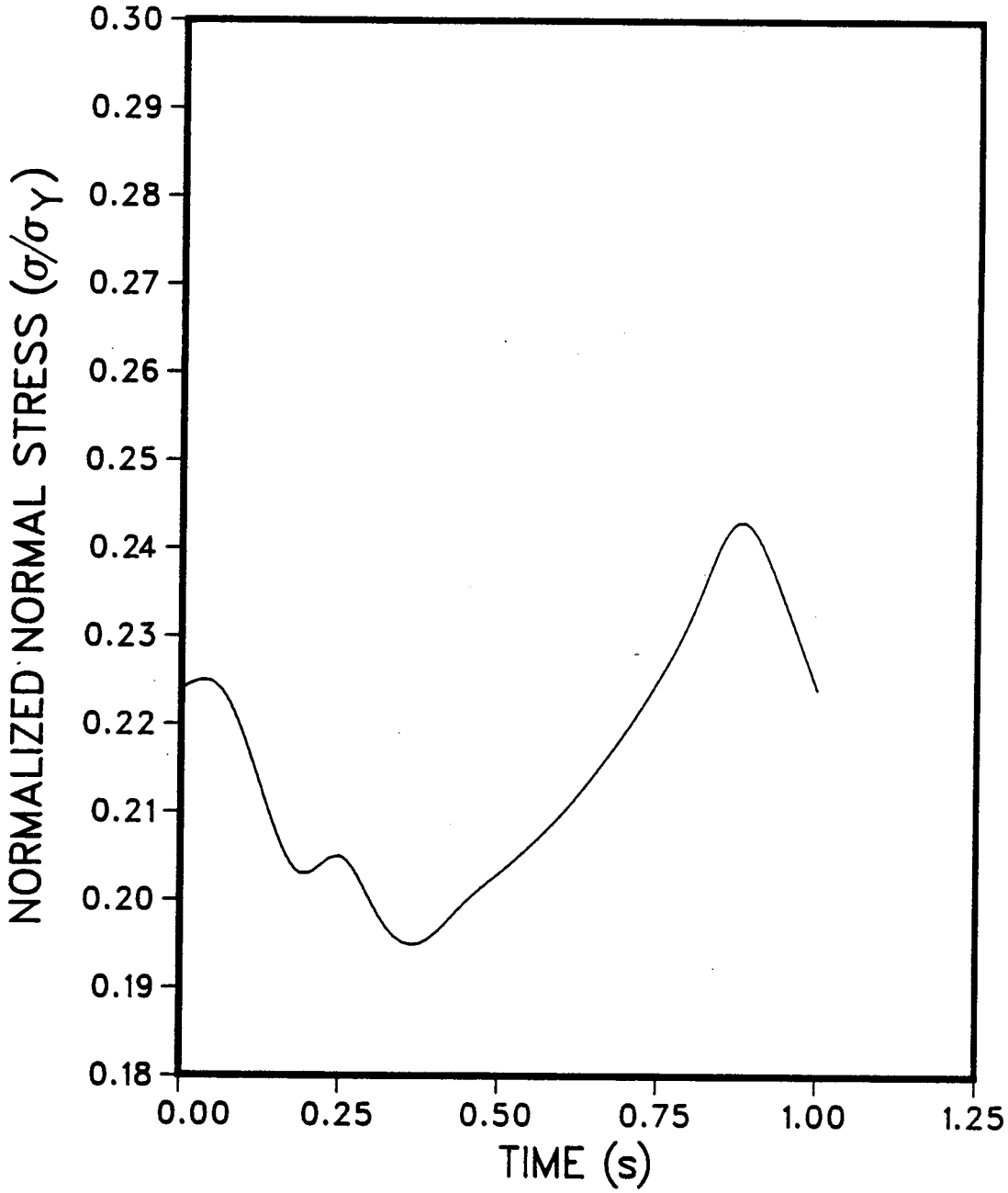

Figure 4.14 Normalized normal Stress - Intermediate Frame

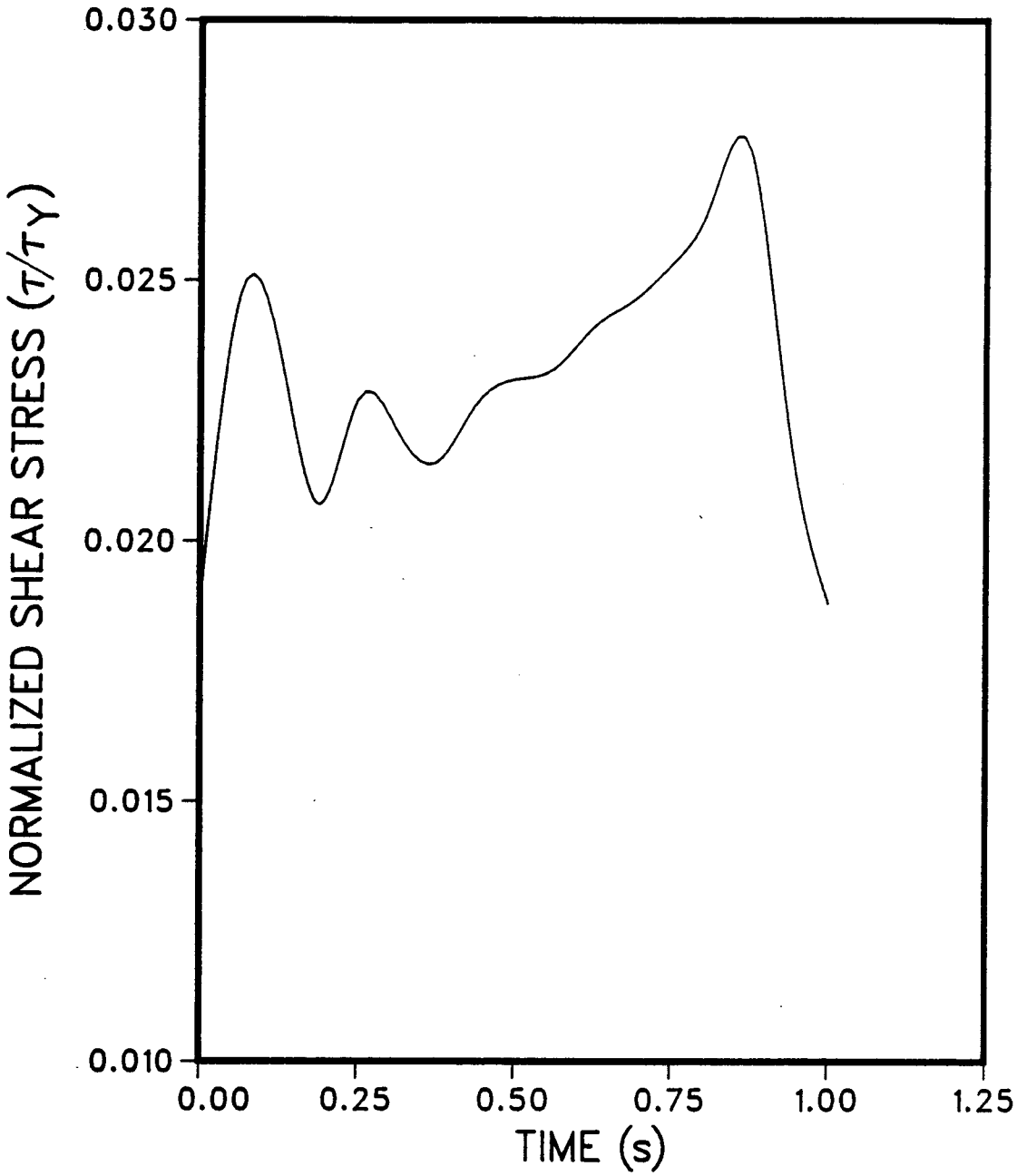

Figure 4.15 Normalized Shear Stress - Intermediate Frame

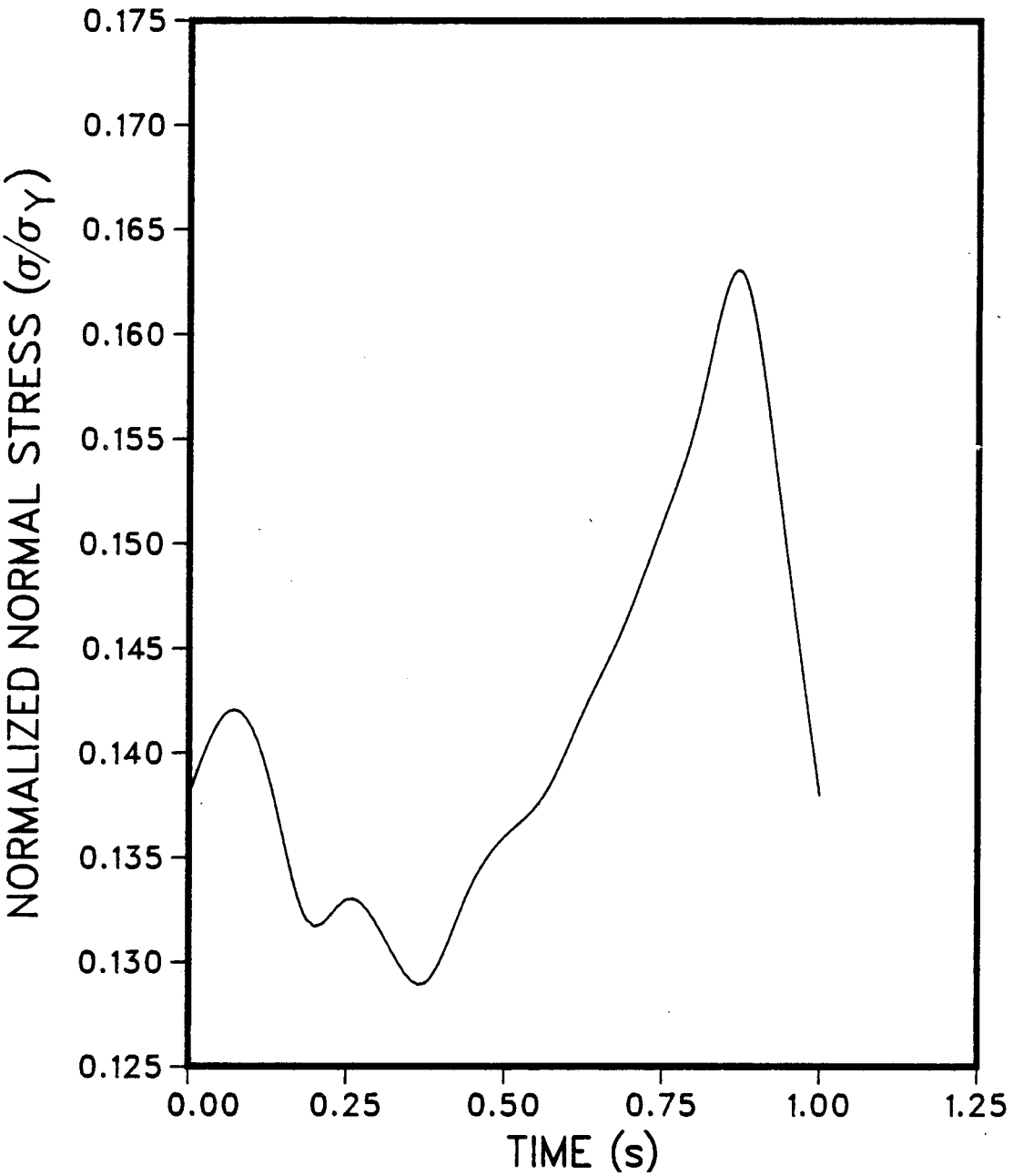

Figure 4.16 Normalized Normal Stress - Horizontal Frame

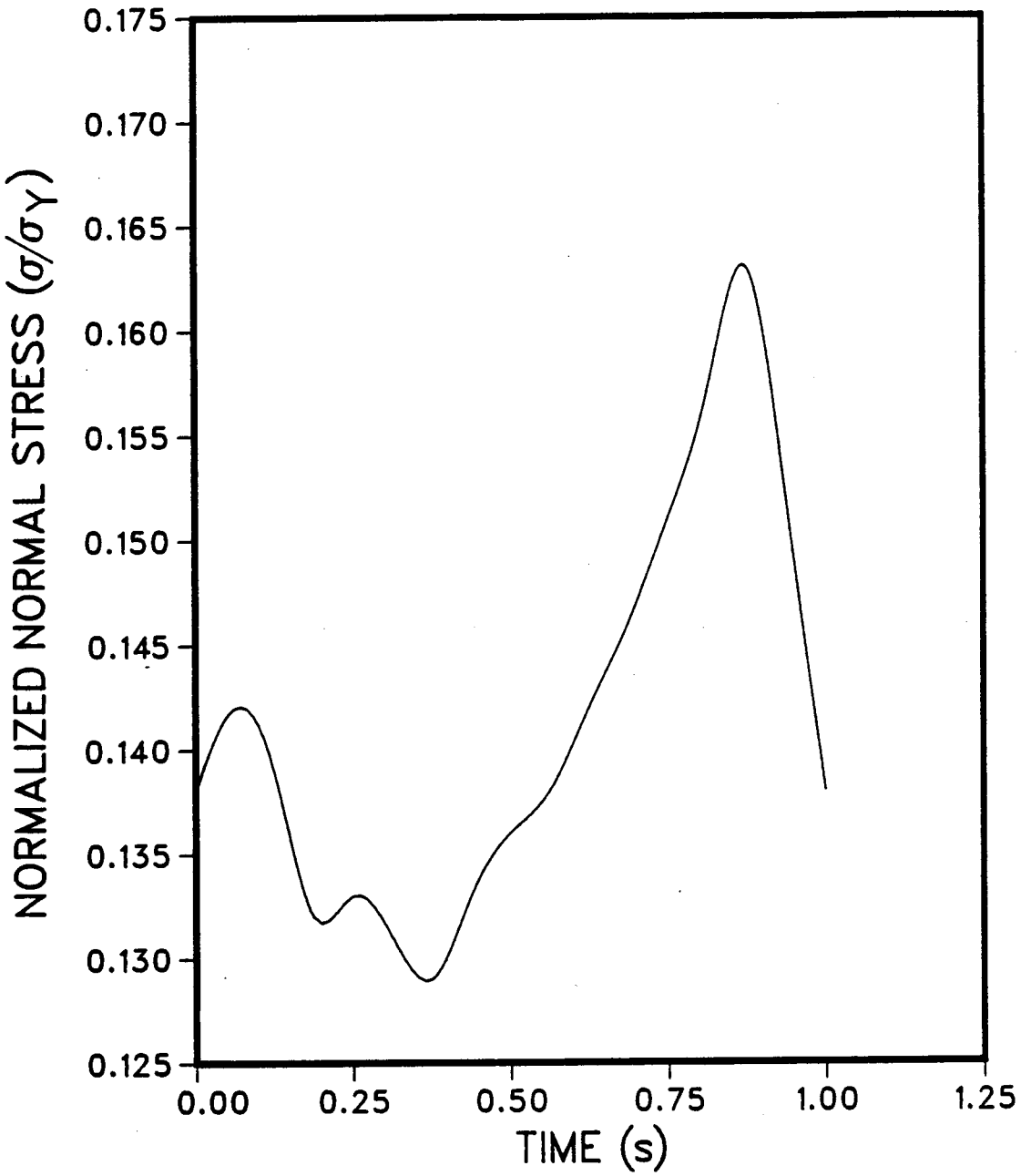

Figure 4.17 Normalized Shear Stress - Horizontal Frame

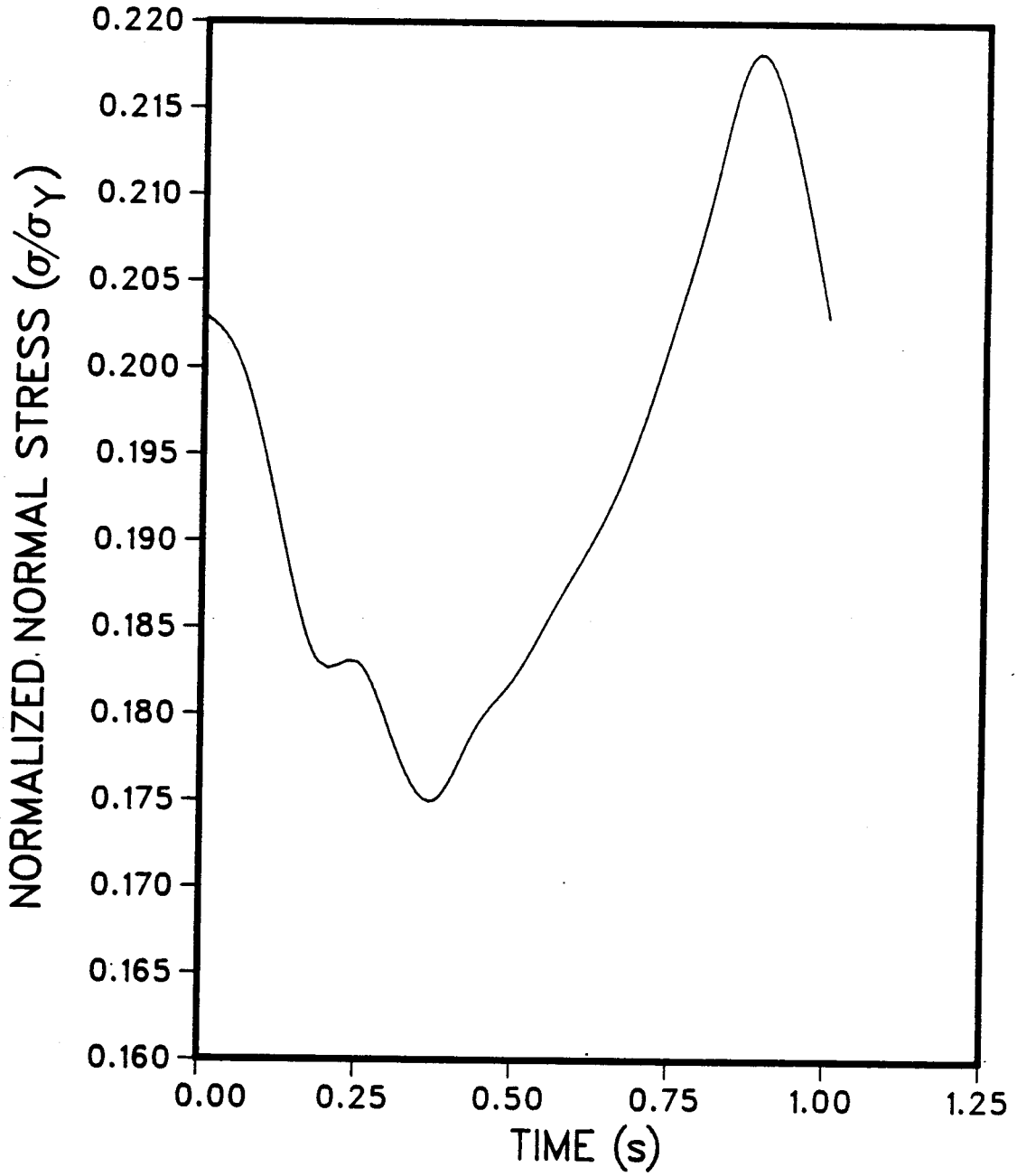

Figure 4.18 Normalized Normal Stress - Bulkhead

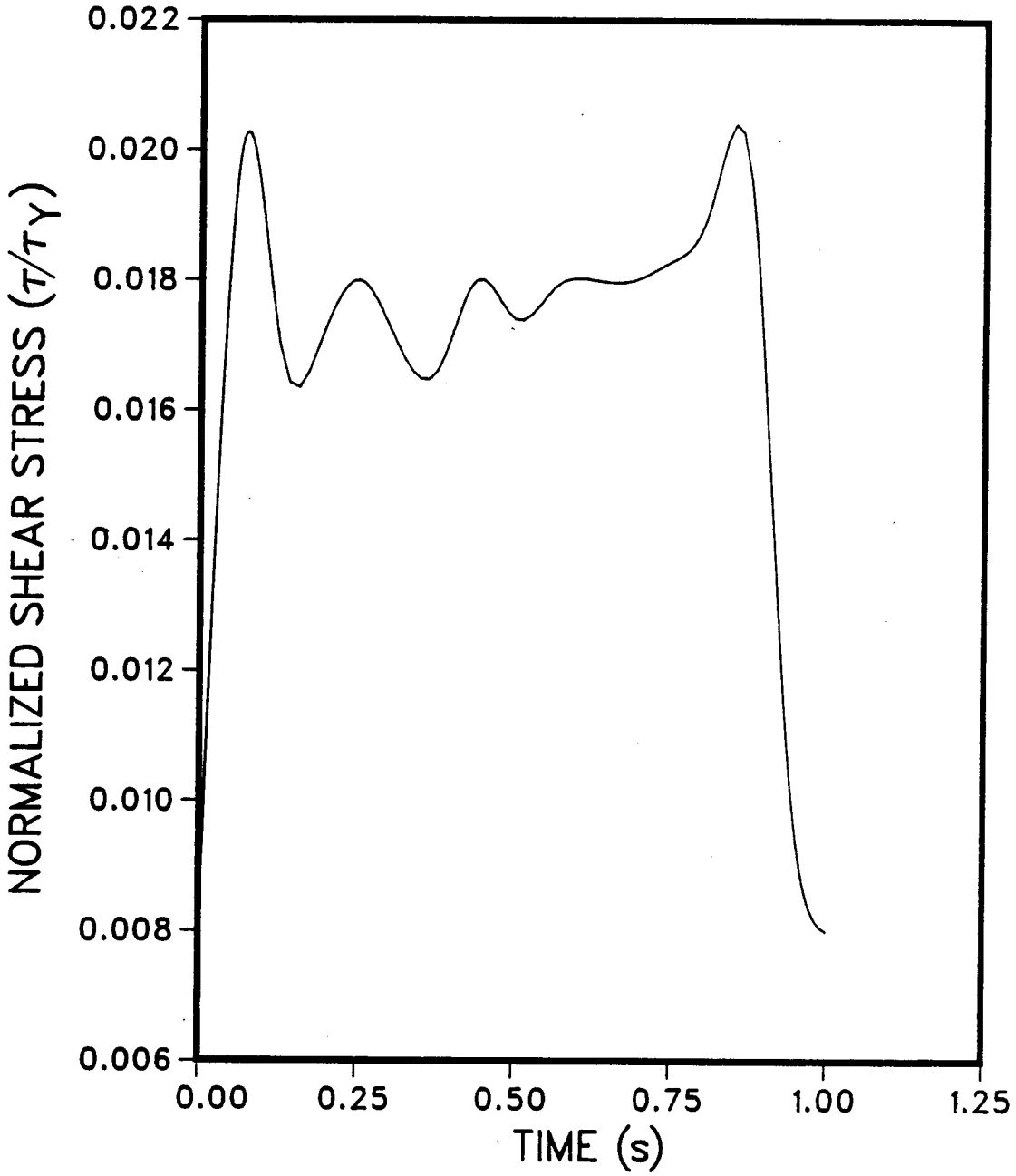

Figure 4.19 Normalized Shear Stress - Bulkhead

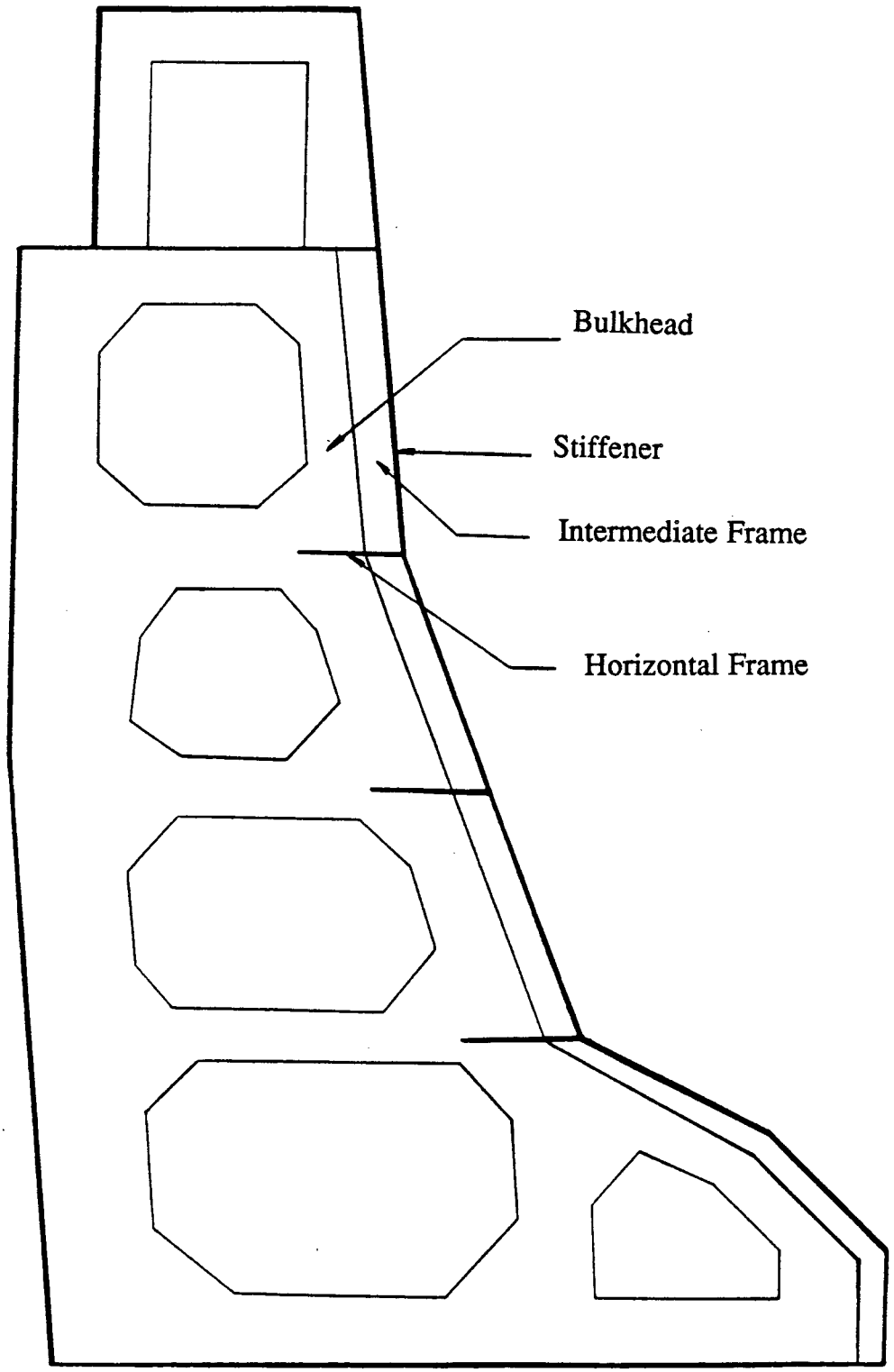

Figure 4.20 Location of Finite Elements Used in Plotting The Stresses

5- INTERACTION ANALYSIS

5.1 Introduction

Ice-structure interaction is a process of action and reaction. What happens on the ice side, for example, depends on the way in which the structure responds to the impinging ice and vice versa. In other words, the two sides of the interaction process affect each other simultaneously. In the dynamic analysis of Chapter 4, the effect of the ice on the structure is represented through an explicit load history. The ice forcing function was recorded in the field during an ice event. Although this is an attractive way of studying ice-structure interactions, it has some drawbacks. Measuring ice forces in the field is expensive and data in most cases is not available in the public domain. In addition to that, ice forces are a function of the geometry of the structure. This means that force records measured on a specific structure might not be applicable to a different type of structure.

Numerical models represent another avenue of approaching ice-structure interaction problems. In this approach, no explicit load history is used to simulate the effect of ice on the structure. Rather, ice itself is represented in the analysis as a structural element. In this case, moving ice is modelled as a train of elements that fail against the structure. The far end of these elements moves at a specified velocity and the near end remains in contact with the structure.

The constitutive behavior of the ice elements is deduced based on the mechanical properties of ice and general observations from indentation tests and

field measurements as reported by a number of investigators. In the interaction analysis, the forcing function between the ice and the structure is an outcome of the solution and that gives an opportunity to study the effect of some parameters such as the ice velocity and thickness on the interaction force.

To begin, a comparison is made between the indentation of an ice sheet by a slender indentor and the interaction between ice and wide structures. The proposed interaction model is then discussed in terms of its different parameters and numerical solution. The model is used in six different cases to study the effect of ice velocity and thickness on the interaction process. Results of all the cases are summarized in terms of the response of the structure and the predicted ice interaction force.

5.2 Interaction between ice and wide structures

In this section a comparison is made between the classical indentation problem in which ice interacts with narrow structures, such as piles or bridge piers, and the situation where ice acts on a wide structure of the order of 10's to 100's of meters width.

5.2.1 Cyclic ice loading during crushing

Based on field observations during the interaction events between MAC and moving ice sheets, Jefferies and Wright (1988) proposed a conceptual framework for the cyclic ice loading during crushing. It may be summarized as follows:

1- The ice moves with constant velocity and when it comes in contact with the structure, the structure deflects and the ice compresses.

2- When the stress in the ice reaches a critical value, the ice crushes.

3- The structure springs back, extruding the crushed ice in the vertical direction.

4- The continuous supply of the ice from the far field causes the repetition of the process described in steps 1 to 3.

This framework is similar to what has been observed by a number of investigators in small scale indentation tests. Michel and Toussaint (1977) and Croasdale et al. (1977) reported that in continuous indentation tests, the ice pressure increased to a peak value at which the ice failed. After failure, the ice pressure usually dropped to about 50 to 60 percent of the peak value before rising again.

The conceptual framework given by Jefferies and Wright is widely accepted for describing the continuous crushing of ice in ice-structure interactions. However, different hypotheses have been proposed for the extrusion process of the crushed ice. Jordaan (1986) suggested that the extrusion takes place entirely during the loading phase of the cycle. Hallam and Pickering (1988), on the other hand, proposed that the majority of the extrusion happens during the unloading phase of the cycle. In general, it is believed that the mass and stiffness of the structure and the ice velocity and thickness are the main parameters that govern the extrusion process. In the writer's opinion, the material properties of the crushed ice are also important factors in the extrusion process.

5.2.2 Ice-wide structure interaction as a special case of the indentation problem

Timco (1986) conducted indentation tests on columnar S2 freshwater ice in the brittle range of strain rate. In his experiments, Timco found that during the interaction process between a flat indentor and ice sheets, there was a highly stressed region in the ice ahead of the indentor. This region extended in front of the indentor typically one to one and a half times the indentor width. This is similar to the bearing problem in soil mechanics. It is well known that the size of the pressure bulb underneath the foundation is a function of its dimensions (Bowels, 1977).

The size of the stressed zone in the ice sheet in the front of the structure is very important to the interaction process. Figure 5.1 shows a schematic representation of the pressure bulb ahead of the indentor. In small scale indentation tests, the width of the indentor is in the order of a few centimeters. In the field, the pile diameter is usually less than one meter and the bridge piers usually have widths less than two meters. This means that during the interaction process with such structures, the size of the pressure bulb ranges between a few centimeters in the case of small indentors and a few meters for bridge piers. In these cases it should be expected that the ice remains completely intact and does not undergo any significant damage due to the interaction until it arrives at a point very close to the structure.During the interaction process between the ice sheets and a very wide structure, typified for example by MAC, the size of the pressure bulb will extend few 100's of meters ahead of the structure. Typically, the width of the structure at the water level is about 90 meters which gives a pressure bulb size in the order of about 200 meters. This means that an element A of the ice,

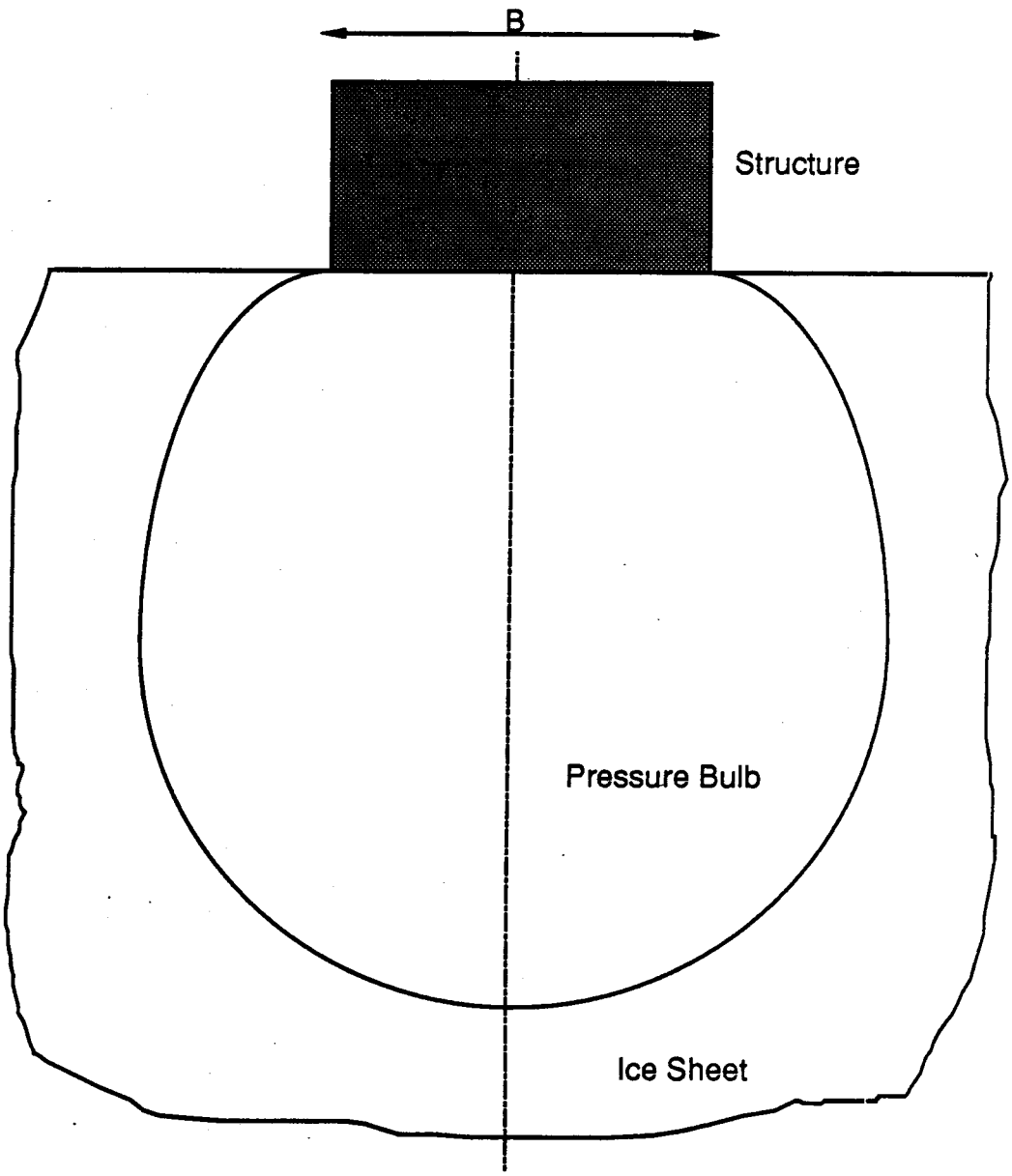

Figure 5.1 Pressure Bulb Ahead of The Structure

shown in Fig. 5.2, will become stressed, because of the interaction, at that distance ahead of the structure. The stress history of the element, as it moves towards the structure, will have a general shape like that shown in Fig. 5.3. The stress intensity will increase as the ice element gets closer to the structure. The saw-tooth shape of the stress history curve is because the interaction force drops to a lower value each time crushing occurs at the interface. This will cause the stress intensity within the stress bulb to vary between two extremes as shown in Fig. 5.4.

The actual stress history for an ice element A is not known in advance because the interaction force itself is not known. However, some very useful points can be drawn from the general shape of the stress history. These are:

1- The stress history will start at zero stress. This is because at points outside the pressure bulb, the ice does not feel the presence of the structure.

2- The ice will crush immediately in the front of the structure when the stress reaches some critical stress value.

3- The time on the stress history curve between zero stress and the failure point can be estimated approximately from the size of the pressure bulb and the ice velocity. For the ice event studied in Chapter 4, the time-to-failure is in excess of 3,000 seconds.

The main difference between the ice-wide structure interaction and the classical indentation problem lies in this last point. Sinha (1978) conducted creep tests on S2 freshwater ice at -10^{o}C for different stress levels. According to his

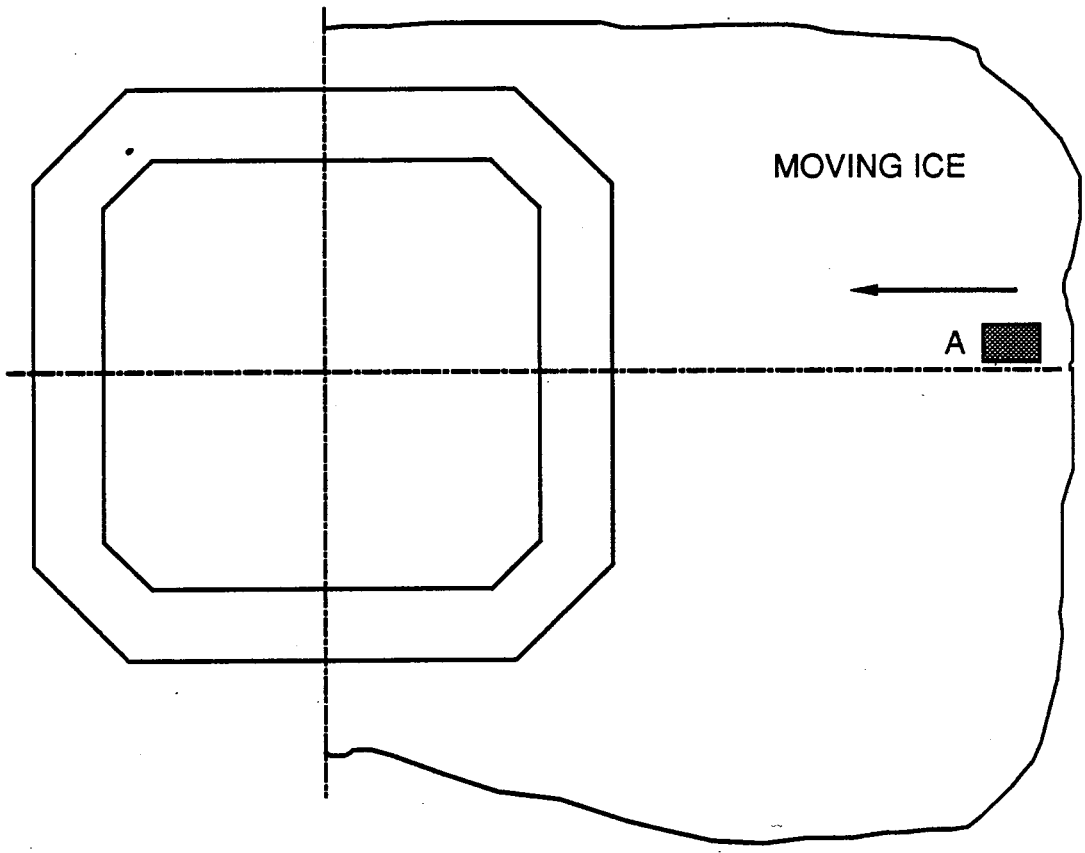

Figure 5.2 Element of Ice A Travelling Towards The Structure

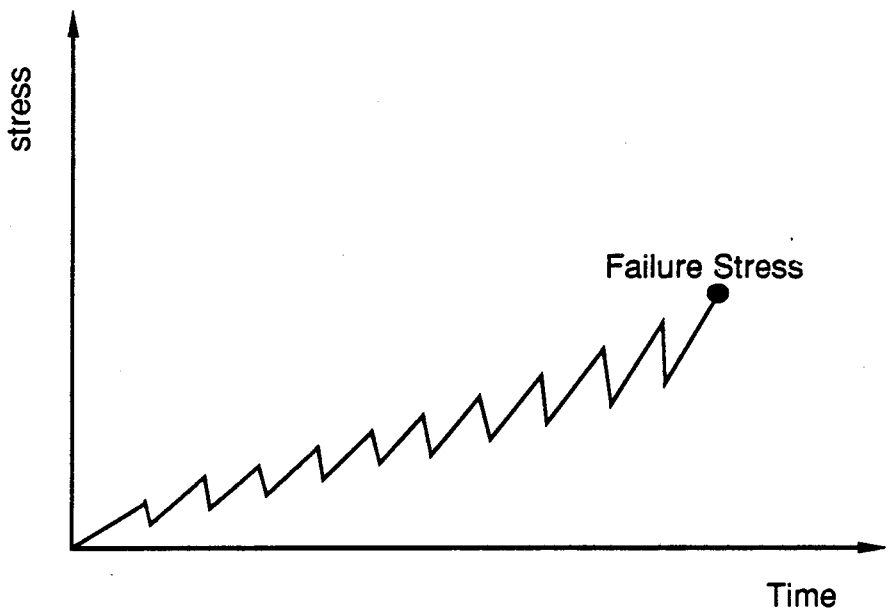

Figure 5.3 General Shape of Stress History on an Ice Element

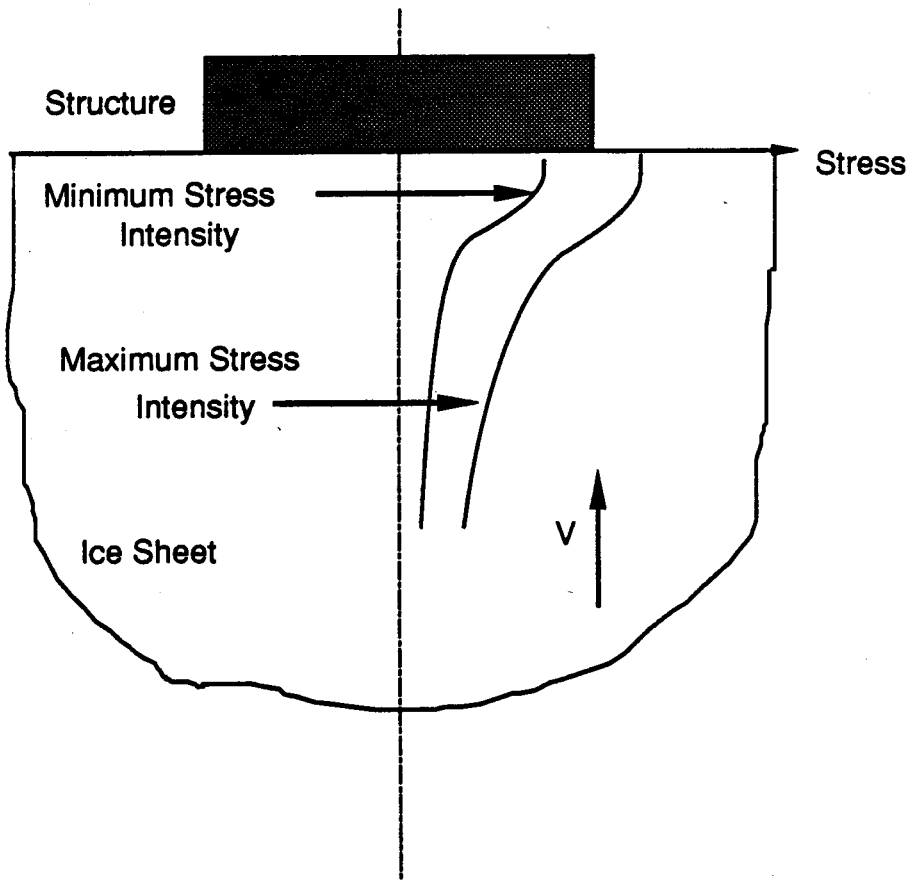

Figure 5.4 Two Extremes of Stress Intensity in Ice Sheet

results, the creep strain under a constant stress of 0.5 MPa after only 100 seconds from loading, is almost the same as the instantaneous elastic strain. This means that the effective modulus of ice (stress / total strain) is almost half the elastic modulus (stress / elastic strain) after a relatively short period of time (100 seconds in this case). This gives an indication that ice might creep quite rapidly and its effective modulus decreases significantly in a short period of time. Under a stress history like shown in Fig. 5.3, it should be expected that significant creep deformations will occur. In addition to that, the saw-tooth nature of the stress history suggests the possibility of fatigue effects.

From this discussion it can be concluded that the main difference between this kind of interaction and the classical indentation problems with small indentors is that in this case there is a significant creep phase of deformation in the ice before it crushes at the structure. This creep phase of deformation will influence the material properties of the ice just before it crushes. In the following section, the interaction model proposed in this study is discussed in detail.

5.3 Interaction model

An interaction model has been developed for use in simulating the moving ice in the interaction analysis. The model is uniaxial, that is it uses spring elements. The assumptions made in developing the model are stated first and then the constitutive behavior of the interaction element are discussed in detail.

5.3.1 Assumptions and limitations

In developing the interaction model, the following assumptions have been made.

1- The ice sheet has a uniform thickness and is wide compared with the width of the structure.

2- The ice floe is very long compared with the width of the structure.

3- Only the crushing mode of failure is considered since this mode produces the maximum ice forces (Kry, 1980).

4- No ice rubble pileup is formed around the structure. This is realistic for structures used in relatively deep water (20 to 50 m depth).

5- The crushed ice does not have any influence on the interaction process after extrusion. In the field, it was observed that the crushed ice moves laterally on top of the ice sheet until it clears around the structure (Jefferies and Wright ; 1988).

6- The ice will be in contact with the structure all the time.

Based on these assumptions, the constitutive behavior of an ice element is proposed. It is discussed in the following subsection.

5.3.2 Constitutive behavior of the interaction model

The saw-tooth shape of the forcing function, shown in Fig. 4.2, in addition to the conceptual framework of the interaction process given by Jefferies and Wright (1988), suggest that a tri-linear force-displacement relationship is a reasonable choice for the interaction model. This leads to four-parameter constitutive relationship for the ice element, as shown in Fig. 5.5.

The four parameters are (S^+), (S^-), F_{max}, and F_{res}. The loading slope (S^+) represents the behavior of the ice during the loading phase. That is, prior to

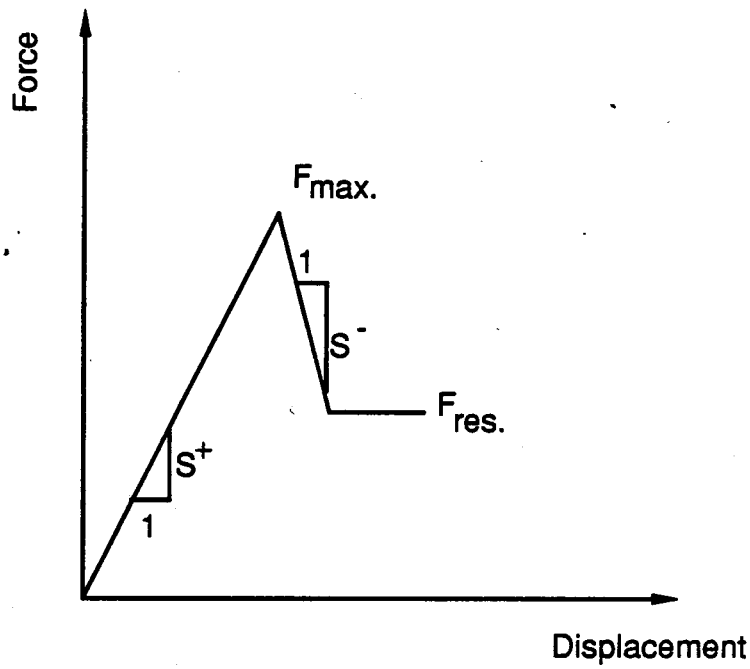

Figure 5.5 Force-Displacement Relationship for Ice Element

crushing. The maximum force (F_{max}) is the critical value of the interaction force at which the ice fails. The negative slope (S^-) represents the unloading phase after crushing. The horizontal plateau (F_{res}) is the residual strength of the ice element after crushing. Each of these four parameters is discussed in detail in the following subsections.

5.3.2.1 The loading slope (S^+)

Vivatrat (1982) plotted ice pressure versus indentation displacement for three tests with different strain rates. He observed that the loading slope in pressure versus displacement curves for the three tests has the same linear slope. He examined several other indentation tests with strain rates between $2x10^{-5}$ and $2x10^{-2}$ s^{-1} and the same phenomenon was observed. Following a procedure similar to that given by Ladanyi (1967) for the problem of cavity expansion in rock mechanics, Vivatrat proposed an expression to calculate the initial loading slope. This is as follows:

$$\sigma = cE\,\Delta/D \tag{5.1}$$

where σ is the indentation pressure, c is a numerical constant with a value of about 0.5, E is the elastic modulus, Δ is the penetration distance, and D is the indentor width. Multiplying both sides by HD and rearranging, this equation can be written as,

$$S^+ = cEH \tag{5.2}$$

where S^+ is the initial loading slope, and H is the ice thickness..

This expression has been developed based on results from small scale indentation tests. It can be used in the analysis of the interaction between ice and slender structures. However, it cannot be used directly in studying the interaction between ice and wide structures. In these cases, the ice undergoes significant level of deformation before it arrives at the structure. Therefore, the solution must be modified in order to take that into consideration.

One approach is to use a reduced value of the elastic modulus E in Eq. (5.2). In general, creep effects in many problems can be taken care of by conducting elastic analysis using an effective or reduced modulus of elasticity (Flugge, 1975). Although rheological models that describe the creep behavior of ice have been developed (Sinha, 1978 and Sunder, 1985), these models are not easily used to evaluate the effective modulus. This is because the stress history on the ice element as it travels towards the structure is not known in advance. However field data, such as the forcing function shown in Fig. 4.2, provides some insight as to suitable values for the reduced modulus. This ice event will be used as a test case to assess the overall performance of the model and to obtain an estimate for the reduced modulus. In this study, the effective or reduced modulus used in evaluating (S^+) is found to be in the range of 20 to 30 percent of Young's modulus of sea ice. This is consistent with the results of Sinha.

5.3.2.2 The maximum force (F_{max})

The second parameter in the proposed interaction model is the maximum ice force F_{max}. This is the force at which the ice fails. In other words, it is the maximum force the ice can support. Ice failure against a structure is function of several parameters. Ice strength, mode of ice failure, area of contact, and

geometry of the structure are among these. The maximum ice force is equal to the effective pressure at failure times the area of contact.

Pressure versus area curves have been developed by a number of investigators, for example Sanderson (1986) and Ashby et al. (1984). These curves are based on data collected from different sources. Data from small scale indentation tests as well as data from field measurements are used in developing these curves. Figure 5.6 shows a typical pressure versus area curve for ice.

5.3.2.3 The unloading slope (S^-)

The unloading slope is a function of parameters such as the structure mass and stiffness, and the ice velocity. Perhaps the most important factors that affect the unloading slope are the extrusion process and the nonsimultanous crushing across the entire contact area. In this study, it is assumed that ice fails in a brittle manner, and the unloading slope is taken as a very high value compared with the loading slope (S^+).

5.3.2.4 The residual force (F_{res})

Croasdale et al. (1974) and Michel and Toussaint (1977) observed that during continuous indentation tests the effective stress dropped to about half of its maximum value after crushing. The recorded forcing function during the ice event considered here, Fig. 4.2, confirms this. Based on that, the residual force in this study is assumed to be a fixed percentage of the maximum force. In all the cases considered, the residual force is taken as 50 percent of the maximum force.

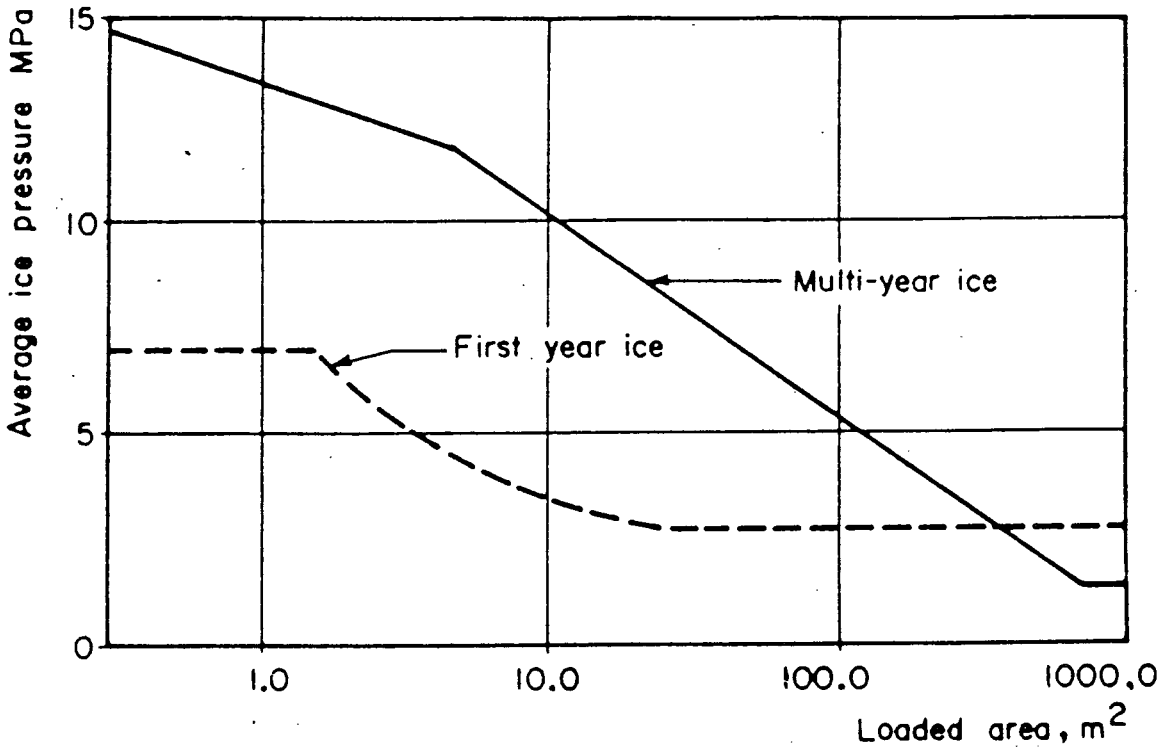

Figure 5.6 Typical Pressure-Area Curve for Ice

The four parameters required to construct the interaction model are now completely defined. In the following section, the implementation of the model in the overall analysis of the problem is discussed.

5.3.3 Finite element representation and numerical solution

The system of equations of motion in the interaction analysis can be written as:

$$[M]\{\ddot{x}\} + [C]\{\dot{x}\} + [K]\{x\} = \{F(t)\} \tag{5.3}$$

which has the same form as Eq. (4.1) and the same definitions hold for the individual terms. However, two differences exist between this equation and Eq. (4.1). In Eq. (5.3), the vector {F(t)} does not include terms from the ice at the contact point between the ice and the structure. The interaction force, in this analysis, is an internal force and does not appear explicitly in equations of motion. In addition, the stiffness matrix [K] has terms that represent the constitutive behavior of the ice element. No contribution from the ice is considered in the mass matrix since it is assumed that the ice moves with constant velocity. Everything else in the two equations is the same.

In order to simulate the interaction process, during which an element of ice crushes against the structure and extrudes, followed by a new cycle of loading, crushing, and extrusion, a new technique has been developed. The ice is represented as a series of elements all of which are attached to the same node on the structure. However, only one is active at any time. After the currently active element finishes its cycle of loading- crushing-extrusion, the next element starts its cycle. This is achieved by adding a horizontal gap to the tri-linear force-

displacement relationship of each element as shown in Fig. 5.7. The length of this gap varies from one element to the other. For the n^{th} element in the series, the length of the gap is equal to the length of the first (n-1) elements. Fig. 5.8 shows the variation of the gap from one element to the other in the series.

To some extent, this technique is similar to the model proposed by Matlock et al. (1969). However, the two models differ in several aspects. In their model it was assumed that the ice fractures instantaneously (unloading time is equal to zero), the ice force drops to zero after crushing, and the force remains at zero until the ice regains contact with the structure.

The Newmark-β integration scheme is used in performing the time stepping calculations as in the direct dynamic analysis of Chapter 4. Within each time step, the solution of the system of the nonlinear equations is handled iteratively using Newton's method. The nonlinearity arises from the dependence of the stiffness matrix on the response of the structure since the constitutive behavior of the interaction element is a function of the response. In the following section, the cases analyzed using the interaction element proposed in this study are discussed along with the results.

5.4 Cases considered using the proposed interaction model

The interaction model is used to study the effect of some parameters on the interaction force. A total of six cases are considered in order to investigate the effect of the ice velocity and thickness. In the first case, the conditions of the ice event during which the forcing function shown in Fig. 4.2 was recorded are simulated. In this case, the ice thickness is 9 m and the ice velocity is 0.06 m/s. The second, third, and the fourth cases have ice thickness of 9 m and velocities of

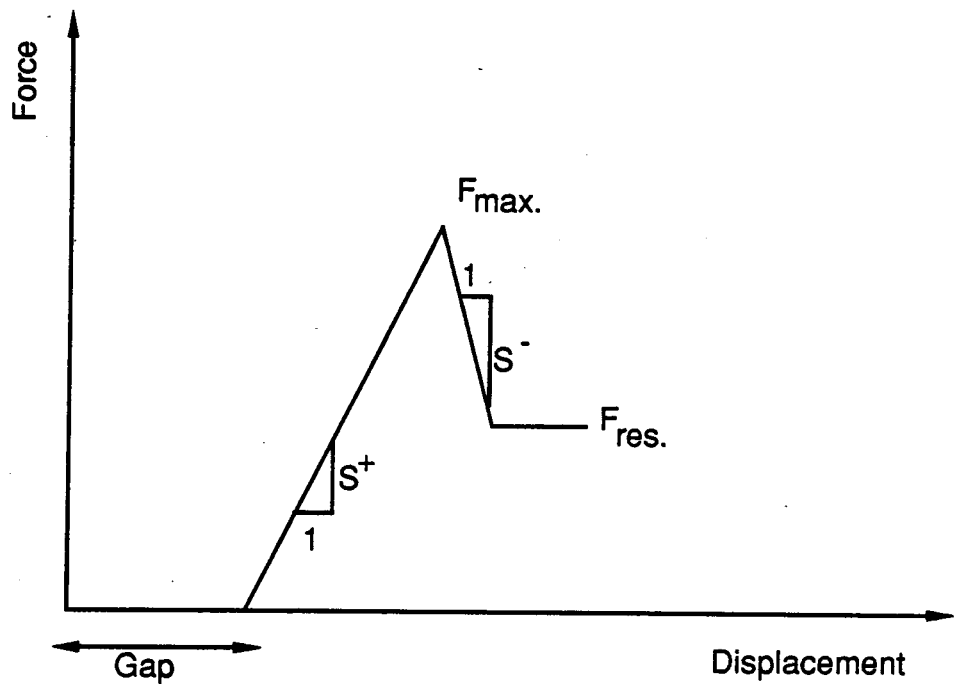

Figure 5.7 Ice Element with A Gap

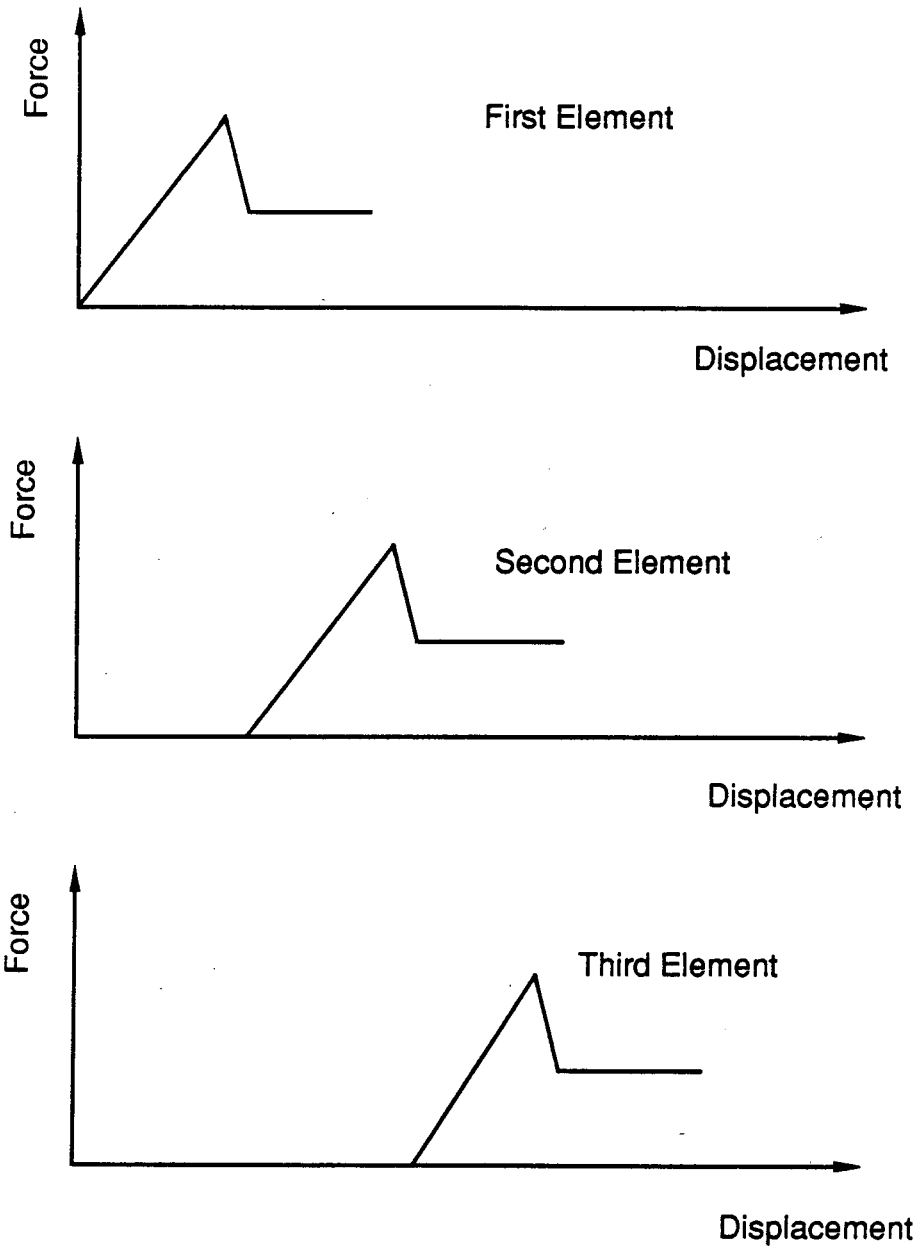

Figure 5.8 Variation of The Gap from One Ice Element to Another

0.04, 0.08, and 0.10 m/s, respectively. The fifth and the sixth cases have ice velocity of 0.06 m/s and thicknesses of 3 and 5 m, respectively. Table 5.1 summarizes the six cases considered in this chapter. Results of the different cases are shown in conjunction with discussion of the effects of the parameters.

5.4.1 Test case

A test case is studied with the model in order to examine its overall performance. The ice event during which the ice forcing function shown in Fig. 4.2 was recorded, is used. All the conditions of the event are known, including the interaction force. The results of the analysis are discussed in the following subsection. Also a comparison is made between these results and those from the direct dynamic analysis of Chapter 4.

5.4.2 Results and comparison

The interaction force for all the cases studied using the interaction model are shown in Fig. 5.9. A typical cycle of the force during the steady state condition is shown in this figure. The solution of the equations of motion is made using the same numerical scheme and time step size as in the case of the direct dynamic analysis of Chapter 4. This is done to avoid differences in the results due to these factors and hence, a direct comparison can be made.

From Fig. 5.9 it can be seen that the predicted interaction force compares well with the recorded forcing function in Fig. 4.2. The interaction forces shown in Fig. 5.9 correspond to the analyzed strip of the structure. This means that these are acting on a strip of 1.22 m width.

Table 5.1 Cases Considered Using The Interaction Model

Case No.	Ice Velocity	Ice Thickness
	m/s	m
1	0.06	9.0
2	0.04	9.0
3	0.08	9.0
4	0.10	9.0
5	0.06	5.0
6	0.06	3.0

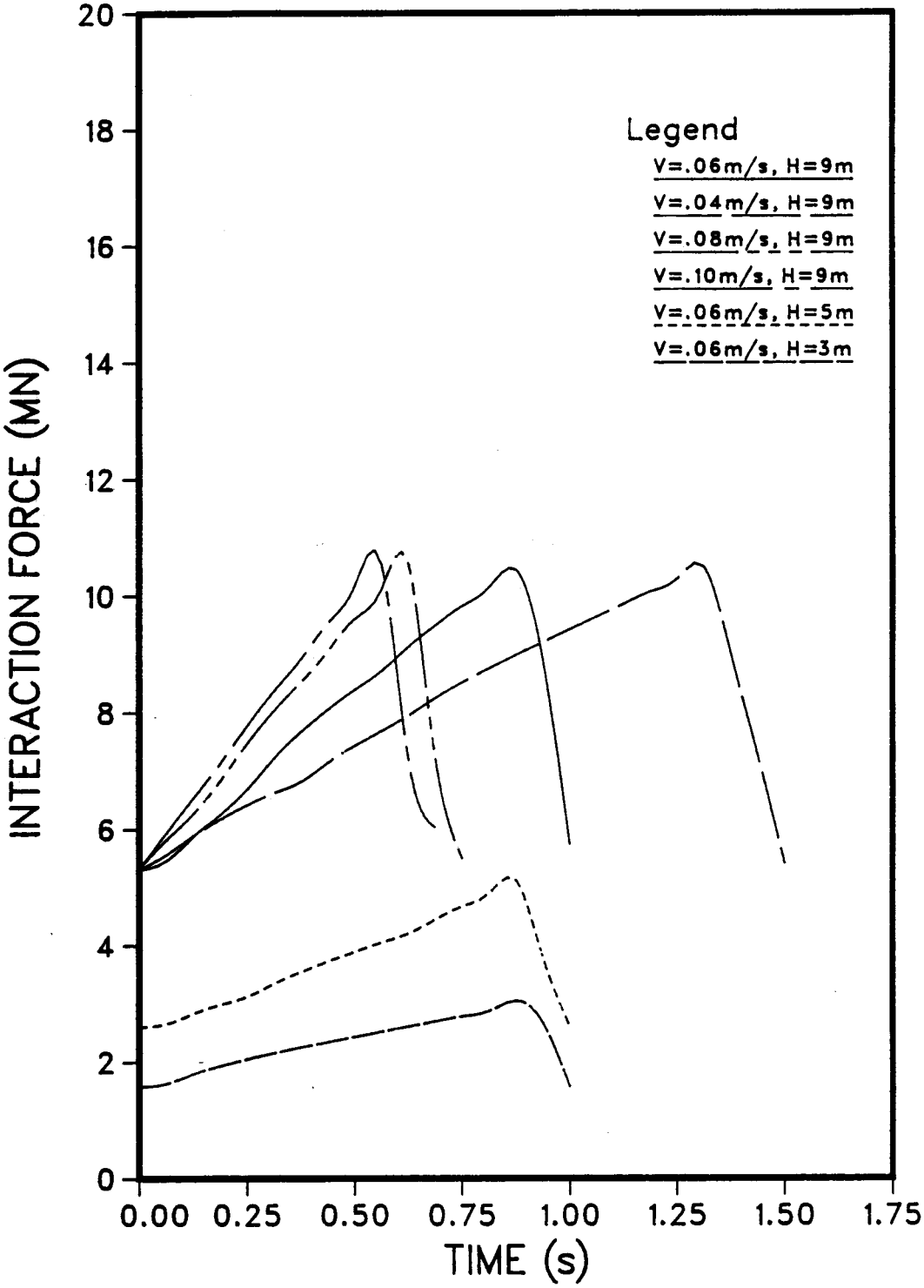

Figure 5.9 Predicted Interaction Forces

The kinematic response of the structure for the first case is also comparable to the response from the direct dynamic analysis. Displacements, velocities, and accelerations at both the ice side and the opposite side are shown in Figs. 5.10 through 5.15.

The maximum displacement on the loaded side is about 75 mm and on the unloaded side is about 2 mm. The velocities on the loaded side and the unloaded side reach values as high as 80 and 20 mm/s respectively. The maximum acceleration response on the loaded side is about 1.3 m/s^2 and on the other side is about 0.33 m/s^2. All these values are in very good agreement with the corresponding values from the direct dynamic analysis of Chapter 4. All these values occurred at the top of the caisson.

5.4.3 Effect of ice velocity

Three cases with different velocities for the ice are studied using the interaction model. Other parameters are the same as for the test case. The three velocities are 0.04, 0.08, and 0.10 m/s. From Fig. 5.9, it appears that the ice velocity has a direct effect on the crushing frequency of the ice. It can be noticed from this figure that the crushing frequency is linearly proportional to the ice velocity. The same phenomenon was reported by Peyton (1966) and Blenkarn (1970). It was found by them from force records measured in the field, that the crushing frequency is proportional to the ice velocity. Maattanen (1980), who conducted indentation tests at CRREL also observed that the crushing frequency is linearly proportional to the ice velocity.

The amplitude of the interaction force, on the other hand, is not significantly affected by the ice velocity. This is expected since the proposed

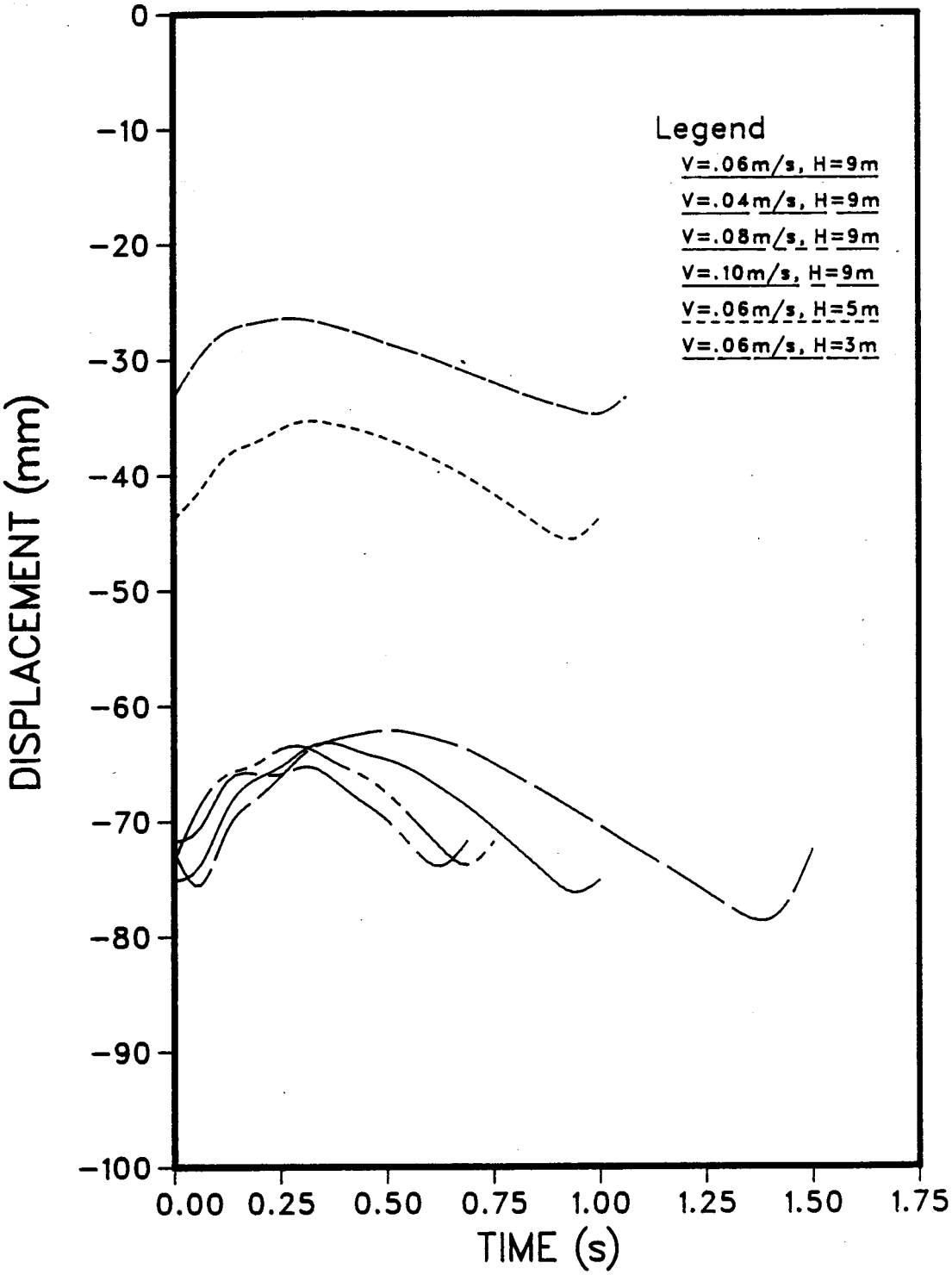

Figure 5.10 Displacement Response - Loaded Side

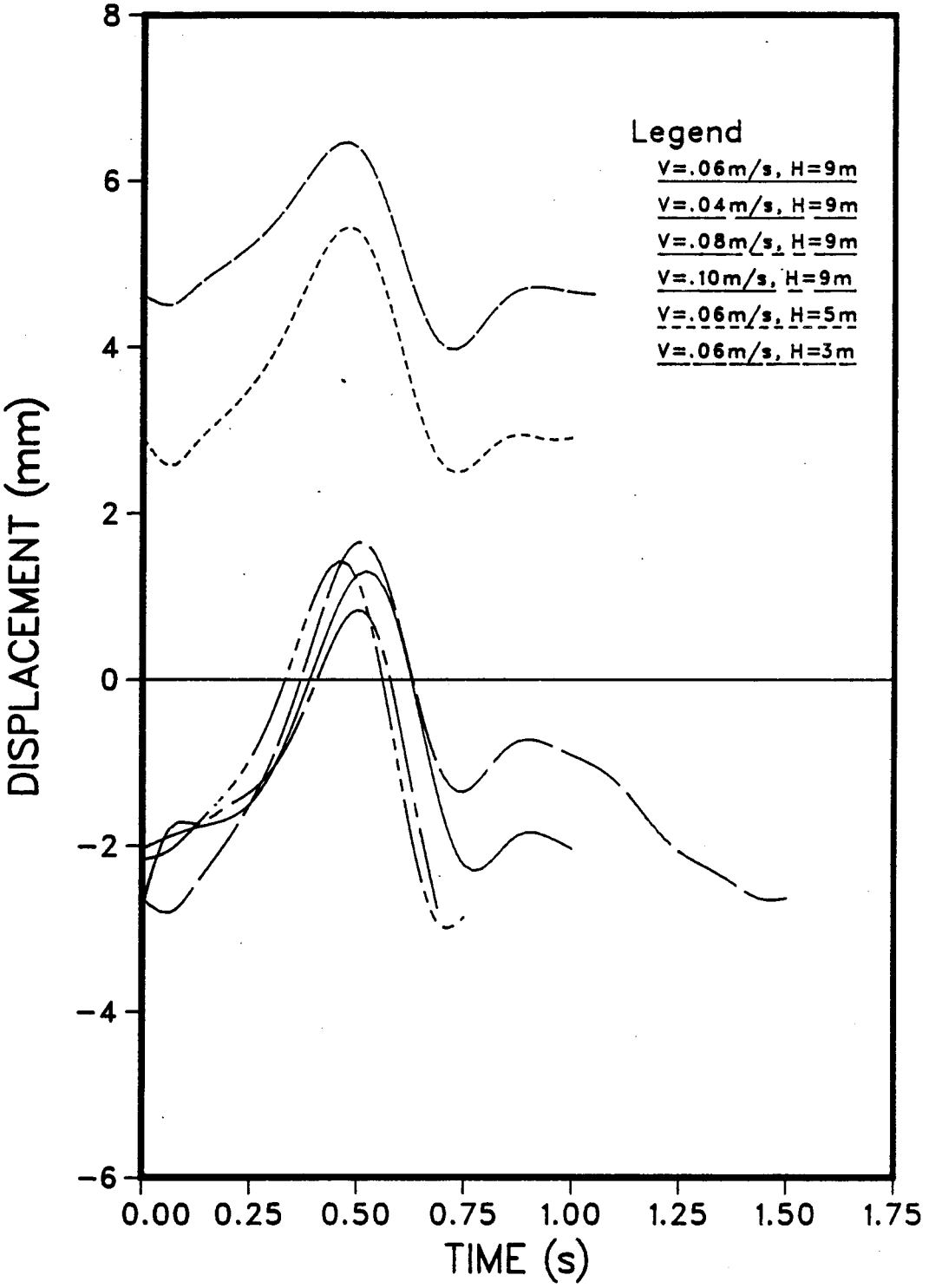

Figure 5.11 Displacement Response - Unloaded Side

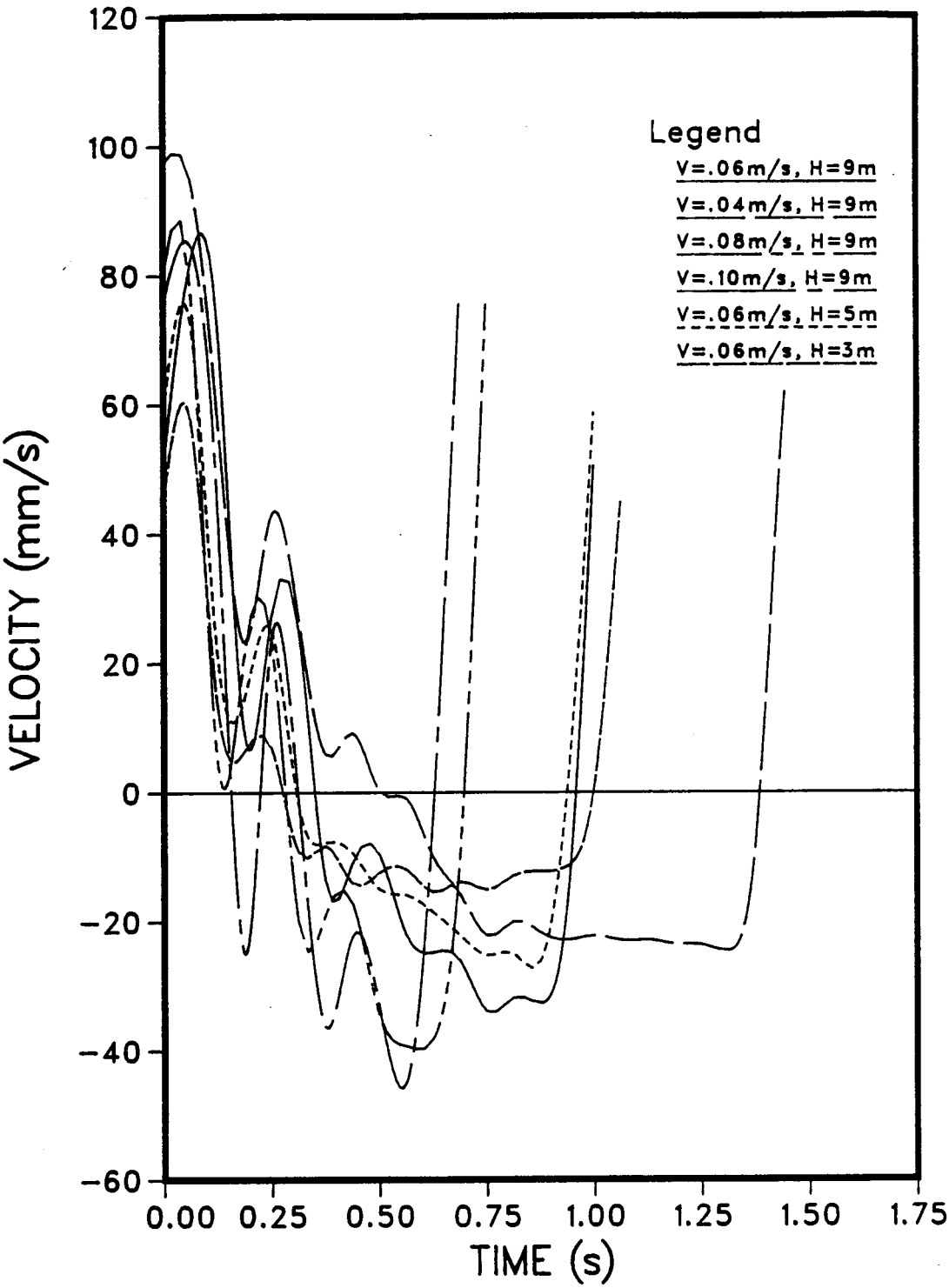

Figure 5.12 Velocity Response - Loaded Side

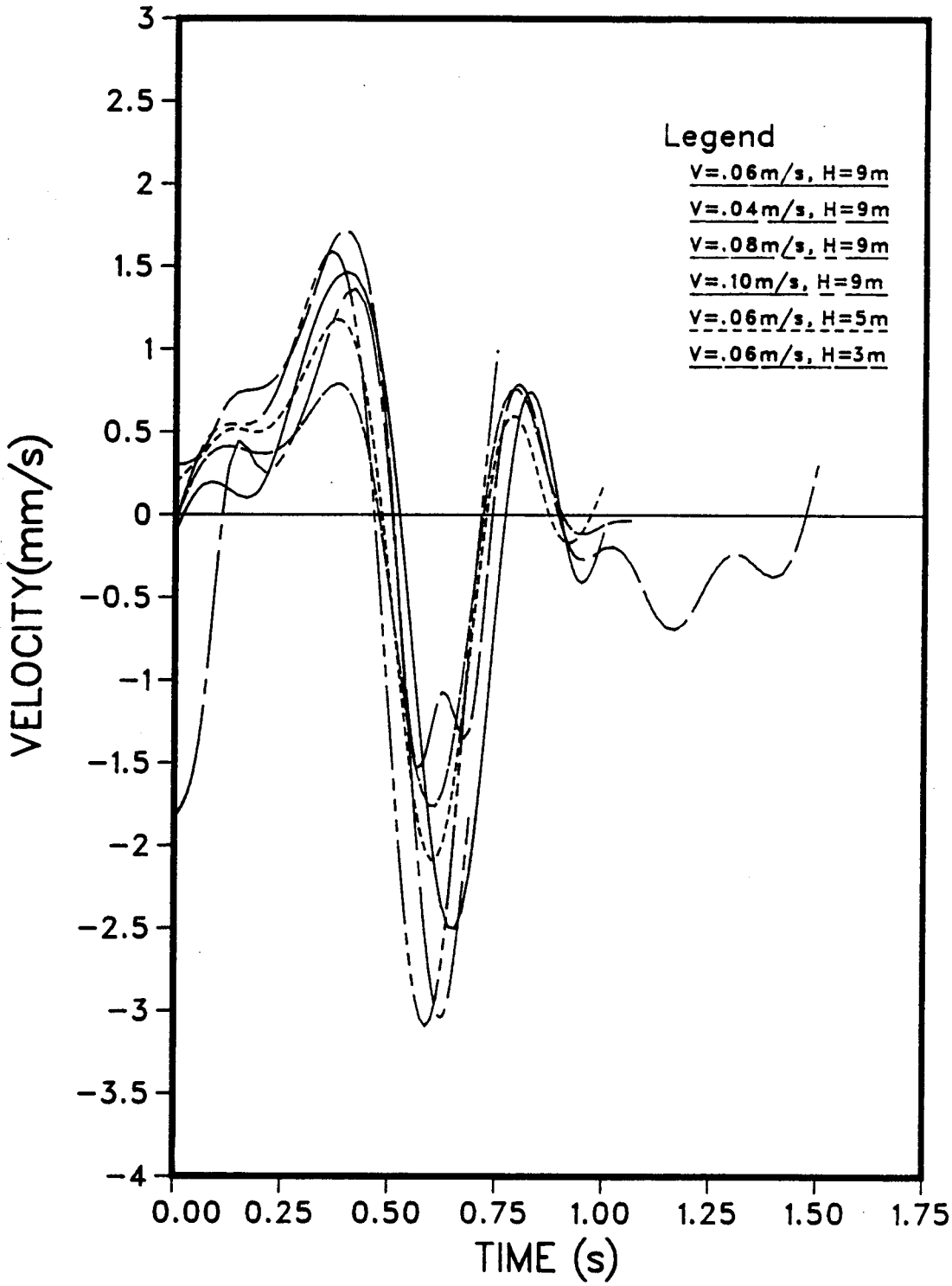

Figure 5.13 Velocity Response - Unloaded Side

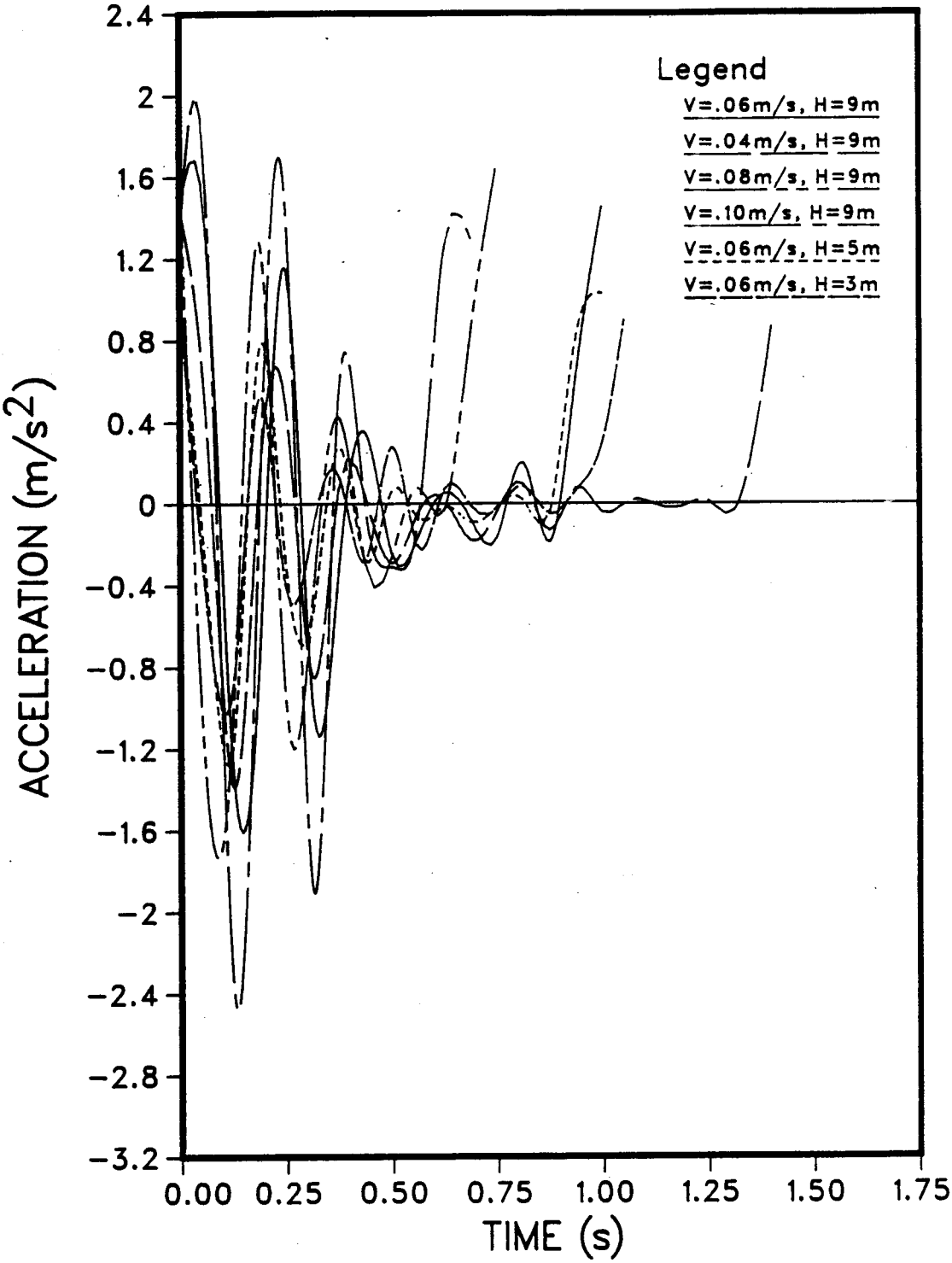

Figure 5.14 Acceleration Response - Loaded Side

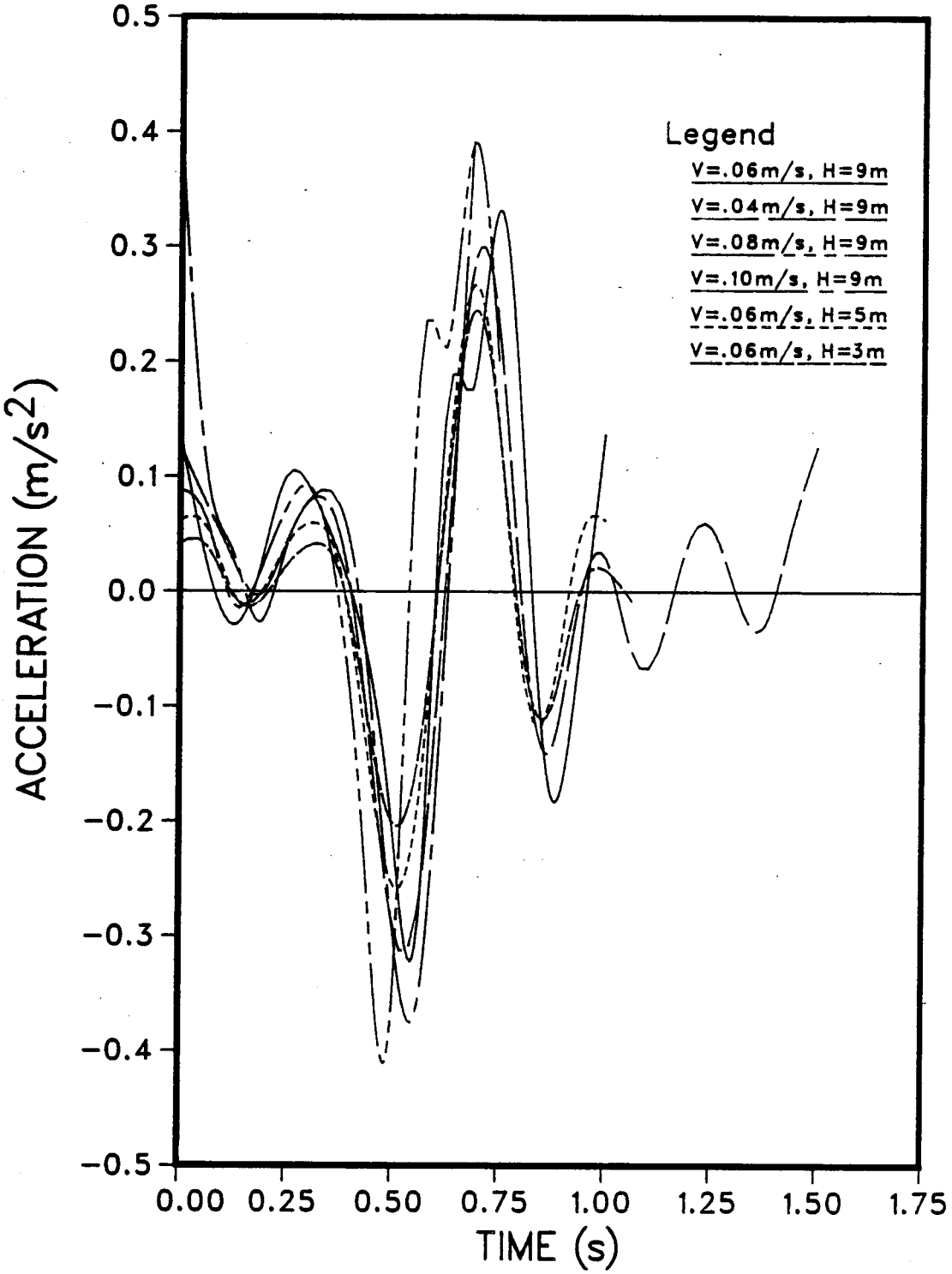

Figure 5.15 Acceleration Response - Unloaded Side

interaction model is based on pressure versus area curve and that does not take the ice velocity into consideration. However, according to the strain rate definition of Bohen and Weingarter (1985), the strain rate in all of the cases studied here lies in the brittle range. Therefore, the effective pressure is independent of the strain rate and hence is not a function of the ice velocity.

The kinematic response of the structure (displacements, velocities, and accelerations) in the three cases indicate that the response does not vary significantly between these cases. This is due to the small range within which the ice velocity has been varied.

5.4.4 Effect of the ice thickness

Two cases are analyzed in order to investigate the effect of the ice thickness on the interaction force and the response of the structure. Ice thicknesses of 3 and 5 m are used, while the ice velocity is kept as 0.06 m/s.

The resulting interaction force for the two cases are shown in Fig. 5.9. It is observed that the amplitude of the force is much less than that of the 9 m thick cases. The reduction in the ice force in these two cases is related directly to the decrease in the two parameters F_{max} and consequently F_{res} in the interaction model. The maximum ice force is equal to the effective pressure times the thickness of the ice sheet times the width of the structure. It is noticed from the pressure versus area curve, shown in Fig. 5.6, that the smaller the contact area the higher the effective pressure. However, the total force in the cases of 3 and 5 m ice thickness is still much smaller than the forces in the cases of 9 m thickness. This is due to the big reduction in the contact area.

It can be seen from Fig. 5.9 that the ice thickness has no significant effect on the crushing frequency. In fact, it is expected that the crushing frequency depends on the size of the crushed zone of ice ahead of the structure. If the size of this zone is a function of the ice thickness, there can be a relationship between the crushing frequency and the ice thickness.

Neill (1976) reported that during interaction between moving ice and piles or bridge piers, the size of the crushed zone varies between 0.2 and 0.5 times the ice thickness. Based on that, Neill suggested that the crushing frequency varies between (2V/H) and (5V/H) (V is the ice velocity and H is the ice thickness). According to the observations of Neill, the crushing frequency is directly proportional to the ice velocity and inversely proportional to the ice thickness.

In the interaction between ice and piles or bridge piers, the ice thickness is usually less than 1.0 m. Failure of ice by flaking on the top and bottom surfaces of the ice sheet is common if the ice thickness is small. If the flaking mode of failure occurs, the length of the crushed zone in front of the structure can be as much as half the ice thickness (Neill, 1976). When the ice thickness becomes in the order of a few meters, one might expect a plane strain condition to exist through the thickness of the ice sheet. In this case, development of the flaking mode of failure in the ice sheet is not possible. Therefore, there is no direct relationship between the crushing frequency and the ice thickness.

In his experiments, Timco (1986) conducted indentation tests on S2 freshwater ice sheets in the brittle range of strain rate. He observed that a thin layer of pulverized ice was formed ahead of the indentor, as shown in Fig. 5.16.

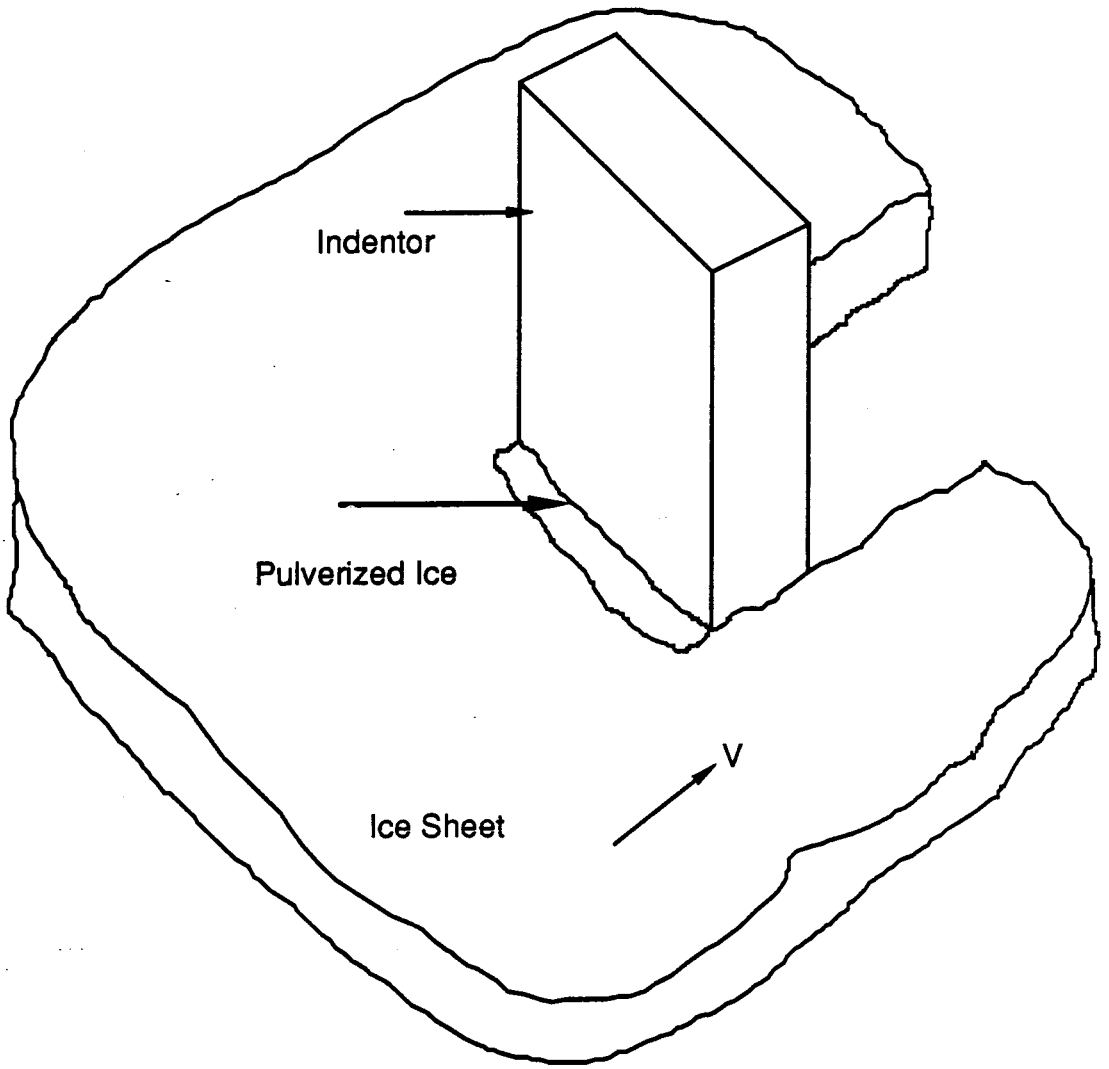

Figure 5.16Thin Pulverized Ice Layer Ahead of Indentor

It seems that this phenomenon is associated with a plane strain condition through the thickness of the ice sheet. In this case the thickness of the ice has little to do with the crushing frequency and that explains why the ice thickness does not affect it.

The kinematic response (displacements, velocities, and accelerations) for the last two cases is shown together with the other cases in Figs. 5.10 through 5.15. It is apparent that the response decreases significantly as the ice thickness decreases. This is because the resultant force gets smaller as the ice thickness decreases. It can be seen from Fig. 5.11 that the displacement at the top of the caisson on the unloaded side is always positive for the cases of 3 and 5 m ice thickness. For the other cases, it varies between positive and negative. The response of the structure shown in these figures is due to both the horizontal and vertical loads. In the cases of 3 and 5 m thickness, the effect of the ice force on the unloaded side of the caisson is not sufficient to counterbalance the deformation under the static vertical loads. Thus, the displacement on the unloaded side of the caisson is positive all the time.

For the sake of completeness, the stresses in the different structural elements for all the six cases considered here are shown in Figs. 5.17 through 5.24. The results are presented for the same set of finite elements used in Chapter 4 so that a comparison can be made. From these figures, it can be seen that the stresses in general are significantly less than the yield stress. An interesting point here can be concluded from the figures. For some elements, the smaller the ice thickness the higher the stresses in the elements. The stresses in the different elements are function of the total force as well as its point of application. According to the Archimedes principle, the ratio between the portion of the ice

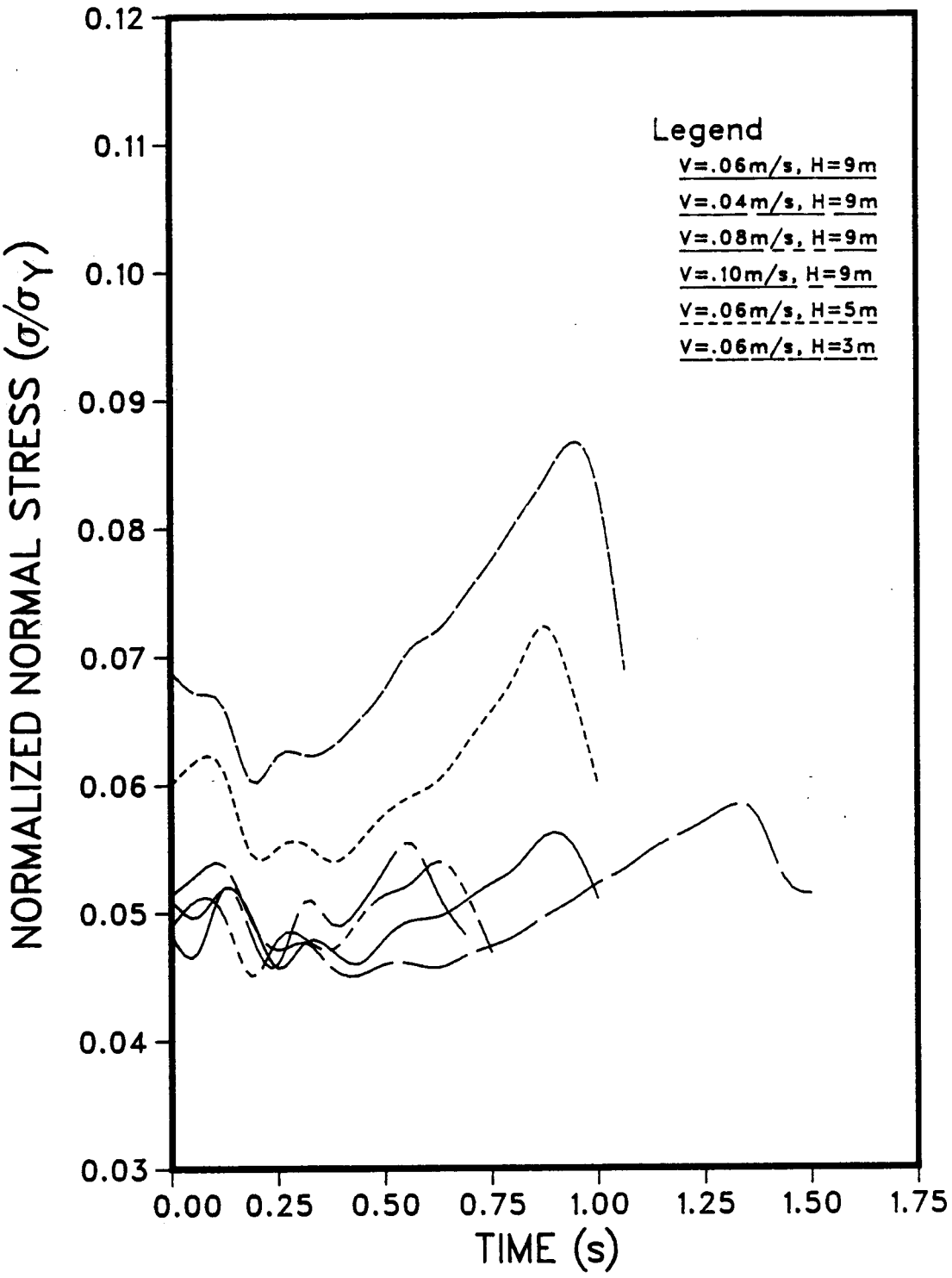

Figure 5.17 Normalized Normal Stress - Stiffener

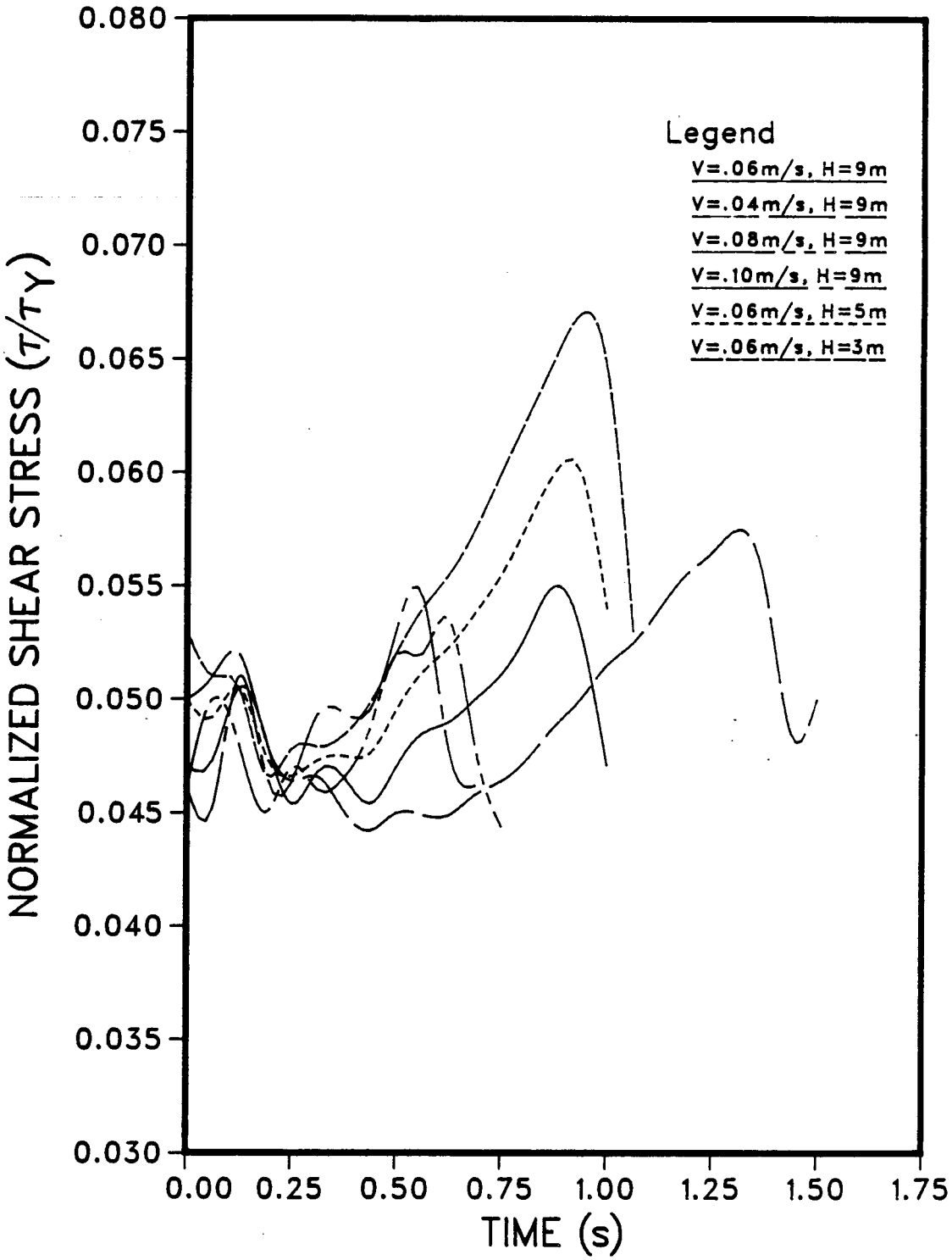

Figure 5.18 Normalized Shear Stress - Stiffener

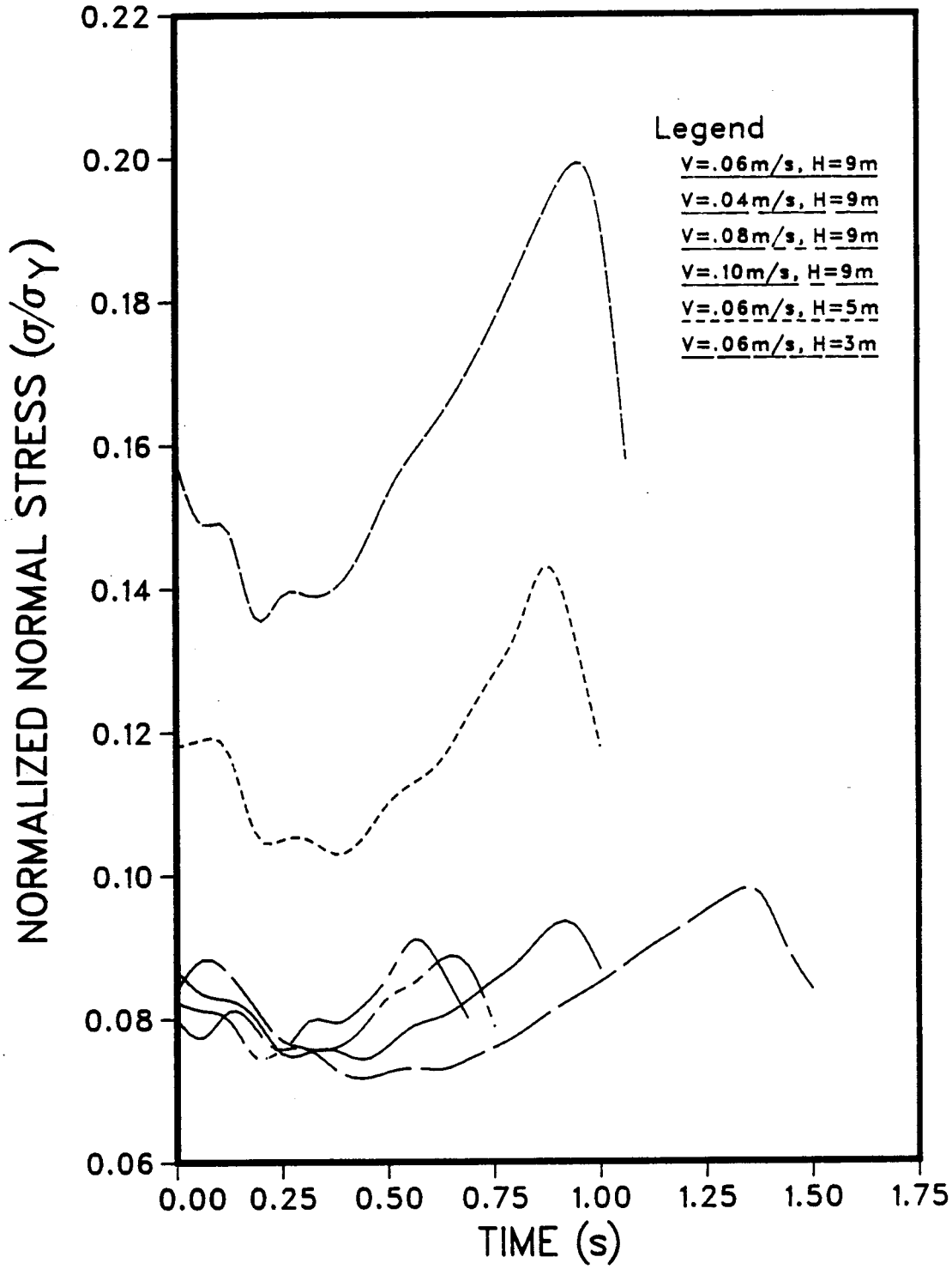

Figure 5.19 Normalized Normal Stress - Intermediate Frame

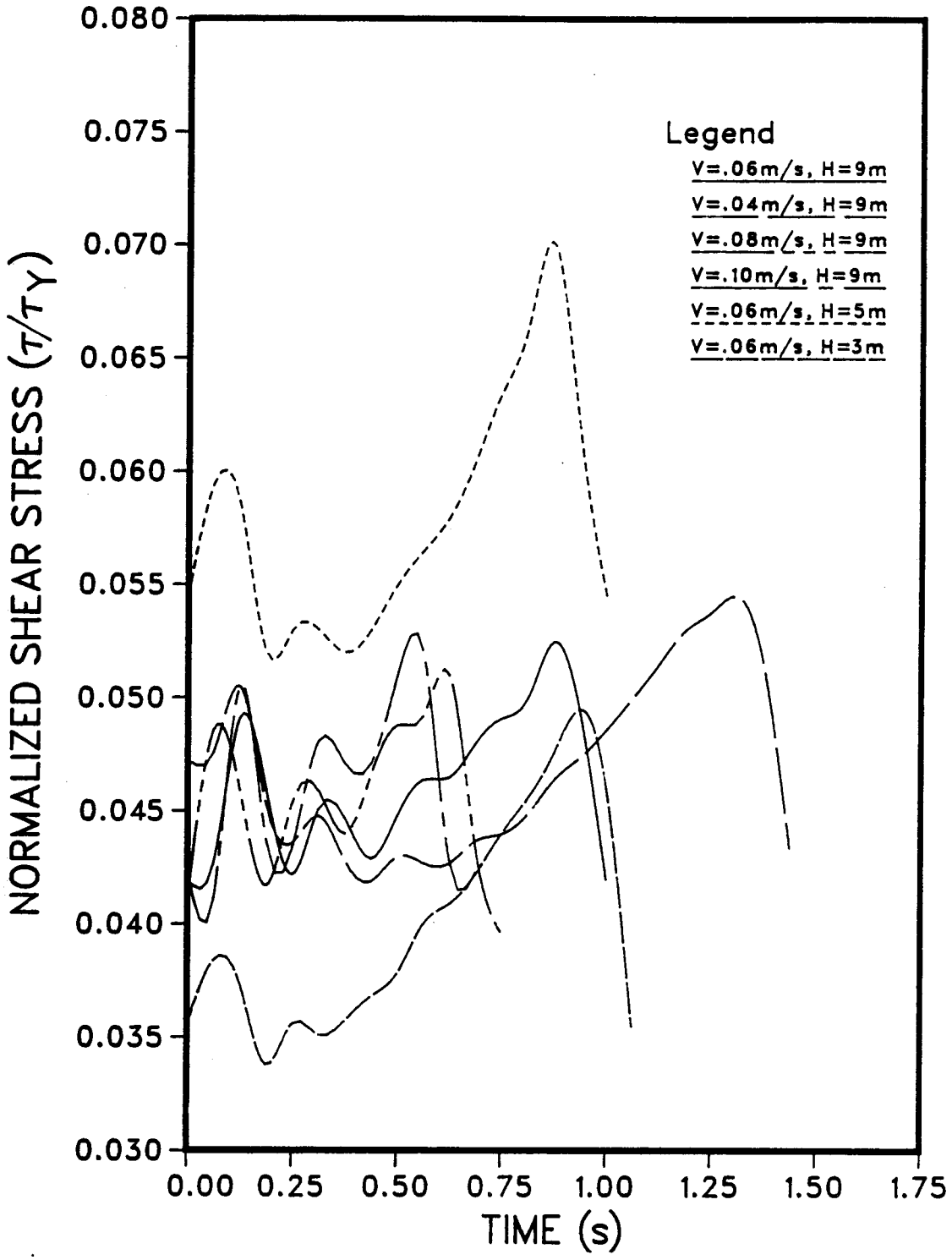

Figure 5.20 Normalized Shear Stress - Intermediate Frame

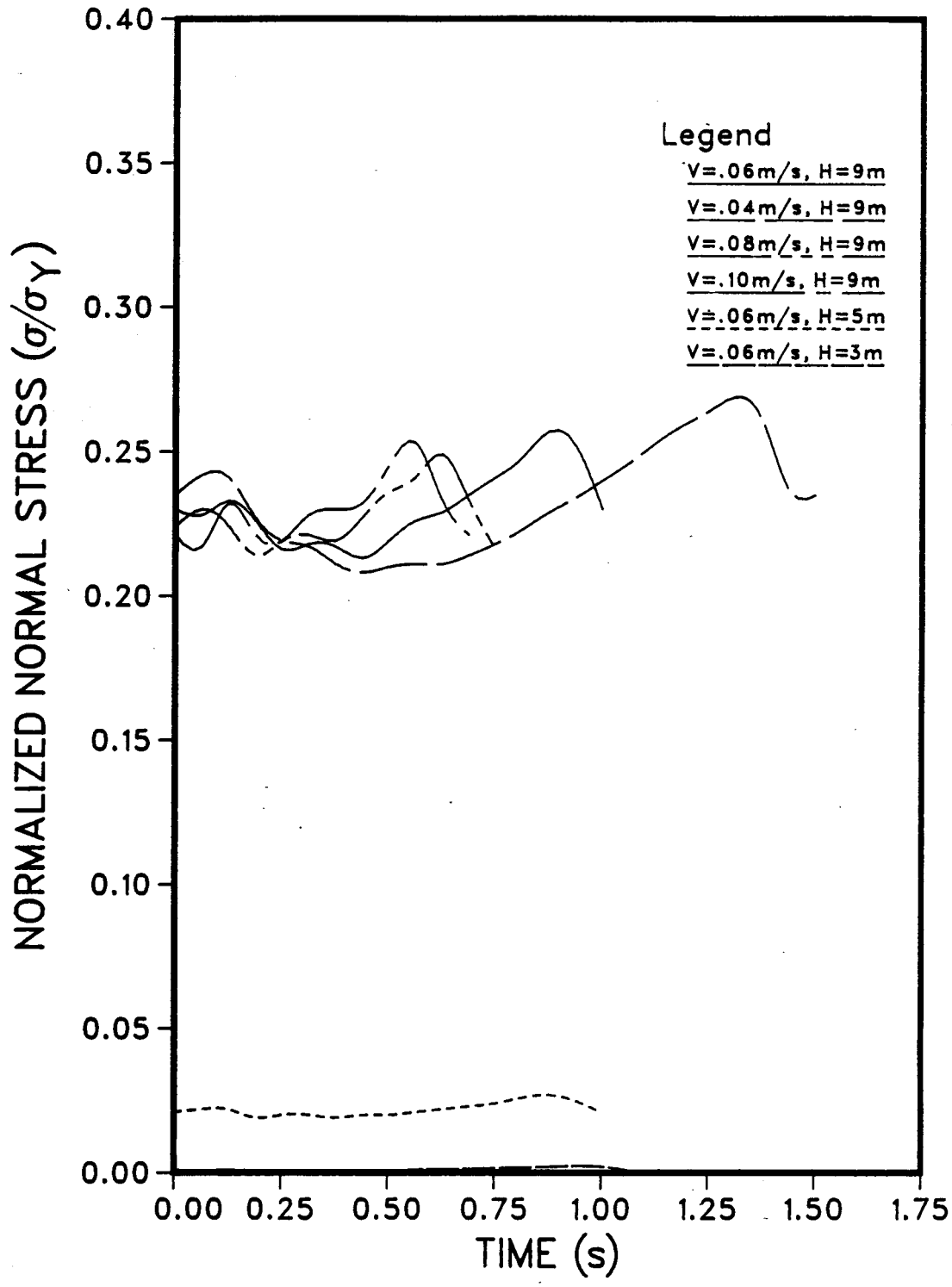

Figure 5.21 Normalized Normal Stress - Horizontal Frame

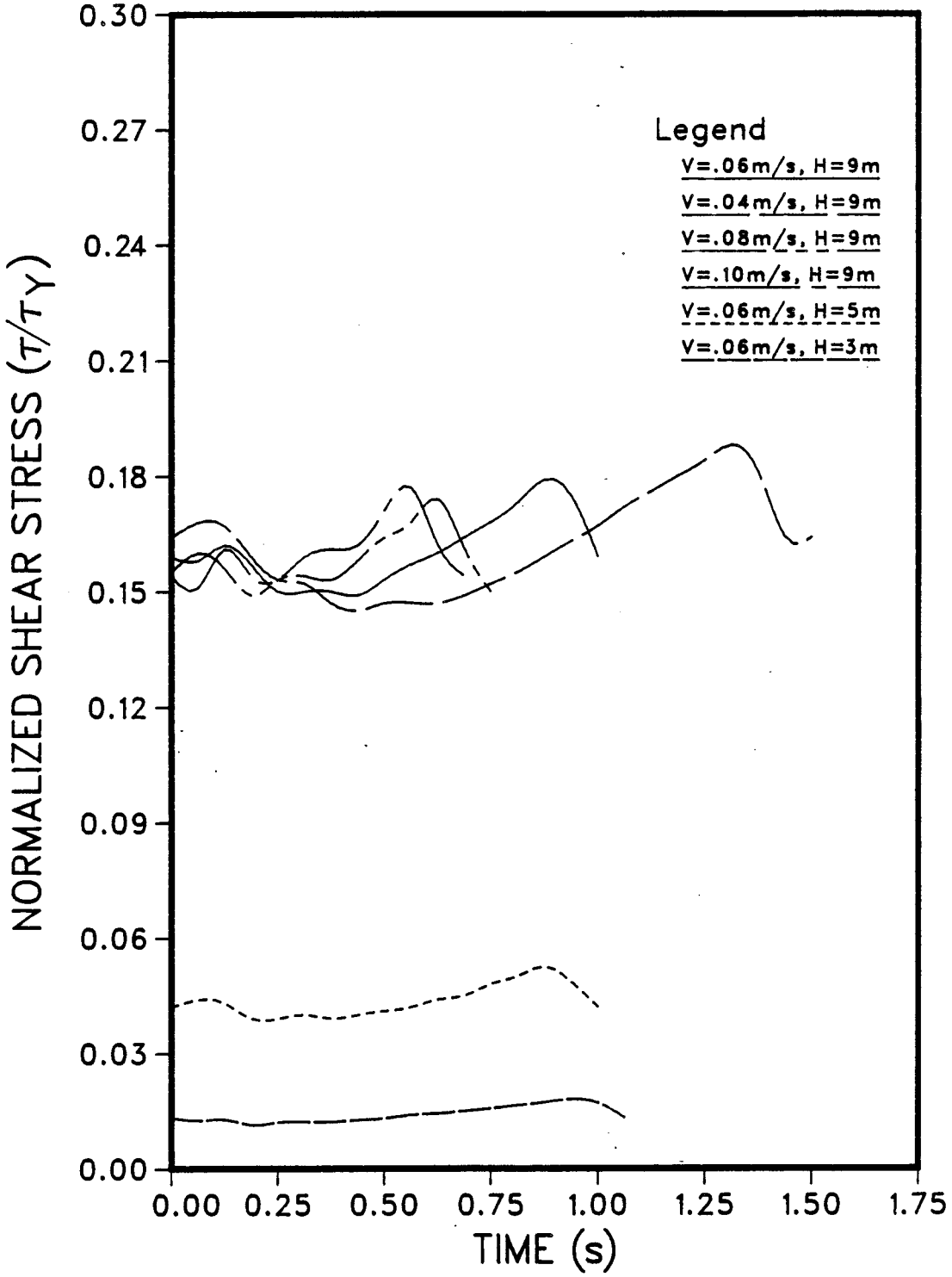

Figure 5.22 Normalized Shear Stress - Horizontal Frame

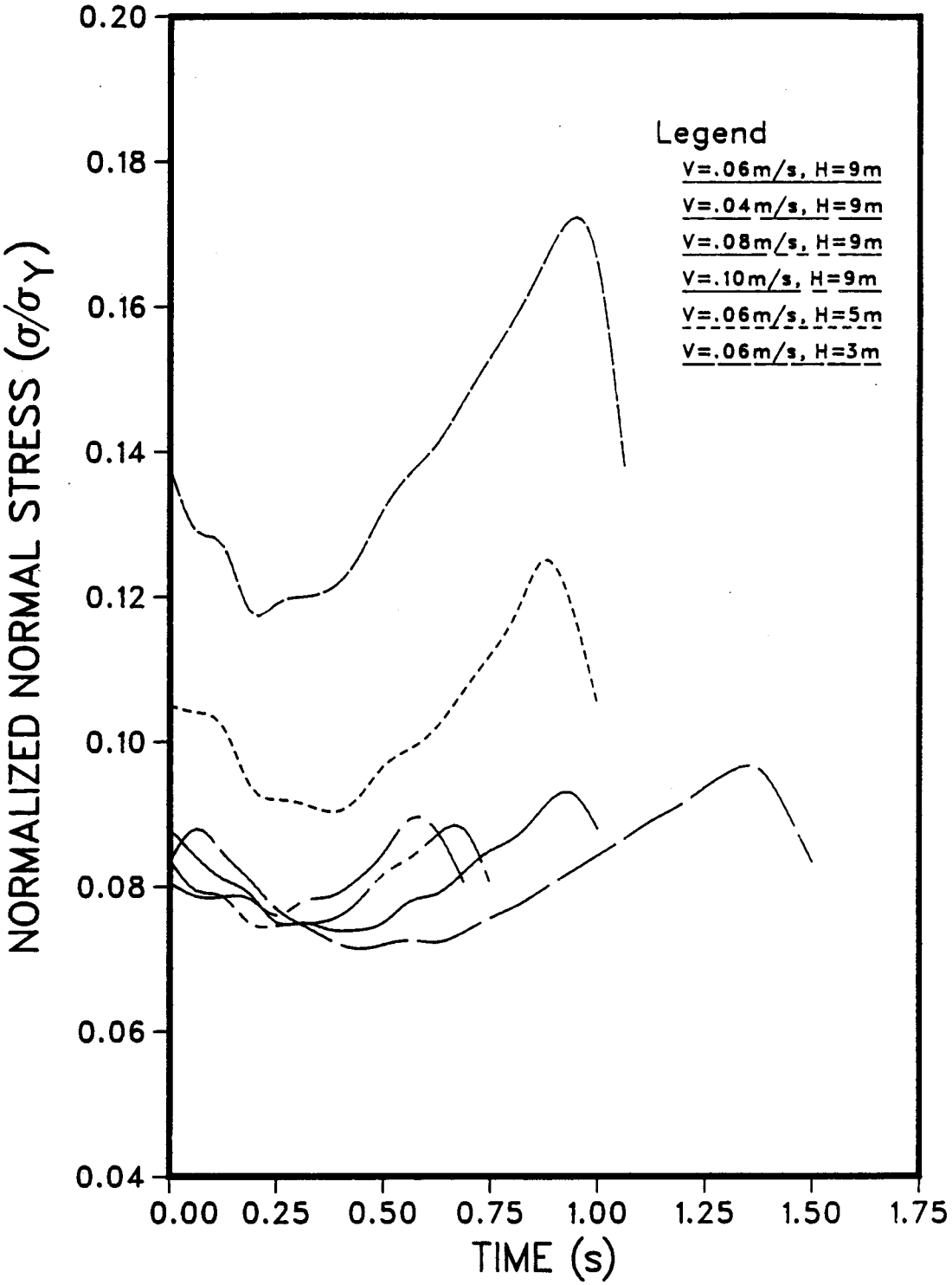

Figure 5.23 Normalized Normal Stress - Bulkhead

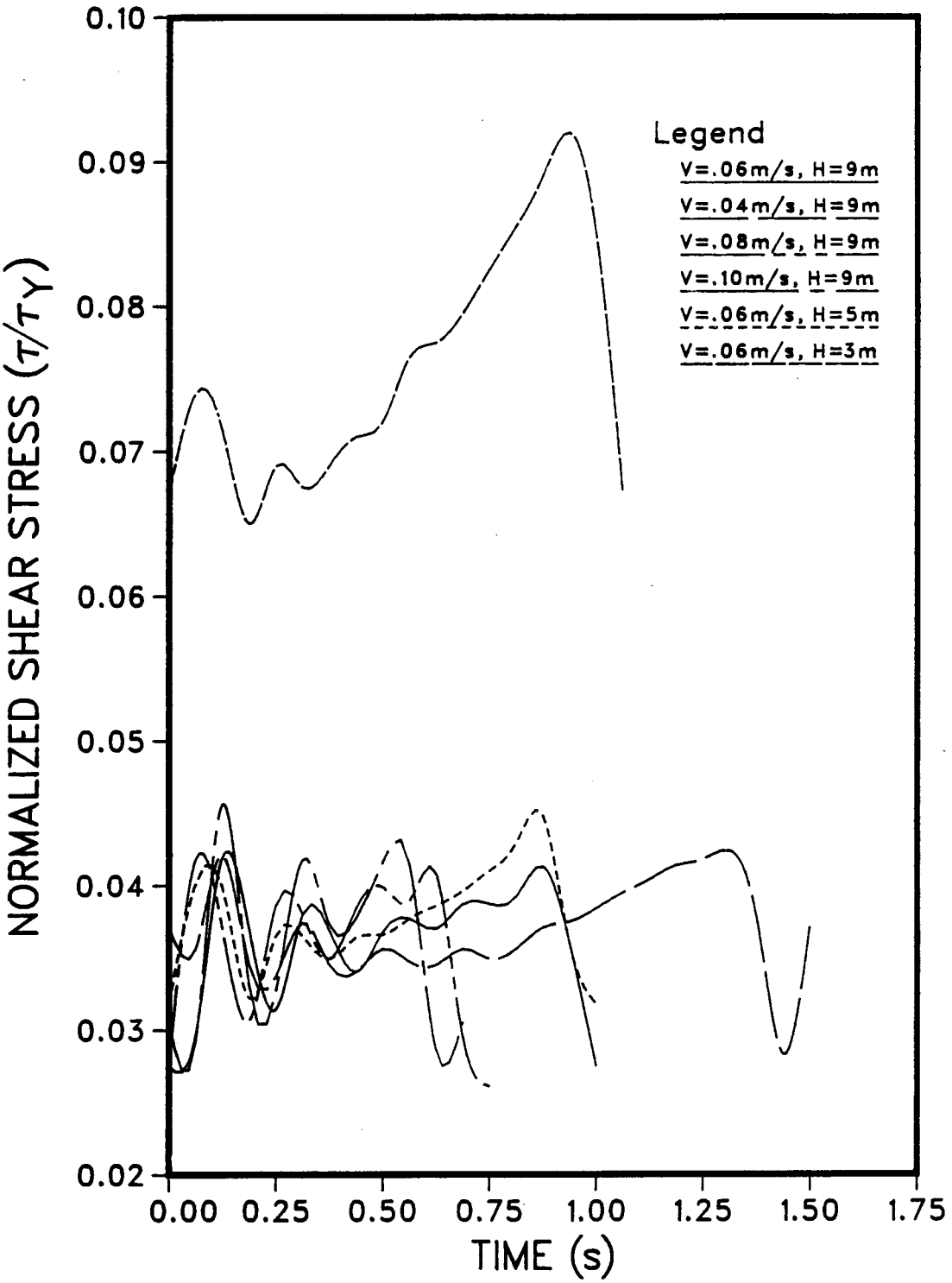

Figure 5.24 Normalized Shear Stress - Bulkhead

thickness that lies below the sea water level and the total thickness of the ice sheet is equal to the ratio between the d ensities of the ice and water. This means that, the point of application of the resultant ice force is a function of the ice thickness. Because of this the smaller ice thicknesses can be more critical for some elements than the bigger thicknesses.

6- VISCOELASTIC INTERACTION MODEL

6.1 Introduction

In the interaction analysis presented in Chapter 5, the structure is represented in detail while the impinging ice is represented in a relatively simple manner. The response of the structure and the stresses in the different structural components are the main concern in that analysis. The behavior of the ice under the variable stress history as it approaches the structure is not simulated in the analysis. However, a reduced modulus of elasticity is used in order to take the effect of the stress history on the ice into consideration. In this chapter, another interaction model is presented. The impinging ice is represented in detail in this model in order to simulate the constitutive behavior of ice in the analysis.

A viscoelastic dynamic analysis for the ice-structure interaction problem is presented in this chapter. In this model, ice is represented in the analysis as a series of elements with the far end moving with a prescribed constant velocity. The behavior of the ice elements is simulated using Sinha's model that describes the long term continuum behavior of ice. A detailed discussion of the viscoelastic model developed by Sinha (1978) is presented in both total and incremental formulations.

The manner in which the crushed ice is represented in the analysis is described along with the proposed failure criterion. The finite element formulation of the viscoelastic behavior is then given along with a derivation of the system of equilibrium equations. Implementation of the viscoelastic finite element formulation in dynamic analysis is shown. A detailed explanation of the

solution algorithm of the system of equations of motion is also presented. Finally, results of several cases that have been analyzed using the proposed viscoelastic interaction model are given.

6.2 Creep behavior of ice

Ice displays a wide range of mechanical properties like elasticity, plasticity, viscosity, and brittle fracture. Loading rate, temperature, and degree of confinement are among the factors that affect the constitutive behavior of ice. Creep studies on ice show that the material undergoes significant creep deformations when subjected to permanent stresses (Sinha, 1978).

Many models have been developed in order to describe the continuum behavior of ice. Some of these models are based on standard viscoelastic models (Maxwell fluid and Maxwell-Kelvin standard solid) Shapiro (1978) and Ting (1985). Other models represent the constitutive behavior of ice as a continuum undergoing damage e.g. Michel (1981) and Karr (1984). A semi-empirical uniaxial model for ice has been proposed by Wang (1982) in order to describe the uniaxial behavior of sea ice under constant strain rate, constant stress rate, and constant stress conditions. According to the model, decomposition of the total strain into elastic and viscous strain components is not possible. In the following subsection, the creep equation developed by Sinha (1978), which has been used in this study, is discussed in detail.

6.2.1 Sinha's creep equation

Sinha (1978) conducted a series of uniaxial compression creep tests on transversely isotropic columnar-grained S2 ice at -10^{o}C. The long axes of the

grains were normal to the loading direction which is the case encountered in ice-structure interaction. Based on his results, Sinha developed a creep equation to describe the long term behavior of ice under constant stress. In his equation, Sinha decomposed the total strain (ε_t) into three components. These are, a pure elastic and instantaneously recoverable strain (ε_e), a delayed elastic recoverable strain (ε_d), and a permanent or viscous strain (ε_v). Thus, the total strain can be written as,

$$\varepsilon_t = \varepsilon_e + \varepsilon_d + \varepsilon_v. \tag{6.1}$$

The associated rheological model consists of a spring, a Kelvin element (a spring in parallel with a dashpot), and a dashpot all in series (Fig. 6.1). The different strain components can be calculated using the following expressions given by Sinha:

$$\varepsilon_e = \sigma/E,$$

$$\varepsilon_d = c_1 (d_1/d)\, (\sigma/E)^s\, [1-\exp(-a_T t)^b], \text{ and}$$

$$\varepsilon_v = \dot{\varepsilon}_{v1}\, t\, (\sigma/\sigma_1)^n \tag{6.2}$$

where E is Young's modulus, c_1 is a constant corresponding to the reference grain size, d_1; b, n, s, and a_T are constants; and $\dot{\varepsilon}_{v1}$ is the viscous strain rate for unit or reference stress, σ_1. Both a_T and $\dot{\varepsilon}_{v1}$ are temperature-dependent. Sinha suggested the values shown in Table 6.1 for these constants.

Sinha (1981) developed an incremental form of his creep equation in order to predict the uniaxial deformation behavior of ice under variable loading conditions. In developing this incremental form, Sinha assumed that an

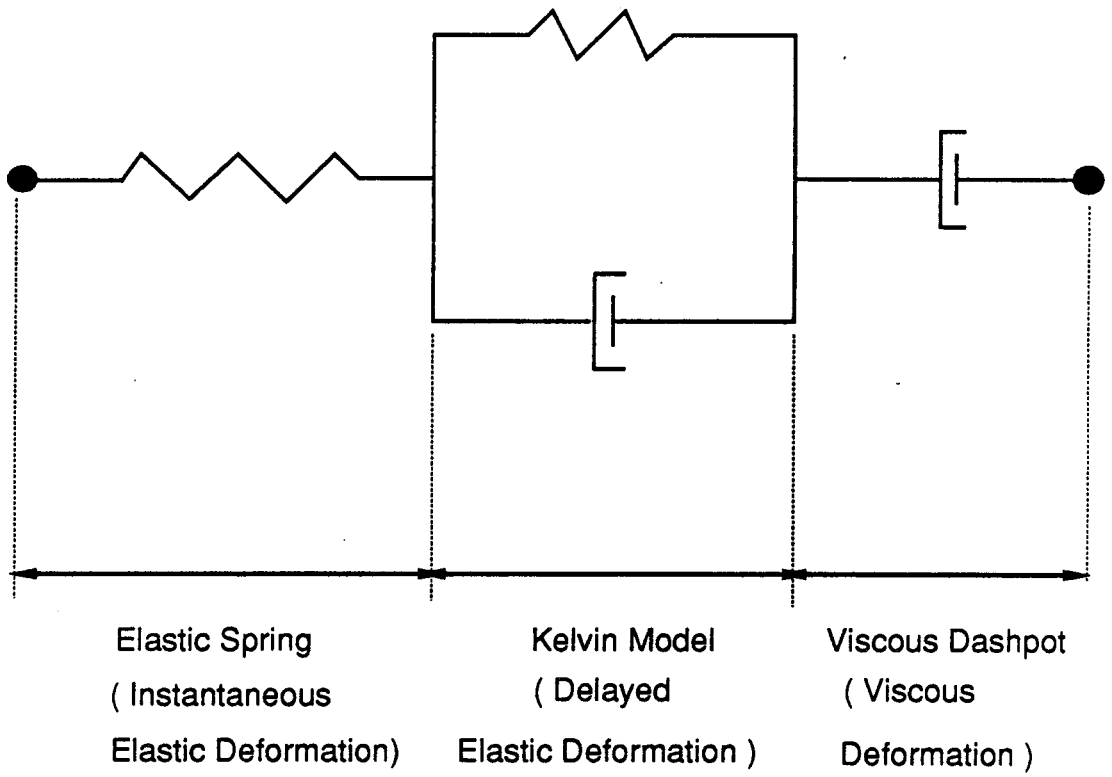

Figure 6.1 Rheological Model of Ice

Table 6.1 Numerical Values of The Constants of Sinha's Model

$E = 9.5$ GPa

$C_1 = 9.0$

$n = 3.0$

$b = 0.34$

$s = 1.0$

$a_T = 2.5 \times 10^{-4}\ s^{-1}$ at -10°C

$\dot{\varepsilon}_{v1} = 1.76 \times 10^{-7}\ s^{-1}$ at -10°C

$\sigma_1 = 1.0$ MPa

$d_1 = 1.0$ mm.

arbitrarily increasing stress history can be represented as a series of stress increments, each acting during an interval of time Δt. Supposing that $\Delta\sigma_1$, $\Delta\sigma_2$,.....$\Delta\sigma_N$, and $\Delta\sigma_{N+1}$ are the stress increments applied at times 0, Δt, $2\Delta t$,....., (N-1)Δt, and NΔt then, $\Delta\sigma_1$ is the total stress during the first interval of time, $\Delta\sigma_1+\Delta\sigma_2$ during the second interval, and so on. At time zero there is elastic strain due to $\Delta\sigma_1$ with no delayed elastic or viscous components. At the end of the first time interval the total strain consists of an elastic component produced by $\Delta\sigma_1+\Delta\sigma_2$ and delayed elastic and viscous components due to $\Delta\sigma_1$ applied for time Δt. The total strain due to the entire stress history can be written as follows:

$$\varepsilon_t = (1/E)\sum_{i=1}^{N+1}\Delta\sigma_i + (c_1/E)(d_1/d)\sum_{i=1}^{N+1}\Delta\sigma_i\,[1-\exp(-(a_T(N+1-i)\Delta t)^b]$$

$$+\varepsilon_{v1}\,(\Delta t/\sigma_1)\sum_{i=1}^{N}(\sum_{j=1}^{i}\Delta\sigma_j)^n. \qquad (6.4)$$

This equation represents the qualitative behavior of see-ice as well as freshwater-ice and the only difference would be in the numerical values of the parameters. Since the proposed model is not intended to be a predictive tool, at this stage, Sinha's model is used in this study. In the following section the finite element formulation for viscoelastic materials is discussed.

6.3 Finite element formulation for viscoelastic problems

The equilibrium equations of a finite element system can be described using the principal of virtual work (Zienkiewicz, 1977). This principle states that the equilibrium of a body requires that for any compatible virtual displacement field that satisfies the essential boundary conditions, the total internal virtual work

is equal to the total external virtual work. Figure 6.2 shows a body with volume V and surface area S subjected to a system of body forces F, surface tractions T on S_T , and known boundary conditions on S_U. The equilibrium condition of this body, according to the principle of virtual work (virtual displacements), can be written as

$$\int_V \langle F \rangle \{\delta u\}\, dv + \int_{S_T} \langle T \rangle \{\delta u\}\, ds = \int_V \langle \sigma \rangle \{\delta \varepsilon\}\, dv \qquad (6.5)$$

where $\{\delta u\}$ is any continuous displacement field defined in V that is compatible with the known boundary conditions on S_U ($\{\delta u\}=\{0\}$ on S_U) and $\{\delta \varepsilon\}$ is its associated virtual strain field. The vector $\{\sigma\}$ is any equilibrium stress field that is in equilibrium with T and F. The left hand side of Eq. (6.5) is the external virtual work while the expression on the other side of the equation represents the internal virtual work. The principle of virtual work represents an equilibrium requirement and hence is valid regardless of the material behavior.

The volume V can be divided into finite elements each with simple geometry. The volume of a typical element is denoted as V_e and the part of its surface that is on S as S_e. The displacement field within each element can be approximated using continuous interpolation functions as follows

$$\{U\}=[N]\{q\}. \qquad (6.6)$$

The vector {U} contains the displacements at any point within the finite element, [N] is the matrix of interpolation functions, and {q} is the vector of the nodal degrees of freedom.

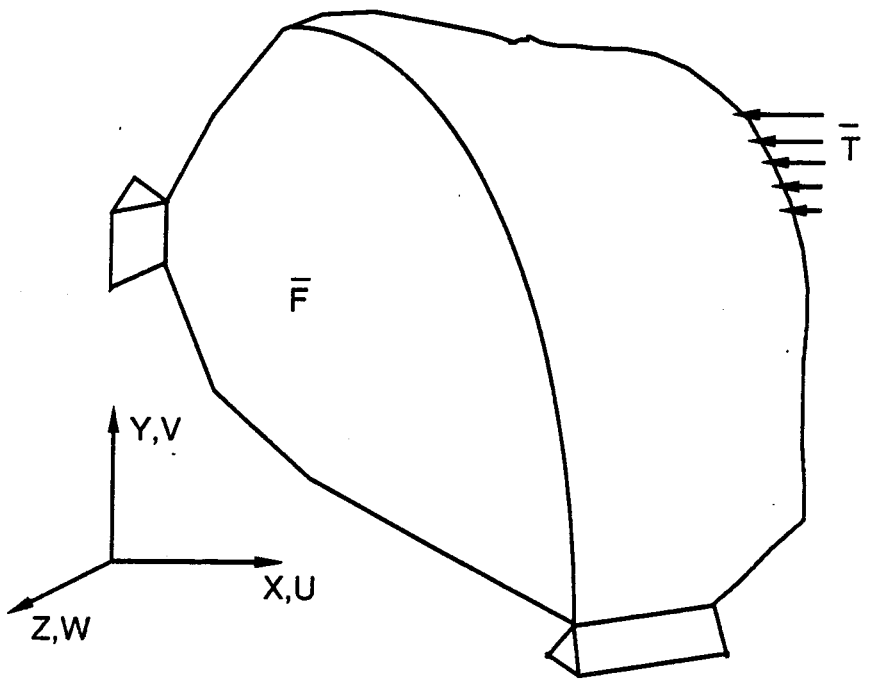

Figure 6.2 A General Body under A System of Body Forces and Surface Tractions

Since the strains can be calculated by differentiation of the displacements, the strain vector at any point can be written as

$$\{\varepsilon\}=[B]\{q\} \tag{6.7}$$

where [B] is a matrix that contains the spatial gradients of [N]. The principle of virtual work can now be written for the body as

$$\sum\int_{V_e} <\delta\varepsilon>\{\sigma\}\, dv= \sum\int_{V_e} <\delta u>\{F\}\, dv + \sum\int_{S_{T_e}} <\delta u>\{T\}\, ds \tag{6.8}$$

In this equation, the summation is made on all the finite elements in the body except for the last term where only the elements with sides on part S_T of S are considered. Substituting Eqs. (6.6) and (6.7) into (6.8), one gets

$$\sum\int_{V_e} <\delta q>[B]^T\{\sigma\}dv=\sum\int_{V_e} <\delta q>[N]^T\{F\}dv+\sum\int_{S_{T_e}} <\delta q>[N]^T\{T\}ds \tag{6.9}$$

Since $\{\delta q\}$ are arbitrary virtual nodal displacements, it follows that

$$\sum\int_{V_e} [B]^T\{\sigma\}\, dv= \sum\int_{V_e} [N]^T\{F\}\, dv + \sum\int_{S_{T_e}} [N]^T\{T\}\, ds. \tag{6.10}$$

Using the elastic constitutive relationship $\{\sigma\}=[E](\{\varepsilon\}-\{\varepsilon_0\})$ where [E] is the elasticity matrix and $\{\varepsilon_0\}$ is the initial strain field, Eq. (6.10) can be written as

$$\sum\int_{V_e} [B]^T[E]([B]\{q\}-\{\varepsilon_0\})dv=\sum\int_{V_e} [N]^T\{F\}dv +\sum\int_{S_{T_e}} [N]^T\{T\}\, ds. \tag{6.11}$$

The initial strain term can be transformed to the right hand side of this equation leading to

$$\sum\int_{V_e} [B]^T[E][B]\, dv\, \{q\} = \sum\int_{V_e} [N]^T\{F\}dv + \sum\int_{S_{T_e}} [N]^T\{T\}\, ds$$

$$+ \sum\int_{V_e} [B]^T[E]\{\varepsilon_0\}\, dv. \qquad (6.12)$$

This equation can be written in the abbreviated form as

$$\sum[K_e]\{q\} = \sum\{P_e\} + \sum\{P_0\} \qquad (6.13)$$

where $[K_e]$ is the element stiffness matrix , $\{P_e\}$ is the corresponding external load vector, and $\{P_0\}$ is the equivalent initial strain load vector. Carrying out the summation on all the finite elements in the body, the overall system of equilibrium equations can be obtained as

$$[K]\{r\} = \{R\} + \{R_0\} \qquad (6.14)$$

where [K] is the global stiffness matrix of the structure, {r} is the nodal degrees of freedom, {R} is the external load vector, and $\{R_0\}$ is the initial strain load

In this derivation, it has been shown that the initial strain field can be taken into consideration through an equivalent additional load vector. The last term on the right hand side of Eq. (6.12) represents the additional load vector for an initial strain field $\{\varepsilon_0\}$. Since in viscoelastic problems, the strains vary as functions of time, the problem can be treated incrementally as a series of elastic problems. At each time step the viscoelastic strain is calculated due to the previous stress history. This viscoelastic strain can be considered as an initial strain for the next step and hence, a corresponding equivalent load vector can be evaluated and added to the external load vector. Another elastic solution can be carried out at the new time step and the procedure can be repeated for any desired

time span (Creus, 1986). In the following section, the viscoelastic dynamic analysis of the ice-structure interaction process is discussed.

6.4 Viscoelastic dynamic analysis

In the viscoelastic dynamic analysis of the ice-structure interaction problem, the ice is represented as a train of two-node truss elements as shown in Fig. 6.3. In this analysis, the structure is represented as a single degree of freedom system since only the global behavior of the structure is of interest and not the local response of the different structural elements. The problem is a displacement-controlled one with the far end of the ice moving with a constant prescribed velocity. The constitutive behavior of the ice elements before crushing is represented using Sinha's model. This is done to take into consideration the effect of the stress history on the element as the ice approaches the structure. At some critical stress value, crushing occurs over a finite number of the ice elements followed by dynamic unloading. The number of the failed elements depends on the stresses in the different ice elements compared with the critical stress (the stress at which the ice fails).

The equations of motion for the ice-structure arrangement can be written as

$$[M]\{\ddot{x}\}+[C]\{\dot{x}\}+[K]\{x\}=\{F(t)\}. \tag{6.15}$$

The mass, damping, and stiffness matrices in this case include contributions from both the structure and the ice. The constitutive behavior of the viscoelastic material contributes to both the damping and stiffness matrices since the stress is a function of both strain and strain rate. In this case the problem becomes nonlinear if any of the springs or dashpots that represent the constitutive

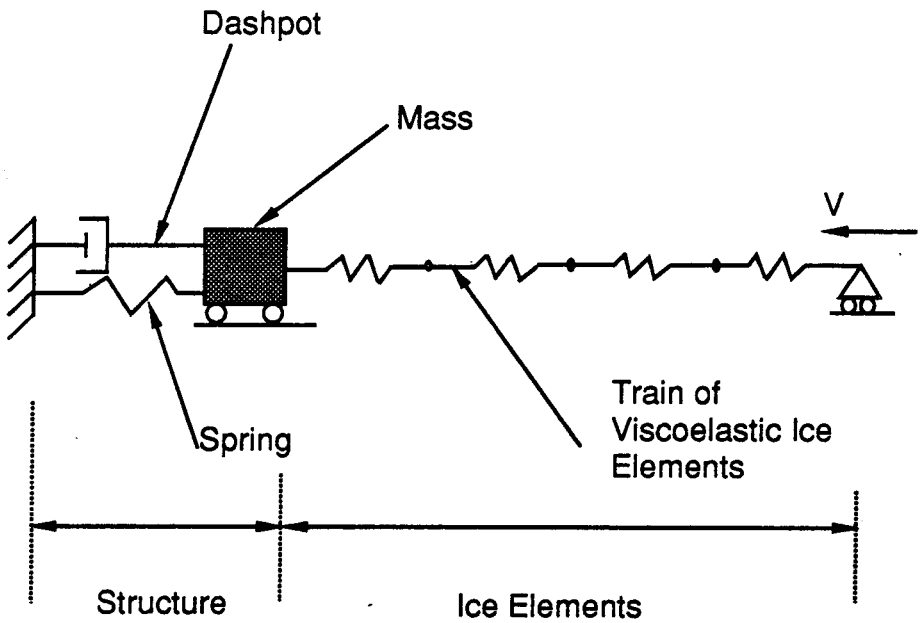

Figure 6.3 Ice-Structure Arrangement in Viscoelastic Analysis

behavior of the material is nonlinear. Sinha's model represent ice as a nonlinear viscoelastic material since the third term of the model is nonlinear. Therefore, representing the constitutive behavior of the ice on the left hand side of Eq. (6.15) results in a nonlinear dynamic problem. In this case both the damping and stiffness matrices are not constants.

The nonlinearity of the problem can be dealt with by treating the viscoelastic constitutive behavior as a series of elastic ones considering the viscous strain as an initial strain at each time step. In this case the viscous effect is converted to an equivalent load on the right hand side of Eq. (6.15) and the problem is solved as a linear elastic one. The solution algorithm in this case can be summarized as follows

1- Starting with a fully elastic condition at time equal zero, a complete solution can be obtained.

2- Using the stresses obtained at the first time step one can get the resulting viscous effect at the second time step using Sinha's model.

3-Solution of the equations of motion at the second time step is now possible after converting the viscous strains into equivalent set of external forces.

4- Steps 2 and 3 can be repeated any number of times in order to determine the response of the structure and the interaction force during the required period of time.

The solution algorithm outlined above is applicable as long as the moving ice behaves as a viscoelastic material. Once crushing occurs, the viscoelastic model cannot be used for the crushed ice and some other constitutive formula

must be implemented. In the following subsection the failure criterion at which crushing occurs and the behavior of crushed ice are discussed.

6.4.1 Simulation of crushed ice

When the stress in the ice sheet at the point of contact with the structure reaches the critical stress of the ice as determined from the pressure-area curve, crushing occurs. This results in unloading on both the structure and the ice sheet. Due to unloading, the structure springs back and at the same time elastic rebound happens in the intact ice. Because of the continuous supply of ice from the far field, the crushed ice extrudes and the structure comes into contact again with the intact ice. The extrusion process of the crushed ice depends on parameters such as the stiffness of the structure, the ice velocity, and the size of the crushed zone. Perhaps the most important factors governing the extrusion process are the mechanical properties of the crushed ice and how they vary during the extrusion.

Kurdymov and Kheisin (1976) conducted impact tests in which a rigid ball was dropped on a flat ice surface. They found that a very thin layer of crushed ice formed at the contact surface between the ball and the ice. This layer of crushed ice is very similar to the thin layer of pulverized ice found by Timco (1986) in his indentation tests in the brittle range. In their analysis, Kurdymov and Kheisin treated the thin layer of the pulverized ice as a viscous fluid.

More recently, Jordaan and Timco (1988) presented a solution for an ice sheet of thickness H being indented continuously by an indentor moving with a constant velocity V_0 as shown in Fig. 6.4. In their solution, Jordaan and Timco treated the crushed ice as a Newtonian viscous fluid and they found that the force on the iindentor can be calculated as

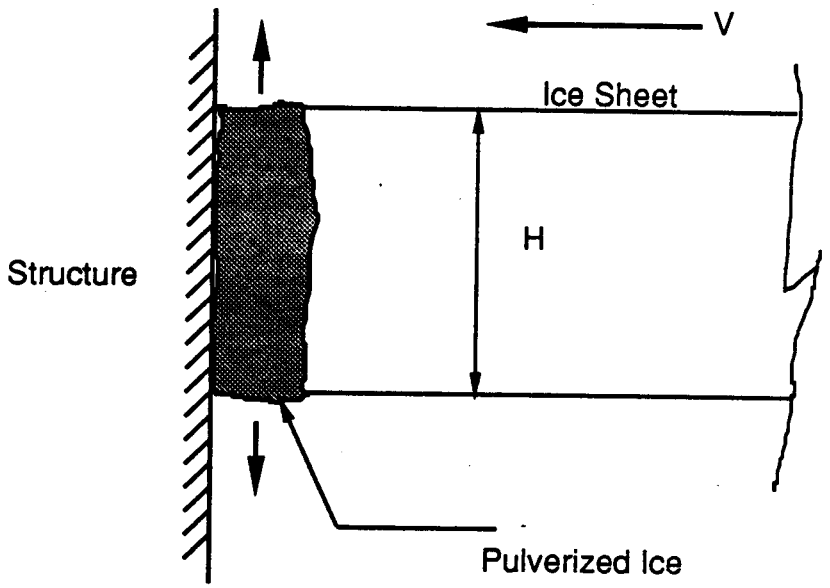

Figure 6.4 Extrusion of Pulverized Ice

$$F(t) = \mu V_0 (H/L)^3 \qquad (6.16)$$

where F is the force on the indentor, μ is the viscosity of the crushed ice, and L is the thickness of the crushed layer at time t. According to this equation the force on the indentor is inversely proportional to the cubic length of the crushed zone. Vivatrat (1982) plotted ice pressure versus penetration distance for indentation tests with different strain rates. It was concluded from his curves that the ice force is almost inversely proportional to the crushed zone length. Also, representing the crushed ice as a Newtonian viscous fluid does not take into consideration the change in the material properties of the pulverized ice that occur during the extrusion. However, simulating the crushed ice as a viscous fluid in the analysis has some advantages. The representation of a viscous fluid in a numerical analysis is straightforward.

In this study the crushed ice is assumed to behave as a nonlinear viscous fluid during the extrusion. The nonlinearity is introduced through the viscosity which changes during the extrusion process. During extrusion, the crushed ice is squeezed between the structure and the intact ice. It is expected that the properties of the crushed ice change during the extrusion and that its load carrying capacity increases as the length of the crushed zone decreases. Comprehensive studies on the mechanical behavior of crushed ice are not available in the literature. However, preliminary study on the geotechnical properties of rubble ice has shown that its shear strength increases significantly as the void ratio decreases (Gale et al., 1987). The assumption used here, to represent the increase in the shear strength, as the length of the crushed zone decreases, can be written as

$$\mu = \mu_0(1-\varepsilon), \tag{6.17}$$

where μ is the viscosity of the crushed ice, μ_0 is its initial viscosity, and ε is the strain in the crushed ice. This is defined as the change in its length divided by the initial length of the crushed zone. The value of ε varies between zero and -1. Within a cycle of crushing and extrusion, ε takes the value zero when crushing occurs since at that time the size of the crushed zone is a maximum and none of the crushed ice has been extruded. During the extrusion process, the length of the crushed zone decreases and the value of ε decreases. When the crushed ice is almost completely extruded the numerical value of ε approaches -1. It is noticed that ε in this case is not as usually used in theory of elasticity since it goes from zero to -1 in which case a logarithmic strain provides a better strain measure. However, ε is a parameter that can be used to track the extrusion process.

Equation (6.17) represents a linear increase in the viscosity of the crushed ice as its length decreases (ε in Eq. (6.17) is always negative). This assumption seems to be consistent with the observations of Vivatrat in his indentation tests and also reflects the observed increase in shear strength of crushed ice during compression (Gale et al., 1987).

Representing the crushed ice as a nonlinear viscous dashpot in the interaction analysis makes the damping matrix nonlinear (Eq. (6.15)). Since the strain in the crushed ice is assumed to be completely viscous, its effect can be taken into consideration through an equivalent external load as discussed earlier, if the material is represented as a viscoelastic material. In order to take advantage of this approach, the crushed ice is simulated in the numerical solution as a viscoelastic material that consists of a nonlinear viscous dashpot in series with a

stiff spring as shown schematically in Fig. 6.5. The total strain in this spring-dashpot system is equal to the elastic strain in the spring plus the viscous strain in the dashpot. The elastic strain is very small due to the high stiffness of the spring. This causes the total strain in the spring-dashpot system to degenerate to the viscous strain in the dashpot.

Having established the constitutive behavior of the crushed ice in this fashion, the solution algorithm outlined above for viscoelastic materials can be used in studying the ice-structure interaction problem. In the following section, the viscoelastic model is used to perform an interaction analysis for several cases.

6.5 Test problems

The first four cases studied in Chapter 5 in which the ice thickness is 9 m and the ice velocity varies from 0.04 to 0.10 m/s are analyzed using the viscoelastic model. The structure is represented as a single degree of freedom system. The stiffness of the spring in the single degree of freedom system (K) is taken as the global stiffness of the structure (67 GN/m, Jefferies and Wright; 1988). The mass (m) is calculated in such a way that the natural frequency of vibration of the system is equal to the natural frequency of the first mode of vibration of the actual structure (ϖ^2= K/m). A viscous damper that has a damping coefficient of about 20 percent of the critical damping is used in order to represent the damping of the system.

In the four cases, the ice-structure system is represented using the arrangement shown in Fig. 6.3 where the ice is simulated as a train of elements with the far end moving with a prescribed constant velocity. In order to allow for the decrease in the stresses in the ice sheet as one moves away from the structure,

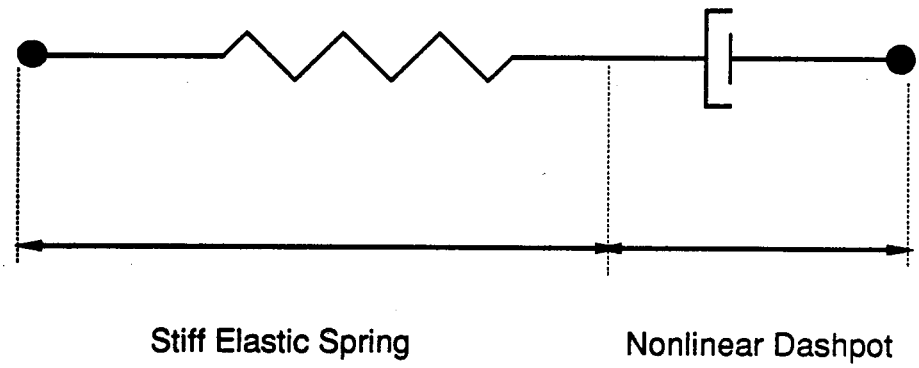

Figure 6.5 Representation of Crushed Ice in Finite Element Analysis

the area of the ice elements is assumed to increase linearly using a slope of 2:1 to determine the limits of the stressed zone as shown in Fig. 6.6 (D. Sego, personal communications). This slope is used extensively in soil mechanics to calculate the vertical stresses under foundations. Timco's experiments (1986) show that the stressed zone in the ice sheet ahead of the indentor is similar to the stressed zone in soil under foundations.

The resulting interaction force during a typical cycle of loading-crushing-unloading for the four cases is shown in Fig. 6.7. The results show that the interaction force has the same features of the force obtained using the 4-parameter interaction model introduced in Chapter 5. The ice force increases almost linearly until crushing occurs at a critical value of stress then unloading starts and the cycle repeats itself. The results of the viscoelastic model show that the frequency of the ice interaction force is a direct function of the ice velocity which is consistent with the results from the first interaction model. The interaction forces shown in Fig. 6.7 correspond to the entire structure and not just a strip from it.

The magnitude of the interaction force is dependent on the numerical value of the viscosity of the crushed ice. To the writer's knowledge, no data on this material property is available in the public domain for crushed ice. In order to get a magnitude of the interaction force that is comparable to that of the recorded forcing function of Fig. 4.2, a value of μ_o that lies in the range of $1x10^7$ and $1x10^8$ N s/m^2 is required. These values of viscosity are comparable to those of materials such as bitumen when being tested at temperatures close to its melting point (Jackson, 1976).

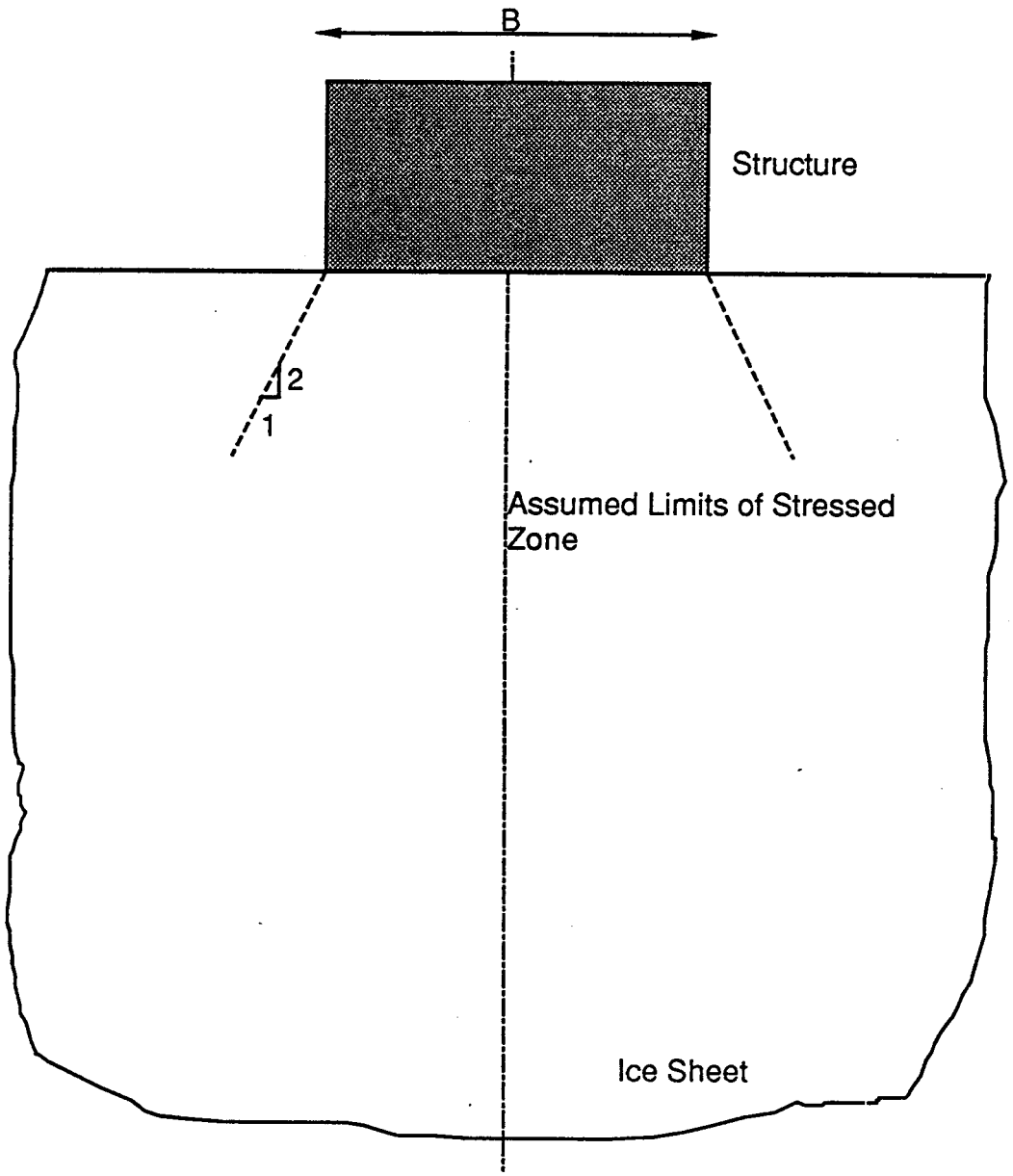

Figure 6.6 Assumption Used in Increasing the Area of Ice Elements

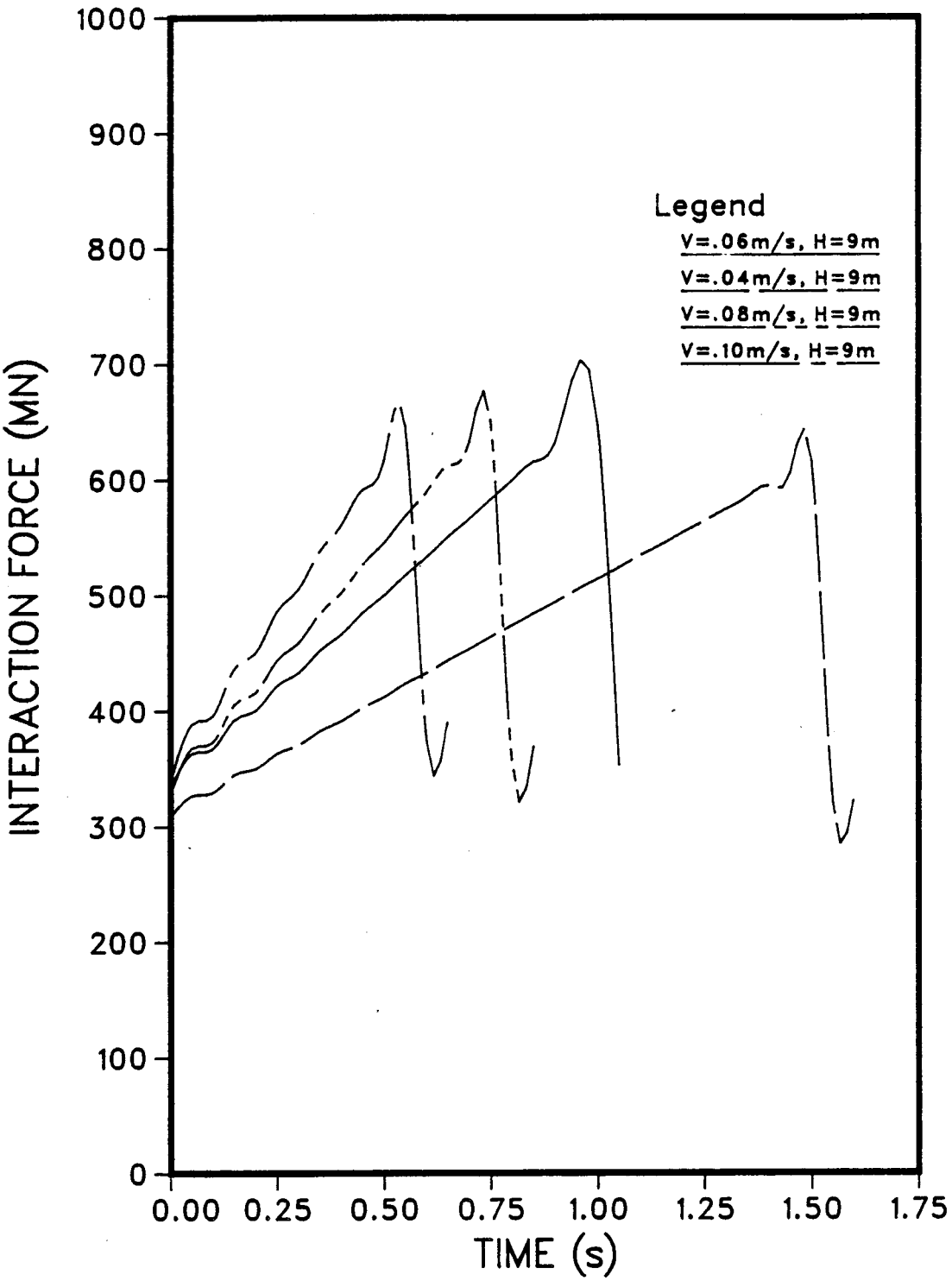

Figure 6.7 Interaction Force from Viscoelastic Model

In the four-parameter interaction model, presented in Chapter 5, a reduced modulus of elasticity is used in evaluating the loading slope (S^+). The first case studied in Chapter 5 is used as a test case in order to provide a reasonable estimate of the reduced modulus. This reduced modulus was found to be in the range of 20 to 30 percent of the Young's modulus of the sea ice. The results obtained using this value of the reduced modulus in the four-parameter model are in very good agreement with those measured in the field. This means that, comparison between the results of the interaction analysis of Chapter 5 and field measurements is made in order to find out the reduced modulus.

It seems reasonable that the viscoelastic model can be used in conjunction with the four-parameter model in an overall analysis of the ice-structure interaction. The viscoelastic model can be used with a simple representation of the structure under consideration at the beginning. A reasonable estimate of the reduced modulus can be obtained from this step. In the second step of the analysis, the four-parameter model can be employed with a detailed representation of the structure or a representative portion of it. In this step, the response of the structure and the stresses in the different elements can be studied.

It can be concluded from the analysis presented in this chapter that the material properties of crushed ice are an important factor in the ice-structure interactions. The extrusion process is influenced by the properties of crushed ice . The number of studies on crushed ice that have been undertaken to date is very limited and more work is required in order to gain a better understanding of the constitutive behavior of crushed ice.

7. SUMMARY, CONCLUSIONS, AND RECOMMENDATIONS

7.1 Summary

An analytical study has been undertaken in order to investigate the dynamic behavior of caisson-type offshore structures under ice forces. A model structure typified by Gulf Canada's Mobile Arctic Caisson (MAC) was chosen for this study. Two finite element models have been developed for the structure. A detailed two dimensional model was used extensively in this study and a less detailed three dimensional one was developed in order to monitor the behavior of the detailed one. A comparison between the dynamic behavior of the two finite element models through their mode shapes showed that they are in good agreement.

The moving ice has been represented in the analysis in different ways. As a first step, the ice was considered through an idealized forcing function based on field measurements taken by others during an actual ice event. An analysis of the finite element model under the effect of the ice forcing function yielded results that are quite comparable to the recorded response of the structure in the field. Results of the dynamic analysis were presented in terms of the kinematic response of the structure, that is accelerations, velocities, and displacements. The force build-up in different structural components during a typical load cycle were also presented in terms of normalized normal and shear stresses.

In addressing the ice-structure interaction problem, a second approach has been followed in which the impinging ice was represented in the analysis as a

structural element. In this case, the problem has been treated as a displacement-controlled one in which the far end of the ice was assumed to move with a constant velocity. The mechanical behavior of the ice elements has been developed based on known constitutive behavior of ice and also general observations during indentation tests. Several cases have been studied using the proposed interaction model in order to investigate the effect of the ice velocity and thickness on the interaction force.

A second interaction model has also been developed in order to take the long term behavior of ice into consideration. The model is based on Sinha's equation to describe the viscoelastic behavior of ice before crushing. Once crushing occurs, the behavior of crushed ice during extrusion was assumed to be similar to that of a viscous fluid. A solution algorithm for the dynamic viscoelastic analysis has been introduced in which the viscous effect is converted into an equivalent external load. In that sense, the viscoelastic problem can be treated as a series of linear elastic problems. Different cases were analyzed using the proposed viscoelastic model and their results were presented along with discussions of the results and comparison between the results of the two proposed interaction models. In the following section, the main conclusions that have been drawn from this study are summarized.

7.2 Conclusions

The study reported here led to the following conclusions:

1- Dynamic analysis of ice-structure interaction can be done either by representing the ice through a load history or by simulating the ice as a structural element in the analysis. In general, load histories are difficult to obtain.

2. Analyses of caisson-type drilling platforms under ice load histories that have been recorded in the field during ice events have not been published in the past.

3- Dynamic analysis of ice interaction with large scale structures can be done using a representative portion of the structure after ensuring that the global behavior of the actual structure is reflected in the smaller model.

4- Comparison between the modes of vibration of the structure and its representative portion is a reasonable means to check that the smaller model reflects the global behavior of the structure.

5- Damping due to ice can be represented in the analysis using the geometric or radiation damping concept used in dynamic soil-structure interactions.

6- Finite element dynamic analysis conducted on a representative strip of the model structure under a forcing function that was recorded in the field yielded results comparable to the reported field measurements of the structure response.

7- Interaction models that have been developed in the past are either limited to a specific type of structure or need field measurements in order to complete the formulation of the model.

8- The proposed 4-parameter interaction model yielded results that are comparable with reported field measurements.

9- The parametric study conducted using the 4-parameter interaction model shows that the crushing frequency is proportional to the ice velocity.

10- In the interaction between large scale structures and ice floes of few meters thickness, the ice thickness has no significant effect on the crushing frequency.

11- For some structural elements, the smaller ice thicknesses produce higher stresses in the element than the bigger thicknesses due to the change in the point of application of the resultant ice force.

12- Ice can be represented in the analysis in more detail as a viscoelastic material.The proposed viscoelastic ice model yielded results that are comparable with the results of the 4-parameter model.

13- Mechanical properties of crushed ice is an important factor in the extrusion process during ice-structure interaction.

14- The use of a supercomputing facility has allowed a dynamic analysis of a complicated structure using a fairly detailed model.

7.3 Recommendations for future research

Further research and development in the following areas would be of interest:

1- Comprehensive studies on the mechanical behavior of crushed ice under different loading conditions are required.

2- Dynamic analysis of the model structure used in this study under ice forcing functions recorded during different ice events is needed.

3- Tests on ice are required in order to determine the effect of loading-unloading cycles on the mechanical behavior of ice.

4- Constitutive models that describe the behavior of ice under variable strain rate histories are needed.

References

Ashby, M.F., Palmer, A.C., Thouless, M., Goodman, D.J., Hallam, S.D., Murrell, S.A.F., Jones, N., Snaderson, T.J.O., and Ponter, A.R.S. (1986).

"Non-Simultaneous Ice Failure and Ice Loads on Large Structures," Proceedings of the 18th Annual Offshore Technology Conference, Vol. 3, pp. 399-404, Houston, Texas.

Ashwell, D.G. and Gallagher, R.H., Editors, (1976).

"Finite Elements for Thin Shells and Curved Members," John Wiley and Sons, London.

Assur, A. (1958).

"Composition of Sea Ice and its Tensile Strength," in Arctic Sea Ice, U.S.National Academy of Sciences, National Research Council, Publication No. 598, pp. 16-138.

Bercha, F.G. and Brown, T.G.(1985).

"Scale Effects in Ice-Structure Interactions," Proceedings of the 4th International Offshore Mechanics and Arctic Engineering, ASME, Vol. I , pp. 310-314.

Blenkarn, K.A. (1970).

"Measurements and Analysis of Ice Forces on Cook Inlet Structures," Proceedings of the 2nd Offshore Technology Conference, OTC, Vol. 2, pp. 365-378, Houston,Texas.

Bohon, W.M. and Weingarten, J.S. (1985).

"The Calculation of Ice Forces on Arctic Structures" Proceedings of the Conference Arctic'85, pp. 456-464, San Francisco, California.

Bowles, J.E. (1977).

Foundation Analysis and Design," McGraw-Hill, 750p.

Bruce, J.C. and Harrington, A.G. (1982).

"Design Aspects of a Mobile Arctic Caisson," Proceedings of the 14th Anual Offshore Technology Conference, Vol. 3, pp. 405-416, Houston, Texas.

Clough, R.W. and Penzien, J. (1975).

"Dynamics of Structures," McGraw-Hill, 634p.

Crues, G.J. (1986).

"Viscoelasticity-Basic Theory and Applications to Concrete Structures," Springer-Verlag.

Croasdale, K.R. (1984).

Ice interaction with Structures:Recent Developments and Future Trends," Symposium on Offshore Mechanics and Cold Ocean Engineering, Calgary, Canada.

Croasdale,K.R., Morgenstern, N.R., and Nuttall, J.B. (1977).

"Indentation Tests to Investigate Ice Pressures on Vertical Structures," Journal of Glaciology, Vol. 19, No. 81, pp. 301-311.

Croteau, P. (1983).

"Dynamic Interactions Between Floating Ice and Offshore Structures," Univ. of California at Berkeley Report No. UCB/EERC-83/06.

Eranti, E., Haynes, F.D., Maattanen, M., and Soong, T.T. (1981).

"Dynamic Ice-Structure Interaction Analysis for Narrow Vertical Structures," Proc., POAC, Quebec, Canada, Vol. I, pp. 472-479.

Erbatur, M.F. and Maddock, W. (1985).

"Computer Simulation Techniques for Arctic Offshore Design-A Review," Symposium on Offshore Mechanics and Cold Ocean Engineering, Calgary, Canada.

Flugge, W. (1975).

"Viscoelasticity," Springer-Verlag, 194p.

Frankenstein, G. and Gardner, R. (1967).

"Equations for Determining the Brine Volume of Sea Ice from -0.5 to -22.9^{o}C," Journal of Glaciology, Vol. 6, No. 48, pp. 943-944.

Frederking, R. (1977).

"Plane-Strain Compressive Strength of Columnar-Grained and Granular-Snow Ice," Journal of Glaciology, Vol. 18, No. 80, pp. 505-516.

Frederking, R. and Gold, L.W. (1975).

"Experimental Study of Edge Loading of Ice Plates," Canadian Geotechnical Journal, Vol. 12, No. 4, pp. 456-463.

Gale, A.D., Sego, D.C., and Morgenstern, N.R. (1987).

"Geotechnical Properties of Ice Rubble," Ice Rubble Mechanics Report No. 3, NSERC.

Gazetas, G. and Dobry, R. (1984).

"Simple Radiation Damping Model for Piles and Footings," Journal of the Engineering Mechanics Division, ASCE, Vol. 110, No. EM6, pp. 937-956.

Hallam, S.D. and Pickering, J.G. (1988).

"Modelling of Dynamic Ice Loading of Offshore Arctic Structures," Proc. Polarteck'88, Vol. 1, pp. 235-248, Torndheim.

Hausler, F.U. (1981).

"Multiaxial Compressive Strength Tests on Saline Ice with Brush-Type Loading Platens," Proc. IAHR International Symposium on Ice Problems, Quebec, Canada, Vol. II, pp. 526-536.

Jefferies, M.G., Stewart, H.R., Thomson, R.A.A., and Goldby, H.M. (1985).

"Deployment of Beaudril Molikpak at Tarsiut," Symposium on Offshore Mechanics and Cold Ocean Engineering, Calgary, Canada.

Jefferies, M.G., Stewart, H.R., Thomson, R.A.A., and Rogers, B.T. (1985).

"Molikpac Deployment at Tarsiut P-45," Proc. ASCE Speciality Conference 'Arctic 85', pp. 1-27.

Jefferies, M.G. and Wright, W.H. (1988).

"Dynamic Response of Molikpac to Ice-Structure Interaction," Proc. 7th International Conference and Exhibit on Offshore Mechanics and Arctic Engineering, Houston, U.S.A.

Jordaan, I.J. (1986).

"Computational and Finite Element Techniques in Calculation of Ice-Structure Interaction,"Proc. of the 8th International Symposium on Ice, IAHR, Vol. 2, pp. 405-441, Iowa City, IA.

Jordaan, I.J. and Timco, G.W. (1988).

"Dynamics of the Ice Crushing Process," Journal of Glaciology, Vol. 34, No. 118, pp. 318-326.

Karr, D.G. (1984).

"Applications of Continuous Damage Models in Ice Mechanics," Proc. 4th International Conference on Applied Numerical Modelling, Taiwan.

Korzhavin, K.N. (1962).

"Action of Ice on Engineering Structures," U.S.Army Cold Regions Research and Engineering Laboratory, CRREL Translation TL260.

Kry, P.R. (1980).

"Ice Forces on Wide Structures," Canadian Geotechnical Journal, Vol. 17, No.1, February, pp.97-113.

Kurdyumov, V.A. and Kheisin, D.E. (1976).

"Hydrodynamic Model of the Impact of a Solid Ball on Ice," Prikladnaya Mekhanika, Vol. 12, No. 10, pp. 103-109.

Ladanyi, B. (1967).

"Expansion of Cavities in Brittle Media," International Journal of Rock Mechanics and Mining Science, Vol. 4, pp. 301-328.

Lipsett, A.W. and Gerard, R. (1980).

"Field Measurements of Ice Forces on Bridge Piers," Transportation and Surface Water Engineering Department, Alberta Research Council, Internal Report SWE 80/03.

Maattanen, M. (1978).

"On the Conditions of Self-Excited Ice-Induced Autonomous Oscillations in Slender Marine Pile Structures," Finnish-Swedish Winter Navigation Board, Research Report No. 25, Finnish Board of Navigation, Helsinki.

Maattanen, M. (1979).

"Laboratory Tests for Dynamic Ice-Strcture Interaction," Proc., POAC, Tronheim, Norway, Vol. 2, pp. 1139-1153.

Maattanen, M. (1981).

"Ice Structure Interaction-Ice Forces Versus Velocity-Ice-Induced Damping," proc., IAHR International Synposium on Ice Problems, Quebec, Canada, Vol. II, pp. 783-792.

Maattanen, M. (1983).

"Dynamic Ice-Structure Interaction During Continuous Crushing," CRREL Report 83-5.

Matlock, H., Dawkins, W.P., and Panak, J.J. (1969).

"A model for the Prediction of Ice-Structure Interaction," Proc., Offshore Technology Conference, OTC Paper No. 1066, Houston, Texas.

Metge, M., Danielewicz, B., and Hoane, H. (1981).

"On Measuring Large Scale Ice Forces; Hans Island 1980," Proc., POAC, Quebec, Canada, Vol. II, pp. 629-642.

Michel, B. (1978).

"Ice Mechanics," Les Presses de l'Universite' Laval, Quebec, Canada, 449p.

Michel, B. (1981).

"Advances in Ice Mechanics," Proc. of the 6th International Conference on Port and Ocean Engineering Under Arctic Conditions (POAC 81), Universite Laval, Quebec, Canada, pp. 189-204.

Michel, B. and Blanchet, D. (1983).

"Indentation of an S2 Floating Ice Sheet in the Brittle Range,' Annals of Glaciology 4, pp. 180-187.

Michel, B. and Ramseier, R.O. (1971).

"Cassification of River and Lake Ice,"Canadian Geotechnical Jpurnal, Vol. 8, pp. 36-45.

Michel, B. and Toussaint, N. (1977).

"Mechanisms and Theory of Indentation of Ice Plates," Journal of Glaciology, Vol. 19, No. 81, pp. 285-300.

Montgomery, C.J., Gerard, R., and Lipsett, A.W. (1980).

"Dynamic Response of Bridge Piers to Ice Forces," Canadian Journal of Civil Enginerring, Vol. 7, pp. 345-356.

Montgomery, C.J. and Lipsett, A.W. (1981).

"Estimation of Ice Forces from Dynamic Response," Proc. IAHR International Symposium on Ice Problems, Quebec, Canada, Vol. II, pp. 771-780.

Nawwar, A.M., Nadreau, J.P., and Wang, Y.S. (1983).

"Triaxial Compressive Strength of Saline Ice," Proc. of the 7th International Conference on Port and Ocean Engineering Under Arctic Conditions (POAC), Helsinki, Finland, Vol. 3, pp. 193-202.

Neill, C.R. (1972).

"Force Fluctuations During Ice Floe Impacts," Proc. IAHR International Symposium on Ice Problems, Leningrad, USSR, pp. 26-29.

Neill, C.R. (1976).

"Dynamic Ice Forces on Piers and Piles, An Assessment of Design Guidelines in the Light of Recent Research," Canadian Journal of Civil Engineering, Vol. 3, pp. 305-341.

Newmark, N.M. (1959).

"A Method of Computation for Structural Dynamics," ASCE, Journal of Engineering Mechanics Division, Vol. 85, pp. 67-94.

Newmark, N.M. and Hall, W.J. (1973).

"Procedures and Criteria for Earthquake Resistant Design,"Building Practices for Disaster Mitigation, National Bureau of Standards, Gaithersburg, Md., Building Science Series No. 46, Vol. 1, PP. 209-236.

Newmark, N.M. and Rosenblueth,E. (1971).

"Fundamentals of Earthquake Engineering," Prentice Hall, Englewood Cliffs, N.J., 640p.

Nilrat, F. (1980).

"Hydrodynamic Pressure and Added Mass for Axisymmetric Bodies," earthquake Engineering Research Centre, report No. EERC 80-12, University of California, Berkeley, 143p.

Peyton, H.R. (1966).

"Sea Ice Strength," Geophysical Institute, University of Alaska, Report UAG R-182, College, alaska, December, 217p.

Peyton, H.R. (1968).

"Sea Ice Properties," Ocean Industry, Vol. 3, No. 9, September, pp. 59-65.

Peyton , H.R. (1968a).

"Sea Ice Forces," National Research Council, Associate Committee on Geotechnical Research, Subcommittee on Snow and Ice, Technical Memorandum No. 92, NRC No. 9851, Ottawa, Canada.

Peyton, H.R. (1968b).

"Ice and Marine Structures: Part 1-The Magnitude of Ice Forces Involved in Design; Part 2-Sea Ice Properties; Part 3-The Importance of Design Alternatives," Ocean Industry, Vol. 3, No. 3, March, pp. 40-44; No. 9, September, pp. 59-65; No. 12, December, pp. 51-58.

Prager, W. and Hodge, P.G. (1951).

"Theory of Perfectly Plastic Solids," John Wiley and Sons.

Prakash, S. (1981).

"Soil Dynamics," McGraw-Hill, 426p.

Ralston, T.D. (1978).

"An Analysis of Ice Sheet Indentation," Proc. IAHR International Symposium on Ice Problems, Lulea, Sweden, Part I, pp. 13-31.

Reddy, D.V., Cheema, P.S., Swamidas, A.S.J., and Halder, A.K. (1975b).

"Stochastic Response of a Three-Dimensional Offshore Tower to Ice Forces," Proc. IAHR International Symposium on Ice Problems, Hanover, NH, pp. 499-574.

Reddy, D.V., Swamidas, A.S.J., and Cheema, P.S. (1975a).

"Ice Force Response Spectrum Modal Analysis of Offshore Towers," Proc.,POAC, Fairbanks, Alaska, Vol. II, pp.887-910.

Reinicke, K.M. and Ralston, T.D. (1977).

"Plastic Limit Analysis with an Anisotropic Parabolic Yield Function," International Journal of Rock Mechanics and Mining Sciences, Vol. 14, pp.147-154.

Reinicke, K.M. and Remer, R. (1978).

"A Procedure for the Determination of Ice Forces Illustrated for Polycrystalline Ice," Proc. IAHR International Symposium on Ice Problems, Lulea, Sweden, Part I, pp. 217-238.

Richart, F.E., Hall, J.R., and Woods, R.D. (1970).

"Vibrations of Soils and Foundations," Prentice-Hall, Englewood Cliffs, N.J..

Roscoe, K.H. and Burland, J.B. (1968).

"On the Generalized Stress-Strain Behavior of Wet Clay," in Engineering Plasticity, J. Heyman and F.A. Leckie (Editors), Cambridge University Press, Cambridge, pp. 525-609.

Sanderson, T.J.O. (1987).

"A Pressure-Area Curve for Ice," Working Group on Ice Forces, 3rd State-of-the-Art Report," USA Cold Regions Research and Engineering Laboratory, CRREL Special Report 87-17,75-98.

Schwarz, J. (1970).

"The Pressure of Floating Ice Fields on Piles," Proc. IAHR Symposium-Ice and its Action on Hydraulic Structures, Reykjavic, Iceland, Paper No. 6.3.

Schwarz, J., Hirayama, K., and Wu, H.C. (1974).

"Effect of Ice Thickness on Ice Forces," Proc. of the 6th Offshore Technology Conference, Houston, Texas, Paper No. 2048.

Shapiro, L.H. (1978).

"Development of Hadware and Procedures for In-Situ Measurement of Creep in Sea Ice," OCSEAP Annual Report, Research Unit 265, Contract No. 03-5-022-55.

Sinha, N.K. (1978).

"Rheology of Columnar-Grained Ice," Journal of Experimental Mechanics, Vol. 18, No. 12, pp. 464-470.

Sinha, N.K. (1981).

"Deformation Behavior of Ice-Like Materials in Engineering Applications," Proc. of the International Symposium on the Mechanical Behavior of Structural Media, Carleton University, Ottawa, Ontario, pp. 419-430.

Sodhi, D.S. and Morris, C.E. (1986).

"Characteristic Frequency of Force Variations in Continuous Crushing of Sheet Ice Against Rigid Cylindrical Structures," Cold Regions Sciencs and Technology, Vol. 12, pp. 1-12.

Timco, G.W. (1986).

"Indentation and Penetration of Edge-Loaded Freshwater Ice Sheets in the Brittle Range," Proc. of the 5th OMAE Symposium, ASME, Vol. IV, pp. 444-452.

Ting, S.K. and Sunder, S.S. (1985).

"Constitutive Modelling of Sea Ice with Applications to Indentation Problems," CSEOE Research Report No. 3, M.I.T..

Vivatrat, V. (1982).

"Strains and Strain Rates in Sea Ice Indentation," Proc. of the 14th Annual Offshore Technology Conference, Vol. 3, pp. 133-140, Houston, Texas, Paper No.

Wang, Y.S. (1979).

"Sea Ice Properties," in Exxon Technical Seminar on Alaskan Beaufort Sea Gravel Island Design, Anchorage, Alaska, October 15 and Houston, Texas, October 18.

Wang, Y.S. (1981).

"Uniaxial Compression Testing of Arctic Sea Ice," Proc. of the 6th International Conference on Port and Ocean Engineering Under Arctic Conditions, POAC, Universite Laval, Quebec, Canada, pp. 345-355.

Wang, Y.S. (1982).

"A Rate-Dependent Stress-Strain Relationship for Sea Ice," Proc. of the 1st International Symopsium on Offshore Mechanics and Arctic Engineering, ASME, New Orleans, Louisiana, pp. 243-248.

Wu, H.C., Cheng, K.J., and Schwarz, J. (1976).

"Fracture in the Compression of Columnar Grained Ice,"Engineering Fracture Mechanics, Vol. 8, pp. 365-372.

Zienkiewicz, O.C. (1977).

"The Finite Element Method," McGraw-Hill.

RECENT STRUCTURAL ENGINEERING REPORTS

Department of Civil Engineering

University of Alberta

132. *Design Strengths of Steel Beam-Columns* by N.S. Trahair, December 1985.

133. *Behaviour of Fillet Welds as a Function of the Angle of Loading* by G.S. Miazga and D.J.L. Kennedy, March 1986.

134. *Inelastic Seismic Response of Precast Concrete Large Panel Coupled Shear Wall Systems* by M.R. Kianoush and A. Scanlon, March 1986.

135. *Finite Element Prediction of Bin Loads* by A.H. Askari and A.E. Elwi, June 1986.

136. *Shear Behavior of Large Diameter Fabricated Steel Cylinders* by J. Mok and A.E. Elwi, June 1986.

137. *Local Buckling Rules for Structural Steel Members* by S. Bild and G.L. Kulak, May 1986.

138. *Finite Element Prediction of Reinforced Concrete Behavior* by S. Balakrishnan and D.W. Murray, July 1986.

139. *Behavior and Strength of Masonry Wall/Slab Joints* by T.M. Olatunji and J. Warwaruk, July 1986.

140. *Bayesian Analysis of In-Situ Test Data for Estimating the Compressive Strength of Concrete in Existing Structures* by G.J. Kriviak and A. Scanlon, July 1986.

141. *Shear-Moment Transfer in Slab-Column Connections* by S.D.B. Alexander and S.H. Simmonds, July 1986.

142. *Minimum Thickness Requirements for Deflection Control of Two-Way Slab Systems* by D.P. Thompson and A. Scanlon, November 1986.

143. *Shrinkage and Flexural Tests of Two Full-Scale Composite Trusses* by A. Brattland and D.J.L. Kennedy, December 1986.

144. *Combined Flexure and Torsion of I-Shaped Steel Beams* by R.G. Driver and D.J.L. Kennedy, March 1987.

145. *Cyclic and Static Behaviour of Thin Panel Steel Plate Shear Walls* by E.W. Tromposch and G.L. Kulak, April 1987.

146. *Postbuckling Behavior of Thin Steel Cylinders Under Transverse Shear* by V.G. Roman and A.E. Elwi, May 1987.

147. *Incipient Flow in Silos - A Numerical Approach* by R.A. Link and A.E. Elwi, May 1987.

148. *Design of Web-Flange Beam or Girder Splices* by D. Green and G.L. Kulak, May 1987.

149. *Spreadsheet Solution of Elastic Plate Bending Problems* by G.E. Small and S.H. Simmonds, July 1987.

150. *Behaviour of Transversely Loaded Continuous Steel-Concrete Composite Plates* by S.J. Kennedy and J.J. Cheng, July 1987.

151. *Behaviour and Ultimate Strength of Partial Joint Penetration Groove Welds* by D.P. Gagnon and D.J.L. Kennedy, July 1987.

152. *KBES for Design of Reinforced Concrete Columns* by A. Bezzina and S.H. Simmonds, July 1987.

153. *Compressive Behavior of Gusset Plate Connections* by S.Z. Hu and J.J. Cheng, July 1987.

154. *Development of Structural Steel Design Standards* by P.J. Marek and D.J.L. Kennedy, October 1987.

155. *Behaviour of Bolted Joints of Corrugated Steel Plates* by R.W.S. Lee and D.J.L. Kennedy, January 1988.

156. *Masonry Veneer Wall Systems* by W.M. McGinley, J. Warwaruk, J. Longworth and M. Hatzinikolas, January 1988.

157. *Stability of Concrete Plates* by A.O. Aghayere and J.G. MacGregor, February 1988.

158. *The Flexural Creep Behaviour of OSB Stressed Skin Panels* by P.C.K. Wong, L. Bach and J.J. Cheng, April 1988.

159. *Ultimate Strength of Eccentrically Loaded Fillet Welded Connections* by D.F. Lesik and D.J.L. Kennedy, May 1988.

160. *Fatigue Strength of Coped Steel Beams* by M.C.H. Yam and J.J. Cheng, June 1988.

161. *Analysis of Concrete Panels* by B. Massicotte, A.E. Elwi and J.G. MacGregor, July 1988.

162. *Behavior and Design of Reinforced Concrete Ice-Resisting Walls* by R.M. Ellis and J.G. MacGregor, November 1988.

163. *An Analysis of the Performance of Welded Wide Flange Columns* by D.E. Chernenko and D.J.L. Kennedy, December 1988.

164. *Nonlinear Dynamic Analysis of Caisson-Type Offshore Structures* by I.R. Soudy and T.M. Hrudey, March 1989.